NASA TM X-623

NASA TM X-623

TECHNICAL MEMORANDUM

X-623

PRESSURE DISTRIBUTIONS ON BLUNT DELTA WINGS AT A MACH NUMBER OF 2.91 AND ANGLES OF ATTACK UP TO 90°

By James N. Mueller

Langley Research Center
Langley Air Force Base, Va.

[redacted]

NATIONAL AERONAUTICS AND SPACE ADMINISTRATION
WASHINGTON March 1962

[redacted]

1M

[redacted]

NATIONAL AERONAUTICS AND SPACE ADMINISTRATION

TECHNICAL MEMORANDUM X-623

PRESSURE DISTRIBUTIONS ON BLUNT DELTA WINGS AT A MACH NUMBER OF 2.91 AND ANGLES OF ATTACK UP TO 90°*

By James N. Mueller

L
1
5
5
2

SUMMARY

A wind-tunnel investigation was made at a Mach number of 2.91 to evaluate the pressure-distribution characteristics on a family of blunt-leading-edge, slab-type, delta wings at angles of attack up to 90°. Two types of leading-edge bluntness were employed: square and round. For each type of bluntness there were five wing models of 50°, 60°, 70°, 75°, and 80° leading-edge sweep.

The results of the investigation indicated that, in the angle-of-attack range from 45° to 90°, the effect of leading-edge shape on wing pressures was confined primarily to the leading-edge surfaces. The windward pressures were essentially constant over the slab surface for angles of attack less than 45°; at greater angles of attack the strong, curved, bow shocks created by the wings produced significant negative pressure gradients in the streamwise direction. At angles of attack greater than about 35°, a simple expression related to sweep theory and Newtonian theory is shown to predict qualitatively the wing pressures normal to the leading edge. A compilation of asymptotic center-line slab-surface pressures, normalized by the stagnation pressure behind a normal shock, for angles of attack from 0° to 90° and Mach numbers from 2.91 to about 22 shows that oblique-shock theory at a Mach number of ∞ predicts the pressures up to angles of attack of about 40°. The experimental hypersonic maximum center-line pressures are generally bracketed by a hypersonic series approximation corresponding to moderate sweep and a modified Newtonian prediction corresponding to 90° sweep. Pressures on the leeward wing surfaces are essentially constant at angles of attack greater than 20° and are easily predicted.

[redacted] Unclassified.

[redacted]

INTRODUCTION

Knowledge of the pressure distributions on winged configurations at high angles of attack (up to 90° and beyond) is currently of considerable practical interest. For example, orbital manned vehicles entering planetary atmospheres may make use of high angle-of-attack capability to vary their lift and drag and to provide maneuverability during reentry (refs. 1 to 5).

Pressure distributions have been measured at high angles of attack (up to 90°) on basic bodies such as cylinders and cones (for example, refs. 6 and 7); for other shapes, however, little data exist above angles of attack from 40° to 50°. Recently, however, the general evolvement of the basic delta planform, or modifications thereto, as a primary shape for consideration in the design of vehicles with high lift-drag ratios has given impetus to the determination of aerodynamic forces and moments and pressure distributions over these shapes at supersonic and hypersonic Mach numbers over the angle-of-attack range from 0° to 90°. Recent experimental results obtained on delta-wing configurations at supersonic and hypersonic speeds are presented in references 3 and 4 and 8 to 11.

L
1
5
5
2

The purpose of the present investigation was to obtain pressure distributions on blunt delta wings through an angle-of-attack range from 45° to 90° (limited data were also obtained at angles of attack from 0° to 45° on one model) in order to further the knowledge of experimental high angle-of-attack aerodynamic effects at supersonic speeds and to aid in the formulation and development of applicable high angle-of-attack theories. The investigation was made at a Mach number of 2.91 and a test-section unit Reynolds number of about 0.400×10^6 per inch.

This report includes an appendix by Eugene S. Love, of the Langley Research Center, which presents the derivation of a five-term approximation of the pressure coefficient on a flat plate for angles of attack from 0° to 90°.

SYMBOLS

A,B,C,... coefficients in series (see appendix)

C_p pressure coefficient, $\dfrac{p - p_\infty}{\frac{\gamma}{2} M_\infty{}^2 p_\infty}$

$C_{p,min} = -\frac{1}{M_\infty^2}$

l	surface distance measured from wing apex along leading edge in chord plane (fig. 1(a))
M	Mach number
n	exponent in series $(n = 2)$
p	pressure
R	Reynolds number
r	wing leading-edge radius
s	surface distance measured normal to leading edge and referenced from intersection of leading edge and chord plane (fig. 1(a))
s'	modified surface distance measured normal to leading edge (see sketch 1)
t	wing thickness
α	angle of attack, deg
γ	ratio of specific heats, 1.40
δ	flow deflection angle, deg
Λ	sweep angle, deg

L1552

$$\xi = \frac{C_p - C_{p,min}}{C_{p,max} - C_{p,min}}$$

Subscripts:

min	minimum
e	effective
max	stagnation conditions behind normal shock
t	based on wing thickness
α	property at angle of attack
∞	free-stream conditions

APPARATUS AND MODELS

Wind Tunnel

The investigation was conducted in the Langley 9-inch supersonic tunnel (now deactivated). This tunnel is a continuous operation, closed-return type of tunnel with provisions for the control of the humidity, temperature, and pressure of the enclosed air. The test Mach number is achieved with fixed nozzle blocks forming a test section approximately 9 inches square. Eleven fine-mesh screens in the rela- L
tively large settling chamber ahead of the nozzle aid in keeping the 1
turbulence in the tunnel test section at a low level. During the tests 5
the quantity of water vapor in the tunnel air was kept sufficiently low 5
so that the effects of water condensation in the supersonic nozzle were 2
negligible.

Models

The geometric characteristics and dimensional details of the wing models tested in the investigation are presented in figure 1. The slab wings had delta planforms and the nose and wing tips were rounded. Two basic series of models were constructed, along with several special-purpose models. One basic series had square leading edges, and the other basic series of models had round leading edges. The apexes of the round-leading-edge models were tangent spheres with the same diameters as the cylinders forming the leading edges. In each of the basic series there were five models of different leading-edge sweep ($\Lambda = 80^\circ$, 75°, 70°, 60°, and 50°). The basic square-leading-edge models were designated 1A, 2A, 3A, 4A, and 5A, and the basic round-leading-edge models were designated 1B, 2B, 3B, 4B, and 5B, with the numerical designations corresponding, respectively, to sweep angles of 80°, 75°, 70°, 60°, and 50°. The basic models are shown in figures 1(a) and 1(b), and at the top of figure 1(c). The special-purpose models, designated 2AA, 2BB, 2Ⓑ, 3Ⓑ, and 33B are shown at the bottom of figure 1(c) and in figure 1(d). Models 2AA and 2BB (fig. 1(c), bottom) were geometrically similar in planform and leading-edge shapes to the basic models 2A and 2B, respectively, except that they had absolute thicknesses of only one-half those of the basic models. Models 2Ⓑ and 3Ⓑ (fig. 1(d), top) were constructed to represent the enlarged nose sections of models 2B and 3B, respectively. The dashed lines in the planform views of models 2B and 3B, figures 1(a) and 1(b), respectively, indicate the portions of the nose of the basic models represented by the enlarged-nose-section models (models 2Ⓑ and 3Ⓑ, fig. 1(d)).

Model 33B (fig. 1(d), bottom) was specifically constructed to be tested at $\alpha = 0^\circ$ to 45°, only. Differences between this model and model 3B were in the arrangement for the sting support, the exiting of the pressure tubes from the model, and the absolute size.

The pressure-orifice stations on the various models are shown in figure 1, and the location of the individual orifices on the models are given in table I. All models were instrumented with 0.030-inch-diameter orifices.

L1552

The models were linked to the tunnel angle-of-attack sector by means of a wing support strut which was attached to the leeward sides of the models, as shown in figure 2. Mirrors approximately 1/16 inch in diameter were flush mounted in the base of the strut (fig. 2(b)) and formed a part of the optical angle-of-attack system. (The specific model shown in fig. 2, though typical of those in the program, was not included in the tests.)

TESTS

All tests reported herein were conducted at a free-stream Mach number of 2.91 and at an average test-section unit Reynolds number of 0.400×10^6 per inch.

The pressure coefficients as obtained on the models are given in table I. All pressure data were manually read from a multiple-tube mercury manometer.

The wing support struts of 1/4-inch-diameter cold-rolled steel connected the models to the angle-of-attack sector of the wind tunnel. As the absolute range of the sector was only 25°, two bent wing struts were used in combination with the angle-of-attack sector to obtain the principal test angle-of-attack range from 45° to 90°. Model 33B, tested at $\alpha = 0^\circ$ to 45°, used one sting which was straight and subsequently was bent to obtain the test angles of attack.

PRECISION OF DATA

Tunnel calibration surveys have indicated that the test-section Mach number in the region occupied by the models was 2.91 ± 0.01.

The initial referencing of the angle of attack of each model with respect to stream direction was performed to an accuracy of about $\pm 0.05^\circ$. Relative angle-of-attack settings during a given test were $\pm 0.01^\circ$. Individual pressure coefficients were usually accurate to less than ± 0.01.

RESULTS AND DISCUSSION

Basic Presentation

General.- The pressures measured on the models used in the investigation have been reduced to standard pressure-coefficient form and are given in table I. The pressure-distribution results shown in the figures are generally presented in terms of the pressure-ratio parameter p/p_{max} where p/p_{max} is defined as follows:

L1552

$$\frac{p}{p_{max}} = \frac{C_p}{C_{p,max}} + \frac{p_\infty}{p_{max}}\left(1 - \frac{C_p}{C_{p,max}}\right) \tag{1}$$

For tests at $M_\infty = 2.91$,

$$C_{p,max} = 1.75$$

The schlieren photographs of the test models are presented in figure 3. The data of figure 4 show that the technique of constructing an oversize nose section of a model to represent a particular part of a smaller model is valid. The validity is proved by the excellent comparison of pressures measured at the same nondimensional stations on both models.

Fundamental characteristics of pressure distributions ($\alpha = 0^\circ$ to 90°).- The data obtained in the angle-of-attack range from 0° to 35° on model 33B ($\Lambda = 70^\circ$) are shown in figure 5. This round-leading-edge configuration was the only configuration tested at angles of attack less than 45°.

A fundamental characteristic of the pressure distributions in this angle-of-attack range (neglecting the pressures on the nose cap at station $l/t = 0$) is that the pressures are constant over both the windward and leeward wing surfaces at a given angle of attack. The pressures become constant on the windward side of the wing at about the windward shoulder location ($s/t = 0.785$) at all l/t stations shown and remain constant with further increase in s/t. The level of this pressure in terms of p/p_{max} varies with angle of attack as would be expected. The schlieren photographs of figure 3(f) include a side view of model 3B (similar to model 33B) at $\alpha = 45^\circ$ which shows that the bow shock wave is essentially straight. Therefore, the constant pressure over the windward surface is as might be expected for the angles of attack shown in figure 5, which are equal to or less than 35°.

The leeward wing pressures $\left(\text{generally at } \frac{s}{t} \leqq -0.785\right)$ decrease with increase in angle of attack until $\alpha = 20^{\circ}$ is reached; thereafter, the pressures show negligible variation with further increase in angle of attack. This constant pressure level is consistent with the results reported in reference 12, which show that the pressures on the upper surfaces of wings at high angles of attack approach a limiting value defined approximately by $C_{p,min} = -\frac{1}{M_\infty^{\ 2}}$. The value of p/p_{max} equivalent to $C_{p,min} = -\frac{1}{M_\infty^{\ 2}}$ at $M_\infty = 2.91$ is 0.0289. The measured leeward wing surface pressures shown in figure 5 show good agreement with this value.

L1552

The pressures shown in figure 6 were obtained from three geometrically similar round-leading-edge wings each with a sweep angle of 75°. The nondimensionalized pressures p/p_{max} along different wing contours for a constant s/t location are shown. The small sketches show the location of the wing contour relative to the wing leading edge. The values of l/t from 0 to 0.655 are on the nose cap. Figure 6 illustrates that in the angle-of-attack range from 45° to 90° there are large negative pressure gradients on the windward wing surfaces, as contrasted with the angle-of-attack range from 0° to 35°. The schlieren photographs of figure 3 at angles of attack between 45° and 90° show that a strong curved bow shock is produced and consequently strong entropy and pressure gradients must exist in the flow. For the wing contour shown farthest inboard ($s/t = 1.13$), the pressure gradients approach small values $\frac{d\left(p/p_{max}\right)}{d(l/t)} \approx -0.003$ for the lowest and highest angles of attack shown ($\alpha = 45^{\circ}$ and 90°). The higher angle-of-attack data ($\alpha = 90^{\circ}$) are consistent with results shown in references 8 and 11 wherein a method based on three-dimensional cross flow is developed to treat theoretically the case for $\alpha = 90^{\circ}$ where it is shown that at hypersonic speeds the isobars on a delta wing of 70° sweep at $\alpha = 90^{\circ}$ are essentially parallel to the wing edges, that is, independent of l/t.

The steep pressure gradients on the windward wing surfaces for $l/t < 1$ are in the immediate nose region of the wings and are most evident at $\alpha \leqq 60^{\circ}$.

Figure 7 presents pressure distributions normal to the leading edge obtained on typical round-leading-edge models of this investigation through the angle-of-attack range from 0° to 90°. The data shown in this figure were obtained from models 3B and 33B. It is seen that the pressure distributions for the two stations at $l/t = 1.90$ and 4.56 (figs. 7(a) and 7(b)) are qualitatively similar at all angles of attack; however, for angles of attack greater than 45° a slightly different level of pressure is discernible for the two stations. (This effect was previously seen in fig. 6.)

Pressure distributions on nose cap.- Figure 8 shows the variation of pressures around the nose cap of two typical round-leading-edge wings through the angle-of-attack range from 45° to 90°. The models used to obtain these data (models 2(B) and 3(B)) represent the enlarged nose regions of the basic models 2B and 3B. Four pressure-measuring stations at different l/t values are shown in the figure. Three of the stations were on the nose cap, including one at the model plane of symmetry
($l/t = 0$) and one at the point of tangency of the nose cap and the wing L
leading edge ($l/t = 0.61$ or 0.66). The stations at $l/t = 1.90$ and 1
$l/t = 2.11$ were normal to the wing leading edge, but downstream of the 5
wing-nose—leading-edge juncture. Figure 8 shows that the stations on 5
the nose cap and the stations which are normal to the wing leading edge 2
have pressure distributions which are different at $\alpha \leqq 60°$. The nose-cap pressure distributions are characterized by a peaking of the pressures, similar to that observed on curved, blunt shapes. (See, for example, refs. 13 and 14.) The pressures on the nose cap and those normal to the wing leading edge show much less variation with l/t above $\alpha = 60°$ than below $\alpha = 60°$. It is also apparent that the characteristic pressure distributions around the nose cap of the wings lose their identity above an angle of attack of 60° and assume distributions typical of those normal to the leading edge.

Pressures on basic models.- The pressure distributions obtained over the basic A- and B-series models of this investigation are presented in figures 9 and 10, respectively. The pressures are shown in the form of p/p_{max} plotted against orifice location s/t for three pressure-measuring stations (l/t values) normal to the wing leading edges. Included in these figures are the schlieren photographs of the wings taken during the actual pressure-distribution test. In figure 9, which shows pressure distributions over the square-leading-edge models (basic A-series), the pressure distributions have discontinuities at the corners of the front face, as might be expected $\left(-0.5 \leqq \frac{s}{t} \leqq 0.5\right)$. The gradients in the pressure distributions over the front face are associated with an overexpansion of the flow around the lower-surface sharp corner of the wing leading edge, followed by a flow recompression on the leading-edge face, and thence an expansion around the upper-surface corner of the leading edge to a constant pressure on the leeward side of the wings. These pressure variations on the flat face are most evident on the models of least leading-edge sweep at angles of attack of 45° to 60° where the local Mach number is highest (figs. 9(c) to 9(e)). The pressure distributions at the three different l/t stations appear essentially independent of l/t location at the lowest and highest angles of attack shown (45° and 90°). This effect can also be observed in figure 11 which shows supplementary pressure distributions obtained on geometrically similar, but thinner, models of the 2A and 2B configurations for extended l/t values. In the intermediate angle-of-attack range the pressures exhibit a decrease with an increase in l/t along the wing leading edge caused by pressure bleed-off effects within the shock envelope.

Pressure distributions on the basic B-series (round-leading-edge) models (fig. 10) are smooth and without irregularities at all angles of attack in contrast to those obtained on the square-leading-edge wings. The effect of changing the location of the pressure-measuring stations (different values of l/t) is greater for the pressure distributions at intermediate angles of attack between 45° and 90°.

Effect of Leading-Edge Shape

Figure 12 is presented to show a direct comparison of the pressure distributions over the A- and B-series wings (that is, square and round leading edges) at selected angles of attack and at several l/t stations on the wings. The purpose of testing and evaluating the pressure distributions over the square-leading-edge wings was primarily to assess leading-edge-shape effects on wing pressures but not with the view that these types of wings would be used in practical applications. The Reynolds number based on leading-edge thickness is about $R_{\infty,t} = 1.5 \times 10^5$ for these wings.

Significant differences in the pressure distributions over the square- and round-leading-edge wings (A- and B-series models, respectively) appear in the immediate leading-edge regions of the wings, that is, in the regions defined by $-0.5 \leqq \frac{s}{t} \leqq 0.5$ and $-0.785 \leqq \frac{s}{t} \leqq 0.785$ for the square- and round-leading-edge wings, respectively. But farther inboard there is little difference between pressure distributions for the wings. These observations appear valid over the angle-of-attack range from 45° to 90°, l/t range, and sweep-angle range of this investigation.

Effect of Angle of Attack

Figures 13 and 14 present the pressure distributions over the square- and round-leading-edge wings (basic A- and B-series models), respectively, and show the effects of angle of attack on the wing pressures for several l/t values. The general effects of angle of attack on pressures over both the A-series and B-series models, as shown in the figures, are as would be expected; however, some pertinent details concerning the pressure distributions should be pointed out. It is noted that for the basic A-series models (fig. 13) the angle-of-attack effects (increase in windward pressure with increase in angle of attack) are most evident in the angle-of-attack range from 45° to 70° and for all sweep angles. Any further increase in angle of attack results in only a small percentage increase in the wing pressures (generally less than 10 percent at $\alpha = 90^\circ$) over those at $\alpha = 70^\circ$. This observation is true at all sweep angles. It is also seen that the overall increase in wing pressures over the angle-of-attack range is greatest for the wing with the largest sweep angle, and least for the wing of lowest sweep angle. (Cf. figs. 13(a) and 13(e).) The difference is attributable to the lower pressure on the wing of largest sweep at $\alpha = 45^\circ$ and essentially the same pressures on all the wings at $\alpha = 90^\circ$. The leading-edge surfaces of the wings experience angle-of-attack effects when the sweep angles are about 70° or less; however, these effects are seen to be opposite in nature to those experienced on the windward surfaces. (See figs. 13(c) and 13(e).) These counter effects can be ascribed, intuitively, to the geometry of the wing leading edge (or face of the wing) and its angle of exposure to the local flow direction. For example, at $\alpha = 90^\circ$ the flow would be expected to be generally parallel to the leading-edge face of the wing (angle of exposure about zero), and consequently the face pressures would be essentially negligible. Figures 13 and 14 show that, with an increase in l/t, the increase in windward surface pressures with increase in angle of attack appears to tend toward a more linear variation.

L
1
5
5
2

Effect of Wing Sweep

The effects of leading-edge sweep angle on the pressure distributions over the round-leading-edge (or series B) models are shown in figure 15 for a range of angles of attack. Although a small spread of l/t values is included in the data, l/t does not significantly affect the comparisons shown, and the conclusions drawn from these data are believed to be general. The major effect of leading-edge sweep angle, that is, decrease of pressures on the wing windward slab surface with increase in sweep angle, is usually confined to angles of attack from 45° to less than 60°. At angles of attack of 60° and greater the effects of sweep become small. The effects of sweep are negligible on the leeward surface pressures of the wings (that is, for $s/t < 0$). Also it is seen that the effects of sweep are similar for the three ranges of l/t locations shown in figure 15.

Prediction of Wing Pressures

Chordwise center-line pressures.- Figure 16 presents a compilation of the asymptotic value of the experimental pressures obtained on the windward chordwise center line of delta wings of various sweep angles in the Mach number range from 2.91 to 22 (present data, refs. 6, 8, 9, 11, and 15, and unpublished data from the Langley 11-inch hypersonic tunnel). The pressure-coefficient ratio shown as the ordinate scale of figure 16 represents the measured pressure coefficient on the wing at the angle of attack normalized by the stagnation pressure coefficient behind a normal shock. (Individual data points are normalized by the value of $C_{p,max}$ applicable to the specific test Mach number of the data.) Shown also are various theoretical curves (A to D) which are compared with the experimental data.

A five-term hypersonic approximation of the pressure coefficient on a flat plate for angles of attack from 0° to 90° is derived in the appendix. The results of this work are shown as curve A in figure 16. (Especially note that curve A extends throughout the range $\alpha = 0^{\circ}$ to 90° and that it is coincident with the oblique-shock theory $M_{\infty} = \infty$ (curve B) at $\alpha \lessapprox 40^{\circ}$.) Curve A on the basis of its derivation should represent the pressures on a moderately swept flat plate for hypersonic Mach numbers. Curve C ($\sin^2\alpha$), or the familiar modified Newtonian theory, defines a lower limit for the pressure data and represents the case for an infinite cylinder which can be considered as a delta wing with $\Lambda = 90^{\circ}$. Experimental confirmation of this theory has been obtained many times; for comparison in this figure the experimental work of reference 6 for the pressures on the windward meridian of a semi-infinite cylinder is shown. Excellent agreement between the $\sin^2\alpha$ curve and the experimental data is evident. It is seen that the trend of the data for increasing sweep angle (at a constant angle of attack) follows the trends established by the two theoretical cases of moderate sweep (curve A) and $\Lambda = 90^{\circ}$ (curve C). The exact oblique-shock theory for $M_{\infty} = \infty$ (ref. 16), curve B, gives good prediction of the wing pressures up to $\alpha \approx 40^{\circ}$, at all the test Mach numbers shown; this prediction agrees with the experimental results of the present investigation better than oblique-shock theory for $M = 2.91$ (ref. 16), curve D. Curves A and C generally bracket the experimental pressures in the angle-of-attack range from 0° to 90°.

L1552

<u>Pressures normal to leading edge</u>.- Figure 17 shows pressure distributions normal to the wing leading edges of the basic round-leading-edge models at angles of attack and the results of a method which attempts to predict these pressures. The ordinate scale is defined as

$$\xi = \frac{C_p - C_{p,min}}{C_{p,max} - C_{p,min}}$$

where

C_p measured wing pressure coefficient

$C_{p,max}$ stagnation pressure coefficient behind normal shock

$C_{p,min} = -\dfrac{1}{M_\infty^2}$

It should be pointed out that the maximum limit (which is 1) of the pressure parameter ξ corresponds to a measured wing pressure coefficient which is equal to the stagnation pressure coefficient behind a normal shock. The minimum limit (which is 0) of ξ corresponds, on the other hand, to a measured wing pressure coefficient of $-1/M_\infty^2$. The explanation of the abscissa s'/r, used in figure 17, is as follows: In reference 17 an analysis relating to the equivalent two-dimensional flow on an infinite sweptback wing at α is presented. The primary interest in this analysis concerns the direction of the flow defined by the angle α_e in part (c) of figure 18.6 of reference 17 and shown in sketch 1 relative to the blunt leading edge of the round-leading-edge delta wings of this investigation as follows:

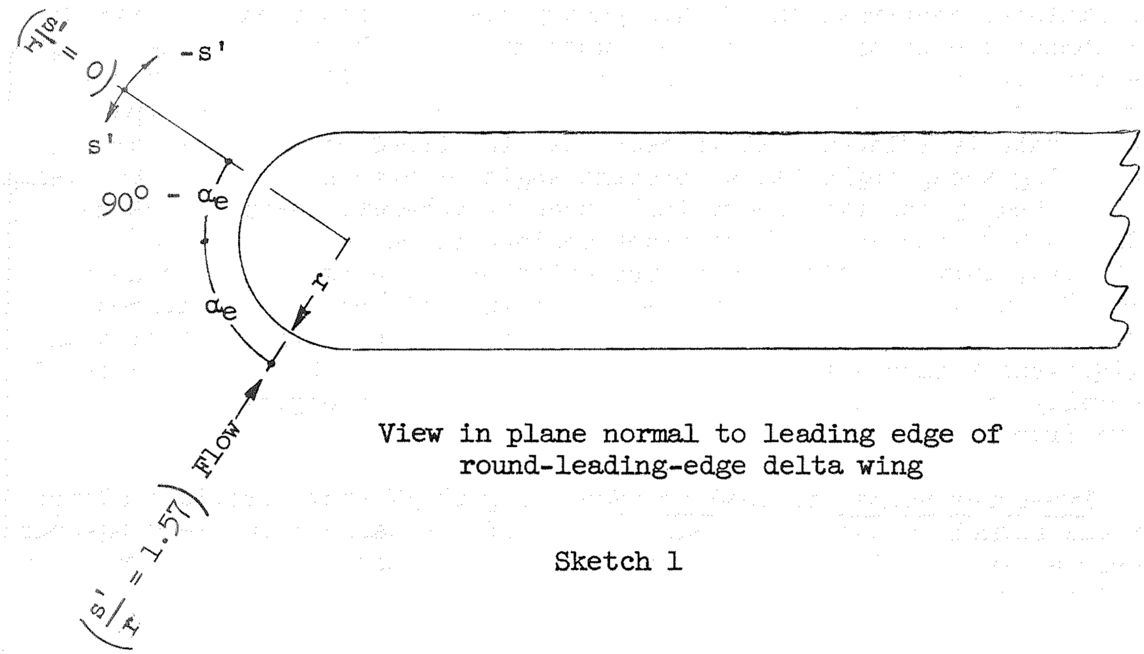

View in plane normal to leading edge of
round-leading-edge delta wing

Sketch 1

As illustrated in sketch 1, the origin of s' is defined as 90° away from the indicated flow direction and toward the leeward side of the wing. Thus, at $s' = 0$ (the tangency point of the flow direction and wing surface) the pressure coefficient would be zero for Newtonian flow. The flow direction angle α_e is given by (ref. 17)

$$\alpha_e = \arc\tan \frac{\tan \alpha}{\cos \Lambda}$$

Therefore, the origin of s' is a function of α and Λ, and these wing variables are considered in the following wing pressure prediction method.

The formulation of the expressions $A \sin^2 \frac{s'}{r}$ and $C \sin^2 \frac{s'}{r}$ (shown in fig. 17) is an outgrowth of the preceding discussion to define s', and the fact that the A and C curves of figure 16 represent an approximation to the upper and lower limit, respectively, of the pressures obtained on the windward slab surface of moderately to highly swept delta wings. (See fig. 16 and attendant discussion.) The constants A and C represent the values of ξ as obtained from curves A and C for specific angles of attack. The parameter $\sin^2 \frac{s'}{r}$ is commonly used when plotting pressures on cylindrical and spherical noses of bodies in supersonic and/or hypersonic flow where the pressures follow, in general, a sine-square-law type of variation. (See refs. 14 and 18.) When $\frac{s'}{r} = 1.57$ radians maximum pressure is supposedly realized on the wings, and the expressions reduce to the values of ξ indicated by the constants A and C. $\left(\sin^2 \frac{s'}{r} = 1 \text{ at } \frac{s'}{r} = 1.57 \text{ radians.}\right)$

The application of the expressions obtained from the concepts of sweepback theory and hypersonic considerations are shown in figure 17 for a range of sweep angles and angles of attack. The experimental data shown in figure 17 were obtained in the present investigation ($M_\infty = 2.91$). The expressions predict the trends of the pressure variations very well and generally predict the wing pressures in the forward regions of the wings best, that is, for small l/t values as would be expected. At downstream stations (increasing l/t values) the actual pressures deviate in varying extent from the predicted pressures. Further theoretical and experimental analyses are needed to define the mechanism of the pressure loss with increase in l/t values in order to permit more accurate predictions of the wing pressures. It is believed, however, that because of their simplicity the present expressions will prove extremely useful for obtaining approximate values of the pressures.

CONCLUSIONS

An investigation was made at a Mach number of 2.91 to determine the pressure-distribution characteristics over a family of square- and round-leading-edge delta wings at angles of attack up to 90° and sweep angles from 50° to 80°. The results of the investigation indicate the following conclusions:

1. In the range of angles of attack from 45° to 90° the effect of leading-edge shape on the pressure distributions over the wing models is confined primarily to the leading-edge surfaces.

2. The major effect of leading-edge sweep, that is, decrease of pressures over the wings, is generally confined to angles of attack of less than 60°.

3. The windward pressures on the slab surfaces of the wings are essentially constant for angles of attack less than 45°; at greater angles of attack, the strong, curved bow shocks created by the wings produce significant negative pressure gradients over the wing surface.

4. Pressures on the leeward wing surfaces are invariant with angle of attack above 20° and are essentially equal to the value given by the empirical base pressure coefficient, $C_p = -\frac{1}{M_\infty^2}$, where C_p is the pressure coefficient and M_∞ is free-stream Mach number.

L 1 5 5 2

5. Compilation of center-line slab-surface pressures, normalized by the stagnation pressure behind a normal shock, for angles of attack from 0° to 90° and at Mach numbers from 2.91 to 22 shows that oblique-shock theory at a Mach number of ∞ predicts pressures up to about an angle of attack of 40°. In the angle-of-attack range from 0° to 90°, the experimental hypersonic maximum center-line pressures are generally bracketed by a hypersonic series approximation corresponding to moderate sweep and a modified Newtonian prediction corresponding to 90° sweep.

6. An expression related to sweep theory and the impact theory is shown to give a fair prediction of the wing pressures in planes normal to the leading edge for a wide range of angles of attack and sweep angles.

7. Characteristic pressure distributions around the nose cap of the wings lose their identity above an angle of attack of 60° and assume distributions typical of those normal to the leading edge.

Langley Research Center,
National Aeronautics and Space Administration,
Langley Air Force Base, Va., October 24, 1961.

APPENDIX

HYPERSONIC APPROXIMATION OF THE PRESSURE COEFFICIENT ON A FLAT PLATE FOR ANGLES OF ATTACK FROM 0° TO 90°

By Eugene S. Love

L1552

The adequacy of various hypersonic approximations and modification of Newtonian theory in the prediction of the pressure coefficient C_p on a flat plate for $0^\circ \leqq \delta \leqq 90^\circ$ has been examined by several authors (e.g., refs. 19, 6, 18, and 20). In particular, the case considered here is the plate that remains essentially two dimensional through nearly all of the attached shock regime, but because of edge losses and effects associated with finite aspect ratio, departs significantly from two-dimensionality as the detachment angle is closely approached. (Note: If two-dimensionality can be maintained up to detachment angle, the pressure coefficient should rise immediately to the normal shock value when the angle for shock detachment is exceeded.) For this case no method exists at present that is satisfactory over the entire range of δ except for a value of the ratio of specific heats γ of unity. In the attached shock regime the approximation

$$C_p = (\gamma + 1)\sin^2\delta \tag{A1}$$

is known to give good results except for values of δ near shock detachment and for not too weak shocks (refs. 19 and 20). Similarly, for the normal shock regime the approximation,

$$C_p = \left(\frac{\gamma + 3}{\gamma + 1}\right)\sin^2\delta \tag{A2}$$

is known to give good results within certain restrictions on its application. Both of these expressions (eqs. (A1) and (A2)) reduce to the exact solution for $M_\infty = \infty$ when $\gamma = 1$, and they resolve into the single continuous solution that is desired only when $\gamma = 1$.

In an attempt to derive a satisfactory continuous solution for $1 \leqq \gamma \leqq \frac{5}{3}$, a series expression has been assumed for C_p. The series chosen here is

$$C_p = A \sin^n\delta + B \sin^{2n}\delta + C \sin^{3n}\delta + \ldots \tag{A3}$$

Consider the first term only. By analogy to exact theory, the value of n is taken as 2; thus, the exponents of the terms of the series are known. It is also recognized that the coefficient A is analogous to the coefficients in the various forms of modified Newtonian theory as exemplified in equations (A1) and (A2) and the values of A given in the following table (the better known designations of the modified forms are underlined):

A	A for $\gamma = 7/5$	Designation of theory
2	2	Simple Newtonian, exact shock for $M_\infty = \infty$, $\gamma = 1$
$\gamma + 1$	2.4	Flat-plate modified or oblique shock
$\frac{\gamma + 3}{\gamma + 1}$	1.833	Blunt-nose modified or normal shock
$\frac{2(\gamma + 1)(\gamma + 7)}{(\gamma + 3)^2}$	2.083	Cone modified

L1552

Since the case under consideration here assumes two-dimensionality over nearly all of the attached shock regime, the first condition imposed is that $A = \gamma + 1$. The values of the coefficients for the other terms are dependent on the approach taken and the number of terms retained in the series. The first attempt was made with a three-term series with the additional conditions that $C_{p,max}$ occurs at $\delta = 90^\circ$, and, at $\delta = 90^\circ$, $C_p = \frac{\gamma + 3}{\gamma + 1}$ and $\frac{dC_p}{d\delta} = 0$. The resulting three-term approximation is

$$C_p = (\gamma + 1)\sin^2\delta - \frac{2\gamma^2 + \gamma - 7}{\gamma + 1}\sin^4\delta + \frac{\gamma^2 - 5}{\gamma + 1}\sin^6\delta \qquad \text{(A4)}$$

The predictions given by this equation are compared in figure 18 with exact results at $M = \infty$ for several values of γ. In the attached shock regime this three-term approximation appears to give its best prediction for γ near 7/5 but is less satisfactory at higher values of γ and becomes notably in error at $\gamma = 1$ where it may be assessed over the entire range.

In view of these deficiencies at the extreme values of γ, a five-term approximation was developed. The attempt was made to impose the same conditions as in the three-term development plus the requirement of agreeing with exact theory at $\gamma = 1$. The resulting five-term approximation is

$$C_p = (\gamma + 1)\sin^2\delta + \frac{(\gamma + 3)(\gamma - 1)\sin^4\delta}{\gamma + 1} - \frac{(2\gamma + 5)(\gamma - 1)}{\gamma + 1}\sin^6\delta$$

$$- \frac{\gamma^3(\gamma - 1)}{\gamma + 1}\sin^8\delta + \frac{\gamma^3(\gamma - 1)}{\gamma + 1}\sin^{10}\delta \qquad \text{(A5)}$$

The predictions given by this equation are also shown in figure 18 and are seen to be in excellent agreement with exact oblique-shock theory at all values of γ except near shock detachment. Although not observable in the figure, when $\gamma = 5/3$, equation (A5) gives values of C_p near $\delta = 80^\circ$ that are in excess of $\frac{\gamma + 3}{\gamma + 1}$ but by such a small amount as to be unimportant (the excess is about one-tenth of one percent). Thus, for all practical purposes equation (A5) may be said to satisfy the conditions set forth for $1 \leqq \gamma \leqq \frac{5}{3}$. (It may be noted that for $\gamma = 7/5$ there is little difference between the predictions given by eqs. (A4) and (A5); it may also be shown that for $\gamma = 7/5$ the first three terms of eq. (A5) give a prediction in very close agreement with that from eq. (A4).)

There are few experimental data with which to assess properly equation (A5) primarily because the case considered here assumes a condition of two-dimensionality for values of δ over most of the attached shock regime. Nevertheless, the adequacy of the prediction may be determined from the fair amount of experimental data that have been obtained on delta wings of varying sweep by noting that for such wings the case treated here corresponds to moderate sweep. Consequently, for $M_\infty \gg 1$ the asymptotic downstream value of C_p on the chordwise center line of all moderately to highly swept delta wings should fall between an upper limit as given by equation (A5) and a lower limit as given by equation (A2). The lower limit is established by the fact that the flow conditions inferred by equation (A2) are closely realized on the windward meridian of a semi-infinite circular cylinder as it proceeds through angle of attack; the experimental studies of reference 6 confirm this. The semi-infinite cylinder may for the present purpose thus be regarded as a round-leading-edge delta wing with 90° sweep.

Figure 16 shows that most of the available hypersonic results for moderately to highly swept delta wings do indeed fall between the limits given by the normalized form of equation (A5) for moderate sweep (curve A) and equation (A2) for $\Lambda = 90^\circ$ (curve C). Equation (A5), curve A, appears generally suitable over the entire range of δ for use in design studies that do not involve either very low or very high sweep angles.

REFERENCES

1. Armstrong, William O., Stainback, P. Calvin, and McLellan, Charles H.: The Aerodynamic-Force and Heat-Transfer Characteristics of Lifting Reentry Bodies. NASA TM X-352, 1960.

2. Phillips, William H.: Research on Blunt-Faced Entry Configurations at Angles of Attack Between 60° and 90°. NASA TM X-315, 1960.

3. Clark, Frank L., and Evans, Joanna M.: Some Aerodynamic and Control Studies of Lifting Reentry Configurations at Angles of Attack up to 90° at a Mach Number of 2.91. NASA TM X-338, 1960.

4. Grimaud, John E.: Wind-Tunnel Investigation at a Mach Number of 2.91 of Stability and Control Characteristics of Three Lifting Reentry Configurations at Angles of Attack up to 90°. NASA TM X-455, 1961.

5. Penland, Jim A., and Armstrong, William O.: Static Longitudinal Aerodynamic Characteristics of Several Wing and Blunt-Body Shapes Applicable for Use as Reentry Configurations at a Mach Number of 6.8 and Angles of Attack up to 90°. NASA TM X-65, 1959.

6. Penland, Jim A.: Aerodynamic Characteristics of a Circular Cylinder at Mach Number 6.86 and Angles of Attack up to 90°. NACA TN 3861, 1957. (Supersedes NACA RM L54A14.)

7. Amick, James L.: Pressure Measurements on Sharp and Blunt 5°- and 15°-Half-Angle Cones at Mach Number 3.86 and Angles of Attack to 100°. NASA TN D-753, 1961.

8. Bertram, Mitchel H., Feller, William V., and Dunavant, James C.: Flow Fields, Pressure Distributions, and Heat Transfer for Delta Wings at Hypersonic Speeds. NASA TM X-316, 1960.

9. Lindsay, E. Earl, and Rippey, James O.: Pressure Distribution and Heat Transfer Test on FSL-WADD Delta Wing Configurations at Mach Number 8 - Phase I. AEDC-TN-60-203 (Contract No. AF40(600)-800 S/A 11(60-110)), Arnold Eng. Dev. Center, Oct. 1960.

10. Close, William H.: Hypersonic Longitudinal Trim, Stability, and Control Characteristics of a Delta-Wing Configuration at High Angles of Attack. NASA TM X-240, 1960.

11. Bertram, Mitchel H., and Henderson, Arthur, Jr.: Recent Hypersonic Studies of Wings and Bodies. ARS Jour., vol. 31, no. 8, Aug. 1961, pp. 1129-1139.

L
1
5
5
2

12. Mayer, John P.: A Limit Pressure Coefficient and an Estimation of Limit Forces on Airfoils at Supersonic Speeds. NACA RM L8F23, 1948.

13. Gunn, Charles R.: Pressure Measurements on the Apexes of Two 60° Sweptback Delta Wings (Panel Semi-Apex Angle of 30°) Having 0° and 45° Dihedral at a Mach Number of 4.95. NASA TM X-421, 1961.

14. Oliver, Robert E.: An Experimental Investigation of Flow Over Simple Blunt Bodies at a Nominal Mach Number of 5.8. GALCIT Memo. No. 26 (Contract No. DA-04-495-Ord-19), June 1, 1955.

15. Wallace, A. R., and Swain, W. N.: Pressure Distribution Tests on a 60-Deg and 70-Deg Delta Wing at Mach Numbers of 20 to 22. AEDC-TN-61-14 (Contract No. AF 40(600)-800 S/A 11(60-110)), Arnold Eng. Dev. Center, Feb. 1961.

16. Ames Research Staff: Equations, Tables, and Charts for Compressible Flow. NACA Rep. 1135, 1953. (Supersedes NACA TN 1428.)

17. Shapiro, Ascher, H.: The Dynamics and Thermodynamics of Compressible Fluid Flow. Vol. II. The Ronald Press Co., c.1954, p. 710.

18. Lees, Lester: Hypersonic Flow. Fifth International Aeronautical Conference (Los Angeles, Calif., June 20-23, 1955), Inst. Aero. Sci., Inc., 1955, pp. 241-276.

19. Laitone, Edmund V.: Exact and Approximate Solutions of Two-Dimensional Oblique Shock Flow. Jour. Aero. Sci., vol. 14, no. 1, Jan. 1947, pp. 25-41.

20. Love, Eugene S., Henderson, Arthur, Jr., and Bertram, Mitchel H.: Some Aspects of Air-Helium Simulation and Hypersonic Approximations. NASA TN D-49, 1959.

[redacted]

TABLE I.- ORIFICE LOCATION DETAIL AND TABULATION OF PRESSURE COEFFICIENTS FOR TEST MODELS

(a) Models 1A and 1B

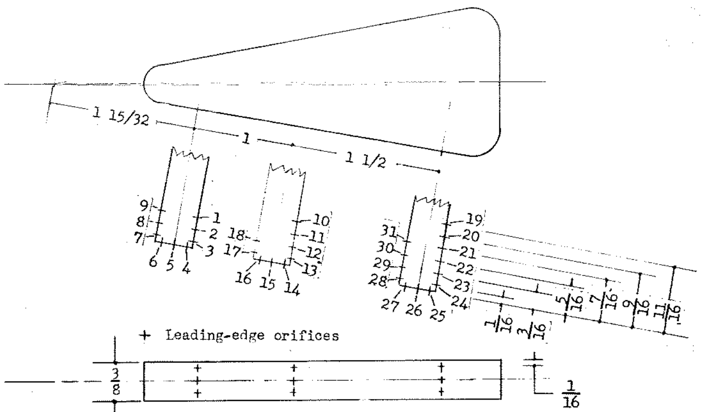

Model 1A

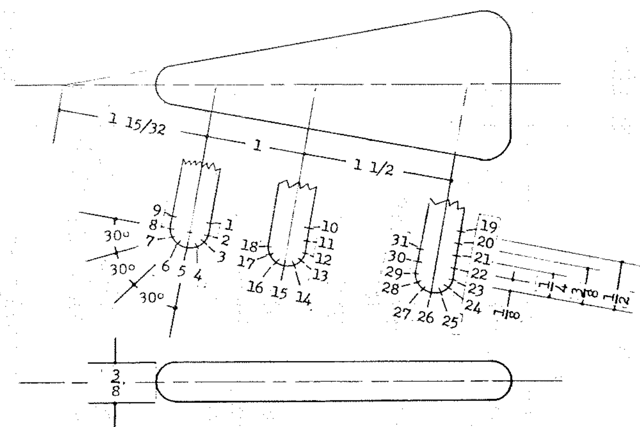

Model 1B

Model 1A

Orifice	Pressure Coefficient, C_p					
	α = 45°	α = 51°	α = 60°	α = 70°	α = 80°	α = 90°
1	1.044	1.231	1.477	1.678	1.742	1.702
2	1.039	1.224	1.467	1.667	1.736	1.686
3	.986	1.158	1.379	1.556	1.608	1.555
4	-.040	-.045	-.054	-.085	-.095	-.111
5	.035	-.003	-.046	-.080	-.086	-.103
6	.125	.099	.019	-.018	-.035	-.068
7	-.132	-.136	-.136	-.113	-.119	-.117
8	-.132	-.136	-.136	-.114	-.119	-.117
9	-.132	-.136	-.134	-.118	-.119	-.117
10	1.032	1.227	1.474	1.664	1.739	1.744
11	1.027	1.221	1.464	1.653	1.724	1.727
12	1.009	1.195	1.429	1.611	1.675	1.674
13	.932	1.097	1.305	1.469	1.521	1.512
14	-.077	-.071	-.083	-.101	-.111	-.120
15	-.066	-.069	-.083	-.104	-.112	-.120
16	.028	.012	-.029	-.077	-.088	-.108
17	-.114	-.116	-.118	-.113	-.116	-.116
18	-.116	-.115	-.118	-.107	-.114	-.115
19	1.029	1.205	1.377	1.514	1.615	1.694
20	1.026	1.204	1.380	1.515	1.621	1.695
21	1.021	1.196	1.375	1.514	1.614	1.686
22	1.008	1.178	1.358	1.496	1.595	1.664
23	.978	1.142	1.317	1.453	1.549	1.609
24	.882	1.029	1.187	1.309	1.397	1.446
25	-.099	-.103	-.112	-.116	-.120	-.119
26	-.099	-.101	-.109	-.122	-.118	-.118
27	-.059	-.070	-.092	-.110	-.114	-.115
28	-.117	-.117	-.117	-.108	-.110	-.109
29	-.116	-.117	-.116	-.110	-.110	-.109
30	-.117	-.117	-.116	-.109	-.111	-.109
31	-.117	-.117	-.116	-.109	-.110	-.109

Model 1B

Orifice	Pressure Coefficient, C_p					
	α = 45°	α = 51°	α = 60°	α = 70°	α = 80°	α = 90°
1	—	—	—	—	—	—
2	1.014	1.195	1.421	1.612	1.676	1.610
3	.815	.935	1.075	1.170	1.170	1.077
4	.299	.329	.361	.373	.356	.302
5	.008	.010	.011	-.002	-.005	-.024
6	-.111	-.112	-.115	-.112	-.118	-.122
7	-.124	-.135	-.134	-.113	-.118	-.114
8	-.129	-.136	-.135	-.118	-.122	-.114
9	-.126	-.134	-.135	-.122	-.124	-.114
10	1.021	1.213	1.468	1.655	1.740	1.739
11	1.012	1.199	1.445	1.622	1.701	1.697
12	.945	1.105	1.313	1.458	1.506	1.485
13	.698	.800	.912	.965	.946	.875
14	.286	.315	.341	.335	.308	.252
15	.014	.020	.019	-.002	-.010	-.036
16	-.117	-.121	-.125	-.118	-.124	-.116
17	-.112	-.115	-.118	-.111	-.116	-.112
18	-.114	-.116	-.119	-.113	-.117	-.112
19	1.010	1.186	1.329	1.440	1.574	1.670
20	1.007	1.182	1.338	1.454	1.584	1.672
21	.997	1.170	1.326	1.440	1.570	1.656
22	.972	1.140	1.300	1.412	1.538	1.614
23	.882	1.021	1.159	1.253	1.360	1.421
24	.604	.673	.730	.756	.809	.837
25	.226	.240	.240	.225	.227	.220
26	-.034	-.035	-.043	-.059	-.062	-.068
27	-.120	-.123	-.126	-.116	-.117	-.109
28	-.115	-.116	-.116	-.113	-.113	-.107
29	-.116	-.116	-.116	-.113	-.112	-.107
30	-.114	-.116	-.116	-.110	-.112	-.108
31	-.115	-.116	-.116	-.113	-.113	-.107

[redacted]

I-1552

TABLE I.- ORIFICE LOCATION DETAIL AND TABULATION OF PRESSURE COEFFICIENTS FOR TEST MODELS - Continued

(b) Models 2A and 2B

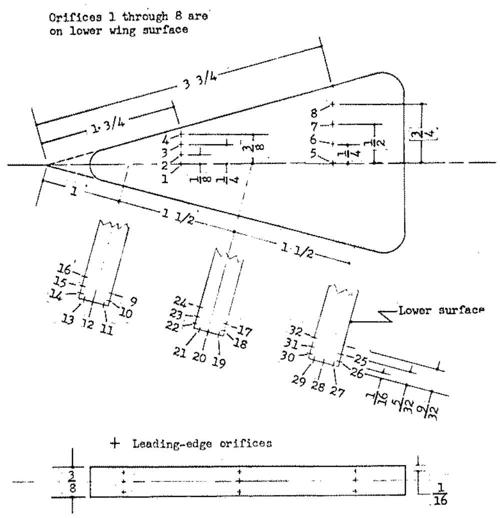

Model 2A

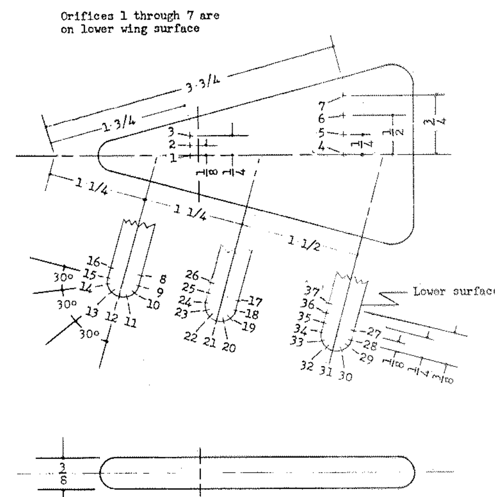

Model 2B

Orifice	Pressure Coefficient, C_p				
	α = 45°	α = 51°	α = 70°	α = 80°	α = 90°
1	0.931	1.102	1.691	1.744	1.699
2	.933	1.104	1.684	1.735	1.689
3	.929	1.093	1.646	1.691	1.643
4	.892	1.039	1.527	1.556	1.507
5	.912	1.088	1.574	1.675	1.726
6	.900	1.078	1.577	1.675	1.720
7	.908	1.080	1.557	1.650	1.700
8	.886	1.040	1.485	1.572	1.619
9	.942	1.109	1.703	1.735	1.618
10	.899	1.055	1.593	1.618	1.491
11	-.027	-.043	-.086	-.115	-.139
12	.140	.063	-.072	-.108	-.129
13	.108	.107	-.005	-.082	-.109
14	-.140	-.131	-.120	-.120	-.123
15	-.142	-.132	-.120	-.120	-.123
16	-.141	-.138	-.120	-.120	-.122
17	.862	1.024	1.539	1.585	1.580
18	.797	.934	1.393	1.425	1.421
19	-.069	-.083	-.126	-.126	-.126
20	-.062	-.086	-.124	-.125	-.125
21	.017	-.029	-.111	-.125	-.125
22	-.129	-.128	-.120	-.121	-.123
23	-.132	-.129	-.121	-.121	-.123
24	-.132	-.128	-.120	-.121	-.122
25	.845	.916	1.371	1.452	1.525
26	.756	.819	1.238	1.313	1.379
27	-.105	-.116	-.120	-.121	-.124
28	-.105	-.115	-.119	-.120	-.123
29	-.048	-.090	-.118	-.120	-.122
30	-.119	-.122	-.115	-.119	-.121
31	-.119	-.121	-.115	-.119	-.120
32	-.119	-.122	-.115	-.119	-.120

Orifice	Pressure Coefficient, C_p					
	α = 45°	α = 51°	α = 60°	α = 70°	α = 80°	α = 90°
1	1.072	1.257	1.517	1.694	1.751	1.696
2	1.072	1.257	1.508	1.679	1.732	1.674
3	1.071	1.228	1.449	1.594	1.628	1.556
4	1.058	1.248	1.435	1.577	1.683	1.732
5	1.055	1.246	1.432	1.569	1.678	1.728
6	1.047	1.232	1.407	1.543	1.645	1.691
7	.994	1.155	1.299	1.412	1.494	1.529
8	1.071	1.263	1.513	1.698	1.740	1.666
9	1.056	1.230	1.456	1.616	1.637	1.548
10	.885	.986	1.098	1.125	1.039	.909
11	.446	.468	.481	.451	.385	.289
12	.058	.055	.043	.010	-.013	-.045
13	-.084	-.085	-.093	-.113	-.115	-.121
14	-.128	-.134	-.130	-.123	-.125	-.112
15	-.125	-.132	-.129	-.121	-.117	-.112
16	-.122	-.129	-.128	-.120	-.117	-.112
17	1.035	1.224	1.443	1.589	1.659	1.641
18	.976	1.139	1.326	1.445	1.493	1.462
19	.732	.799	.840	.832	.791	.712
20	.326	.330	.307	.244	.190	.138
21	.021	.013	-.011	-.043	-.061	-.081
22	-.115	-.118	-.123	-.126	-.120	-.112
23	-.116	-.116	-.118	-.105	-.103	-.101
24	-.117	-.116	-.119	-.122	-.116	-.112
25	-.116	-.117	-.119	-.121	-.116	-.112
26	-.117	-.117	-.119	-.123	-.117	-.112
27	.985	1.131	1.255	1.374	1.489	1.573
28	.922	1.046	1.134	1.223	1.313	1.370
29	.660	.706	.724	.751	.783	.793
30	.237	.231	.197	.173	.162	.147
31	-.017	-.029	-.052	-.073	-.079	-.085
32	-.120	-.120	-.119	-.116	-.112	-.108
33	-.112	-.111	-.112	-.114	-.112	-.108
34	-.111	-.111	-.111	-.113	-.112	-.108
35	-.112	-.111	-.112	-.114	-.112	-.108
36	-.111	-.111	-.111	-.112	-.112	-.108
37	-.113	-.111	-.111	-.112	-.112	-.108

TABLE I.- ORIFICE LOCATION DETAIL AND TABULATION OF PRESSURE COEFFICIENTS FOR TEST MODELS - Continued

(c) Models 3A and 3B

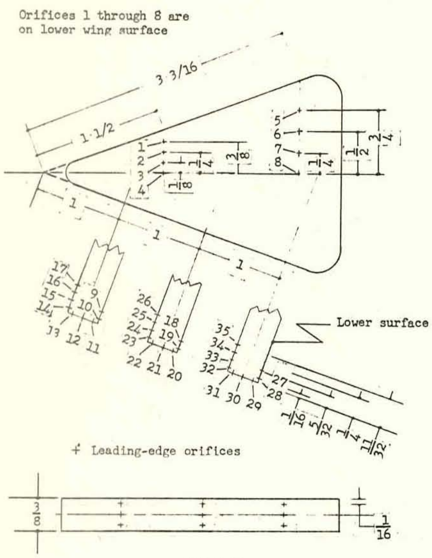

Model 3A

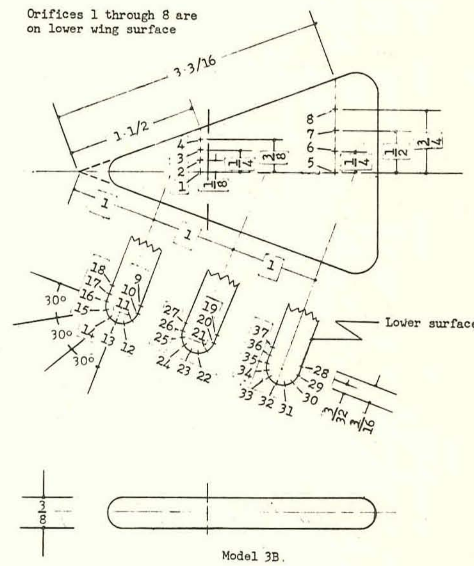

Model 3B

L-1552

Model 3A

Orifice	Pressure Coefficient, C_p					
	α = 45°	α = 51°	α = 60°	α = 70°	α = 80°	α = 90°
1	1.102	1.287	1.502	1.627	1.662	1.599
2	1.110	1.309	1.545	1.688	1.734	1.674
3	1.104	1.307	1.557	1.709	1.760	1.704
4	1.107	1.309	1.560	1.714	1.762	1.712
5	1.100	1.266	1.385	1.500	1.599	1.664
6	1.102	1.277	1.406	1.531	1.636	1.706
7	1.103	1.284	1.415	1.542	1.649	1.719
8	1.100	1.277	1.410	1.540	1.648	1.719
9	1.093	1.281	1.529	1.671	1.682	1.603
10	1.058	1.296	1.429	1.545	1.543	1.459
11	.054	.002	-.050	-.093	-.114	-.118
12	.262	.102	-.022	-.093	-.113	-.118
13	.239	.220	.078	-.052	-.098	-.115
14	-.128	-.130	-.129	-.115	-.111	-.112
15	-.128	-.130	-.129	-.114	-.111	-.112
16	-.128	-.131	-.130	-.114	-.110	-.112
17	-.126	-.130	-.126	-.114	-.109	-.111
18	1.080	1.250	1.435	1.554	1.604	1.590
19	1.030	1.178	1.339	1.441	1.480	1.463
20	-.011	-.049	-.085	-.121	-.117	-.111
21	.041	-.030	-.085	-.119	-.115	-.111
22	.170	.074	-.060	-.112	-.115	-.111
23	-.115	-.115	-.116	-.114	-.111	-.110
24	-.119	-.117	-.116	-.115	-.112	-.111
25	-.119	-.118	-.117	-.115	-.111	-.111
26	-.120	-.120	-.119	-.115	-.110	-.111
27	1.053	1.198	1.314	1.427	1.514	1.568
28	.979	1.104	1.203	1.301	1.376	1.424
29	-.042	-.071	-.107	-.121	-.109	-.110
30	-.036	-.075	-.107	-.120	-.109	-.111
31	.087	-.031	-.095	-.117	-.109	-.110
32	---	---	---	----	----	----
33	-.117	-.115	-.110	-.110	-.107	-.109
34	-.117	-.115	-.112	-.110	-.107	-.109
35	-.116	-.115	-.114	-.111	-.108	-.109

Model 3B

Orifice	Pressure Coefficient, C_p					
	α = 45°	α = 51°	α = 60°	α = 70°	α = 80°	α = 90°
1	1.111	1.311	1.555	1.713	1.762	1.713
2	1.113	1.311	1.552	1.708	1.757	1.701
3	1.113	1.303	1.529	1.669	1.713	1.645
4	1.092	1.251	1.415	1.492	1.490	1.387
5	1.095	1.207	1.382	1.510	1.631	1.713
6	1.098	1.268	1.383	1.510	1.629	1.713
7	1.099	1.264	1.375	1.501	1.618	1.694
8	1.086	1.235	1.334	1.496	1.558	1.627
9	1.116	1.311	1.610	1.717	1.735	1.644
10	1.110	1.292	1.518	1.654	1.640	1.532
11	1.001	1.109	1.203	1.188	1.083	.927
12	.503	.504	.484	.407	.310	.207
13	.074	.059	.029	-.008	-.047	-.076
14	-.079	-.088	-.101	-.118	-.113	-.105
15	-.125	-.124	-.122	-.109	-.102	-.101
16	-.123	-.124	-.123	-.109	-.101	-.102
17	-.121	-.122	-.120	-.106	-.101	-.101
18	-.121	-.122	-.120	-.107	-.101	-.101
19	1.088	1.269	1.465	1.589	1.640	1.623
20	1.057	1.219	1.387	1.486	1.518	1.484
21	.862	.938	.971	.942	.881	.777
22	.386	.373	.313	.240	.170	.105
23	.071	.050	.007	-.032	-.062	-.085
24	-.071	-.082	-.102	-.118	-.108	-.101
25	-.102	-.114	-.115	-.100	-.101	-.090
26	-.114	-.117	-.118	-.103	-.101	-.090
27	-.118	-.120	-.118	-.103	-.101	-.100
28	1.057	1.208	1.318	1.427	1.532	1.590
29	1.003	1.132	1.219	1.345	1.391	1.432
30	.728	.758	.750	.747	.743	.709
31	.273	.242	.182	.139	.107	.124
32	.021	-.003	-.040	-.063	-.078	-.091
33	-.089	-.102	-.118	-.111	-.102	-.103
34	-.117	-.113	-.112	-.103	-.099	-.101
35	-.116	-.113	-.112	-.104	-.100	-.101
36	-.116	-.113	-.112	-.103	-.099	-.101
37	-.115	-.113	-.112	-.103	-.099	-.101

TABLE I.- ORIFICE LOCATION DETAIL AND TABULATION OF PRESSURE COEFFICIENTS FOR TEST MODELS - Continued

(d) Models 4A and 4B

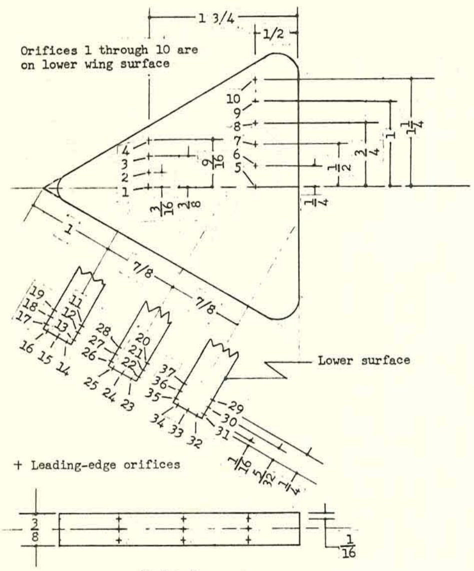

Model 4A

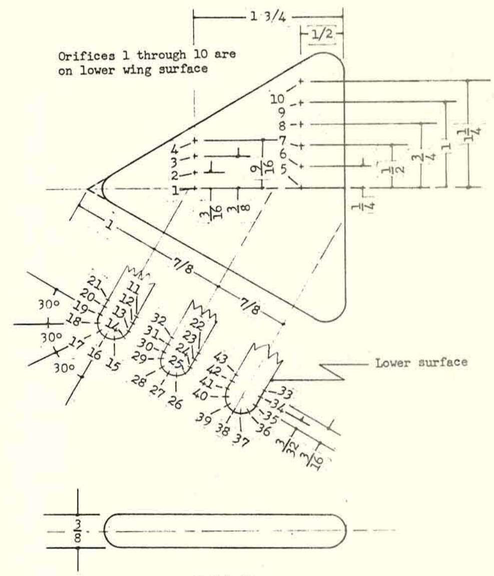

Model 4B

Orifice	Pressure Coefficient, C_p					
	α = 45°	α = 51°	α = 60°	α = 70°	α = 80°	α = 90°
1	1.182	1.397	1.604	1.715	1.744	1.707
2	1.187	1.401	1.603	1.707	1.739	1.696
3	1.199	1.403	1.590	1.678	1.703	1.655
4	1.208	1.385	1.532	1.590	1.597	1.546
5	1.170	1.309	1.426	1.544	1.650	1.718
6	1.174	1.310	1.426	1.544	1.651	1.718
7	1.181	1.316	1.430	1.544	1.650	1.713
8	1.193	1.319	1.428	1.535	1.637	1.696
9	1.204	1.316	1.417	1.514	1.610	1.662
10	1.199	1.286	1.365	1.446	1.523	1.564
11	1.196	1.399	1.597	1.678	1.679	1.608
12	1.200	1.388	1.568	1.635	1.625	1.547
13	1.186	1.341	1.482	1.525	1.503	1.420
14	.200	.062	-.025	-.101	-.119	-.120
15	.453	.263	-.019	-.096	-.118	-.118
16	.416	.367	-.116	-.066	-.113	-.119
17	-.130	-.128	-.113	-.110	-.109	-.115
18	-.130	-.129	-.114	-.110	-.109	-.114
19	-.130	-.129	-.114	-.110	-.109	-.114
20	1.195	1.361	1.502	1.582	1.631	1.613
21	1.189	1.339	1.465	1.534	1.570	1.545
22	1.148	1.268	1.370	1.421	1.443	1.410
23	.076	.012	-.051	-.111	-.118	-.117
24	.369	.040	-.052	-.112	-.120	-.118
25	—	—	—	—	—	—
26	-.114	-.114	-.103	-.110	-.109	-.114
27	-.117	-.117	-.103	-.110	-.109	-.114
28	-.118	-.119	-.104	-.111	-.110	-.114
29	1.185	1.284	1.377	1.453	1.532	1.575
30	1.168	1.260	1.345	1.412	1.481	1.514
31	1.109	1.184	1.255	1.299	1.364	1.385
32	.023	-.035	-.074	-.114	-.117	-.119
33	.209	-.011	-.073	-.112	-.114	-.118
34	.382	.144	-.045	-.102	-.113	-.118
35	-.117	-.114	-.103	-.108	-.108	-.116
36	-.117	-.114	-.101	-.108	-.109	-.117
37	-.116	-.114	-.101	-.108	-.109	-.116

Orifice	Pressure Coefficient, C_p					
	α = 45°	α = 51°	α = 60°	α = 70°	α = 80°	α = 90°
1	1.187	1.399	1.608	1.722	1.755	1.707
2	1.194	1.401	1.608	1.715	1.748	1.693
3	1.208	1.406	1.588	1.667	1.685	1.614
4	1.211	1.349	1.421	1.386	1.307	1.168
5	1.168	1.292	1.399	1.513	1.627	1.710
6	1.172	1.295	1.400	1.517	1.628	1.710
7	1.181	1.301	1.404	1.516	1.624	1.704
8	1.192	1.302	1.400	1.509	1.610	1.686
9	1.213	1.298	1.386	1.482	1.575	1.644
10	1.164	1.171	1.188	1.211	1.232	1.233
11	1.193	1.402	1.608	1.709	1.719	1.640
12	1.198	1.399	1.589	1.677	1.675	1.586
13	1.201	1.382	1.531	1.582	1.548	1.440
14	1.145	1.234	1.226	1.126	.948	.729
15	.868	.876	.804	.673	.510	.347
16	.184	.136	.055	-.005	-.056	-.087
17	-.096	-.109	-.125	-.109	-.106	-.110
18	-.118	-.114	-.114	-.109	-.106	-.110
19	-.118	-.114	-.114	-.107	-.106	-.110
20	-.118	-.114	-.114	-.108	-.106	-.110
21	-.117	-.114	-.114	-.108	-.106	-.110
22	1.187	1.362	1.497	1.591	1.639	1.636
23	1.186	1.350	1.469	1.548	1.581	1.565
24	1.174	1.316	1.402	1.452	1.460	1.427
25	1.047	1.083	1.038	.968	.853	.708
26	.802	.787	.702	.597	.473	.356
27	.159	.112	.045	0	-.043	-.079
28	-.111	-.115	-.113	-.103	-.105	-.111
29	-.101	-.104	-.110	-.102	-.105	-.110
30	-.102	-.105	-.111	-.104	-.105	-.110
31	-.106	-.108	-.111	-.104	-.105	-.110
32	-.112	-.111	-.112	-.105	-.106	-.110
33	—	—	—	—	—	—
34	1.163	1.246	1.310	1.397	1.478	1.546
35	1.135	1.195	1.233	1.289	1.342	1.378
36	.972	.957	.905	.872	.819	.745
37	.678	.630	.550	.491	.414	.337
38	.159	.104	.047	.012	-.023	-.052
39	-.104	-.119	-.119	-.106	-.101	-.110
40	-.122	-.114	-.110	-.104	-.101	-.109
41	-.119	-.112	-.111	-.104	-.101	-.109
42	-.119	-.112	-.111	-.103	-.101	-.109
43	-.119	-.112	-.109	-.104	-.101	-.109

TABLE I.- ORIFICE LOCATION DETAIL AND TABULATION OF PRESSURE COEFFICIENTS FOR TEST MODELS - Continued

(e) Models 5A and 5B

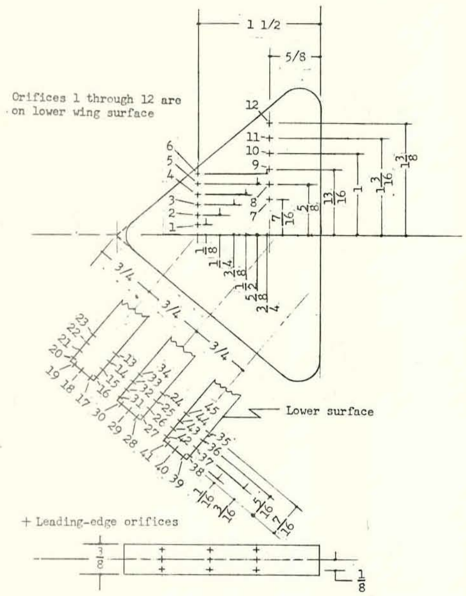

Model 5A

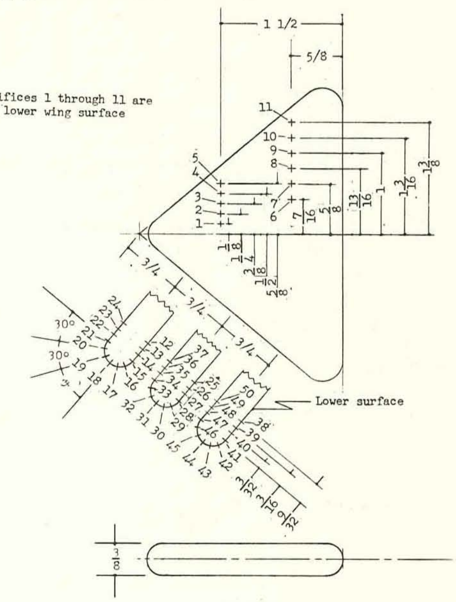

Model 5B

Orifice	Pressure Coefficient, C_p					
	α = 45°	α = 51°	α = 60°	α = 70°	α = 80°	α = 90°
1	1.247	1.450	1.626	1.725	1.748	1.710
2	1.251	1.450	1.620	1.718	1.739	1.696
3	1.265	1.455	1.615	1.703	1.717	1.671
4	—	—	—	—	—	—
5	1.301	1.449	1.563	1.619	1.614	1.563
6	1.305	1.391	1.456	1.484	1.470	1.415
7	1.235	1.347	1.475	1.590	1.674	1.731
8	1.250	1.356	1.479	1.587	1.667	1.720
9	1.267	1.359	1.476	1.579	1.656	1.696
10	—	—	—	—	—	—
11	1.285	1.371	1.463	1.546	1.608	1.636
12	1.241	1.322	1.402	1.475	1.520	1.540
13	1.245	1.457	1.640	1.727	1.741	1.695
14	1.257	1.470	1.652	1.725	1.732	1.669
15	1.258	1.479	1.652	1.711	1.705	1.623
16	1.300	1.401	1.624	1.653	1.620	1.516
17	—	—	—	—	—	—
18	.648	.538	.115	-.074	-.119	-.119
19	.556	.474	.276	.011	-.102	-.119
20	-.127	-.126	-.105	-.105	-.109	-.113
21	-.128	-.127	-.107	-.106	-.109	-.114
22	-.128	-.128	-.108	-.105	-.110	-.113
23	-.129	-.129	-.109	-.105	-.110	-.113
24	1.241	1.412	1.555	1.658	1.710	1.721
25	1.219	1.412	1.557	1.653	1.696	1.695
26	1.250	1.419	1.555	1.625	1.672	1.647
27	1.318	1.441	1.531	1.561	1.580	1.540
28	.421	.087	.015	-.083	-.128	-.117
29	.691	.422	.017	-.083	-.123	-.115
30	.545	.476	.181	-.038	-.110	-.115
31	-.113	-.120	-.104	-.107	-.110	-.114
32	-.116	-.121	-.104	-.105	-.110	-.114
33	-.120	-.121	-.105	-.107	-.110	-.114
34	-.120	-.121	-.105	-.106	-.110	-.113
35	1.223	1.319	1.424	1.532	1.615	1.674
36	1.292	1.376	1.463	1.553	1.624	1.664
37	1.316	1.389	1.468	1.545	1.605	1.629
38	1.228	1.322	1.415	1.527	1.531	1.534
39	.313	.041	-.001	-.087	-.122	-.118
40	.646	.311	-.001	-.086	-.119	-.117
41	.567	.462	.143	-.026	-.099	-.115
42	-.115	-.113	-.103	-.104	-.107	-.114
43	-.117	-.114	-.103	-.105	-.107	-.113
44	-.118	-.114	-.103	-.105	-.109	-.114
45	-.117	-.114	-.103	-.103	-.108	-.113

Orifice	Pressure Coefficient, C_p					
	α = 45°	α = 51°	α = 60°	α = 70°	α = 80°	α = 90°
1	1.246	1.447	1.624	1.720	1.743	1.698
2	1.254	1.452	1.619	1.706	1.728	1.677
3	1.267	1.456	1.611	1.685	1.697	1.642
4	1.285	1.459	1.586	1.637	1.630	1.567
5	1.309	1.443	1.512	1.512	1.462	1.383
6	1.224	1.332	1.455	1.571	1.664	1.727
7	1.233	1.339	1.457	1.569	1.654	1.715
8	1.245	1.343	1.457	1.566	1.644	1.696
9	1.270	1.351	1.457	1.552	1.628	—
10	1.287	1.357	1.446	1.522	1.581	1.606
11	1.281	1.317	1.351	1.350	1.389	1.380
12	1.252	1.463	1.647	1.742	1.733	1.677
13	1.263	1.457	1.657	1.741	1.718	1.645
14	1.277	1.486	1.657	1.717	1.682	1.588
15	1.300	1.493	1.628	1.645	1.579	1.458
16	1.334	1.387	1.308	1.114	.894	.602
17	.939	.865	.646	.402	.228	.099
18	.453	.361	.208	.062	-.027	-.082
19	.074	.024	-.043	-.102	-.116	-.111
20	-.127	-.120	-.108	-.104	-.104	-.109
21	-.117	-.105	-.108	-.104	-.104	-.108
22	-.118	-.117	-.108	-.103	-.105	-.108
23	-.118	-.117	-.108	-.104	-.105	-.110
24	—	—	—	—	—	—
25	1.273	1.421	1.558	1.656	1.694	1.699
26	1.280	1.432	1.566	1.651	1.671	1.663
27	1.297	1.442	1.562	1.623	1.625	1.600
28	1.313	1.439	1.530	1.555	1.523	1.472
29	1.273	1.254	1.158	1.011	.840	.643
30	.843	.731	.536	.349	.215	.108
31	.372	.265	.129	.013	-.043	-.088
32	.045	-.011	-.073	-.115	-.110	-.111
33	-.112	-.109	-.107	-.104	-.105	-.111
34	-.107	-.108	-.106	-.102	-.105	-.110
35	-.108	-.108	-.106	-.102	-.105	-.110
36	—	—	—	—	—	—
37	—	—	—	—	—	—
38	1.255	1.325	1.419	1.531	1.596	1.664
39	1.273	1.348	1.441	1.539	1.596	1.648
40	1.289	1.365	1.451	1.534	1.575	1.604
41	1.298	1.366	1.428	1.484	1.495	1.496
42	1.229	1.196	1.127	1.043	.929	.798
43	.714	.590	.438	.305	.195	.107
44	.296	.197	.089	.008	-.048	-.087
45	.050	-.011	-.068	-.107	-.116	-.112
46	-.120	-.114	-.105	-.100	-.104	-.109
47	-.114	-.112	-.105	-.100	-.104	-.109
48	-.115	-.112	-.105	-.100	-.104	-.109
49	-.116	-.113	-.105	-.100	-.105	-.109
50	—	—	—	—	—	—

L-1552

L-1552

TABLE I.- ORIFICE LOCATION DETAIL AND TABULATION OF PRESSURE COEFFICIENTS FOR TEST MODELS - Continued

(f) Models 2AA and 2BB

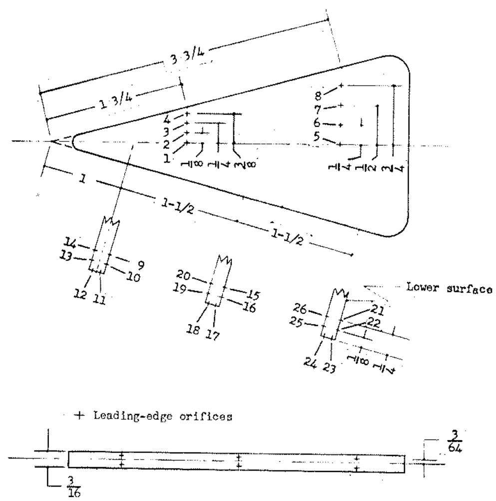

Model 2AA

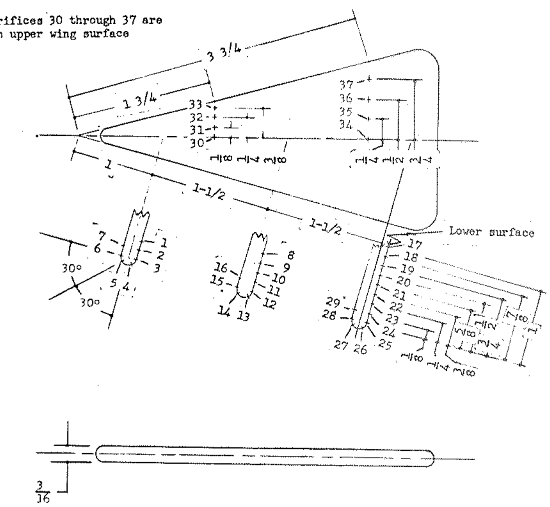

Model 2BB

Orifice	Pressure Coefficient, C_p					
	α = 45°	α = 51°	α = 60°	α = 70°	α = 80°	α = 90°
1	1.074	1.264	1.528	1.691	1.744	1.694
2	1.069	1.255	1.521	1.683	1.738	1.685
3	—	—	—	—	—	—
4	1.026	1.213	1.443	1.571	1.437	1.556
5	1.069	1.260	1.454	1.587	1.420	1.733
6	1.063	1.254	1.448	1.581	1.419	1.731
7	1.052	1.236	1.431	1.559	1.396	1.707
8	1.052	1.227	1.385	1.497	1.591	1.624
9	1.075	1.263	1.538	1.719	1.768	1.659
10	1.067	1.242	1.504	1.662	1.706	1.571
11	0	-.025	-.037	-.111	-.124	-.040
12	.969	.033	.002	-.088	-.103	-.118
13	—	—	—	—	—	—
14	-.099	-.131	-.074	-.121	-.115	-.115
15	1.066	1.242	1.462	1.597	1.664	1.643
16	.978	1.144	1.356	1.487	1.553	1.526
17	-.085	-.113	-.079	-.120	-.115	-.115
18	-.064	-.095	-.073	-.115	-.113	-.114
19	-.102	-.125	-.073	-.115	-.111	-.114
20	-.104	-.126	-.074	-.115	-.111	-.114
21	.960	1.135	1.281	1.408	1.512	1.577
22	.929	1.077	1.212	1.328	1.422	1.483
23	-.110	-.137	-.076	-.112	-.111	-.116
24	-.099	-.124	-.074	-.115	-.110	-.115
25	-.101	-.123	-.073	-.111	-.110	-.115
26	-.101	-.123	-.074	-.111	-.110	-.114

Orifice	Pressure Coefficient, C_p					
	α = 45°	α = 51°	α = 60°	α = 70°	α = 80°	α = 90°
1	1.070	1.251	1.519	1.720	1.770	1.661
2	1.077	1.249	1.505	1.693	1.745	1.627
3	1.009	1.165	1.384	1.530	1.550	1.409
4	.263	.260	.244	.200	.134	.063
5	-.103	-.107	-.113	-.130	-.128	-.123
6	-.138	-.136	-.129	-.123	-.116	-.119
7	-.137	-.136	-.129	-.125	-.116	-.118
8	1.069	1.262	1.500	1.661	1.733	1.736
9	1.072	1.256	1.490	1.649	1.719	1.719
10	1.069	1.241	1.465	1.618	1.686	1.678
11	1.041	1.209	1.407	1.550	1.609	1.595
12	.918	1.048	1.182	1.280	1.317	1.283
13	.160	.147	.111	..071	.040	.008
14	-.132	-.132	-.134	-.124	-.121	-.119
15	-.118	-.123	-.124	-.122	-.116	-.118
16	-.123	-.126	-.128	-.126	-.119	-.119
17	1.071	1.256	1.333	1.439	1.550	1.639
18	1.072	1.259	1.344	1.453	1.562	1.648
19	1.072	1.253	1.348	1.464	1.572	1.656
20	1.065	1.244	1.352	1.922	1.576	1.658
21	1.061	1.238	1.349	1.473	1.578	1.657
22	1.051	1.230	1.343	1.466	1.568	1.644
23	1.035	1.213	1.322	1.444	1.543	1.612
24	.998	1.163	1.268	1.390	1.481	1.541
25	.851	.973	1.053	1.148	1.220	1.262
26	.012	-.005	-.030	-.044	-.050	-.061
27	-.124	-.131	-.129	-.119	-.115	-.119
28	-.122	-.127	-.121	-.116	-.112	-.117
29	-.122	-.126	-.121	-.115	-.112	-.116
30	-.131	-.129	-.126	-.121	-.115	-.118
31	-.132	-.129	-.126	-.121	-.114	-.117
32	-.133	-.131	-.129	-.123	-.115	-.117
33	-.131	-.127	-.127	-.122	-.115	-.117
34	-.128	-.127	-.122	-.119	-.113	-.117
35	-.123	-.122	-.120	-.116	-.112	-.116
36	-.126	-.125	-.120	-.118	-.112	-.116
37	-.123	-.125	-.120	-.117	-.112	-.115

CONFIDENTIAL

TABLE I.- ORIFICE LOCATION DETAIL AND TABULATION OF PRESSURE COEFFICIENTS FOR TEST MODELS - Continued

(g) Models 2Ⓑ

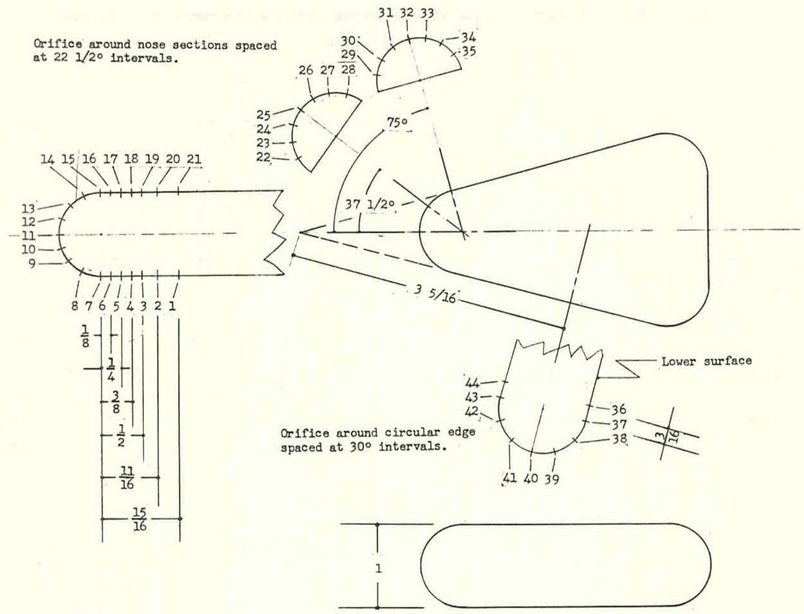

Model 2Ⓑ

L-1552

Orifice	Pressure Coefficient, C_p					
	α = 45°	α = 51°	α = 60°	α = 70°	α = 80°	α = 90°
1	1.075	1.265	1.506	1.673	1.743	1.727
2	1.074	1.269	1.519	1.685	1.745	1.712
3	1.074	1.274	1.527	1.695	1.741	1.699
4	1.070	1.275	1.534	1.701	1.739	1.689
5	1.066	1.278	1.542	1.705	1.739	1.676
6	1.059	1.283	1.553	1.713	1.764	1.654
7	1.032	1.277	1.562	1.740	1.739	1.591
8	1.472	1.601	1.748	1.725	1.448	1.114
9	1.745	1.733	1.644	1.377	.995	.651
10	1.503	1.368	1.086	.769	.461	.226
11	.846	.662	.419	.212	.049	-.041
12	.272	.169	.051	-.036	-.091	-.101
13	-.022	-.058	-.093	-.109	-.107	-.097
14	-.111	-.108	-.105	-.105	-.106	-.101
15	-.104	-.105	-.105	-.104	-.106	-.101
16	-.104	-.105	-.105	-.104	-.107	-.101
17	-.104	-.105	-.105	-.104	-.106	-.098
18	-.103	-.105	-.106	-.104	-.106	-.098
19	-.104	-.105	-.106	-.104	-.107	-.098
20	-.105	-.105	-.107	-.104	-.106	-.098
21	-.102	-.105	-.108	-.102	-.107	-.098
22	1.310	1.464	1.643	1.644	1.437	1.147
23	1.400	1.436	1.450	1.291	.987	.706
24	1.060	.985	.815	.612	.385	.201
25	.589	.472	.317	.178	.057	-.031
26	.157	.092	.014	-.038	-.086	-.101
27	-.052	-.078	-.104	-.089	-.106	-.096
28	-.110	-.107	-.105	-.084	-.106	-.097
29	1.023	1.237	1.475	1.605	1.500	1.320
30	.797	.919	1.042	1.046	.934	.766
31	.441	.475	.496	.464	.362	.259
32	.173	.173	.151	.106	.036	-.018
33	-.045	-.058	-.065	-.092	-.109	-.098
34	-.111	-.112	-.109	-.104	-.105	-.096
35	-.102	-.104	-.105	-.103	-.105	-.096
36	1.055	1.242	1.469	1.608	1.661	1.632
37	.974	1.116	1.273	1.345	1.341	1.276
38	.715	.795	.864	.873	.832	.750
39	.382	.406	.415	.393	.343	.285
40	.045	.042	.032	.014	-0.11	-.033
41	-.096	-.098	-.105	-.116	-.116	-.097
42	-.104	-.105	-.105	-.104	-.105	-.096
43	-.104	-.105	-.106	-.104	-.105	-.096
44	-.105	-.105	-.107	-.104	-.105	-.096

CONFIDENTIAL

L-1552

TABLE I.- ORIFICE LOCATION DETAIL AND TABULATION OF PRESSURE COEFFICIENTS FOR TEST MODELS - Continued

(h) Models 3 Ⓑ

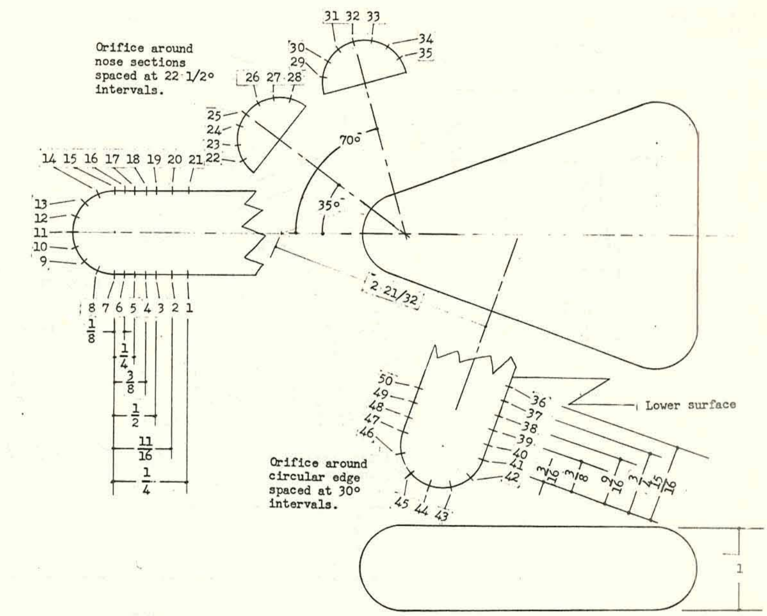

Model 3 Ⓑ

Orifice	Pressure Coefficient, C_p					
	α = 45°	α = 51°	α = 60°	α = 70°	α = 80°	α = 90°
1	1.121	1.311	1.551	1.697	1.778	1.703
2	1.123	1.315	1.562	1.717	1.761	1.688
3	1.122	1.320	1.576	1.731	1.755	1.676
4	1.106	1.313	1.582	1.736	1.750	1.661
5	1.109	1.321	1.595	1.743	1.742	1.639
6	1.063	1.302	1.597	1.749	1.723	1.581
7	1.071	1.322	1.629	1.759	1.686	1.522
8	1.442	1.598	1.742	1.695	1.442	1.106
9	1.736	1.728	1.593	1.305	.904	.559
10	1.444	1.728	.968	.643	.343	.136
11	----	----	----	----	----	----
12	.261	.169	.060	-.019	-.076	-.093
13	-.049	-.061	-.094	-.111	-.106	-.095
14	-.100	-.111	-.111	-.110	-.105	-.094
15	-.101	-.108	-.111	-.110	-.107	-.096
16	-.096	-.105	-.109	-.109	-.105	-.093
17	----	----	----	----	----	----
18	-.101	-.108	-.110	-.110	-.107	-.096
19	----	----	----	----	----	----
20	-.100	-.107	-.109	-.110	-.107	-.095
21	----	----	----	----	----	----
22	1.272	1.465	1.660	1.669	1.457	1.163
23	1.389	1.401	1.390	1.223	.931	.618
24	1.066	.975	.807	.598	.364	.165
25	.573	.459	.314	.187	.063	-.055
26	.118	.066	.002	-.045	-.087	-.098
27	-.074	-.082	-.102	-.111	-.103	-.093
28	-.095	-.106	-.108	-.109	-.103	-.093
29	1.080	1.297	1.533	1.595	1.451	1.227
30	.899	1.018	1.113	1.080	.930	.738
31	.572	.605	.600	.527	.396	.257
32	.198	.192	.167	.117	.042	-.025
33	-.025	-.027	-.044	-.067	-.099	-.098
34	-.102	-.108	-.113	-.114	-.103	-.095
35	-.097	-.106	-.109	-.109	-.103	-.093
36	1.116	1.295	1.475	1.561	1.587	1.471
37	1.127	1.323	1.541	1.677	1.743	1.659
38	1.116	1.317	1.548	1.703	1.774	1.701
39	1.111	1.313	1.548	1.705	1.752	1.691
40	1.109	1.302	1.518	1.658	1.679	1.605
41	1.064	1.203	1.338	1.383	1.311	1.187
42	.842	.907	.939	.900	.786	.668
43	.481	.486	.465	.402	.317	.235
44	.111	.098	.073	.032	-.012	-.044
45	-.075	-.082	-.093	-.107	-.116	-.097
46	-.097	-.109	-.109	-.109	-.107	-.098
47	-.096	-.108	-.109	-.110	-.106	-.098
48	-.096	-.109	-.110	-.110	-.106	-.098
49	-.096	-.108	-.109	-.110	-.106	-.098
50	-.096	-.104	-.107	-.109	-.105	-.096

TABLE I.- ORIFICE LOCATION DETAIL AND TABULATION OF PRESSURE COEFFICIENTS FOR TEST MODELS - Concluded

(i) Models 33B

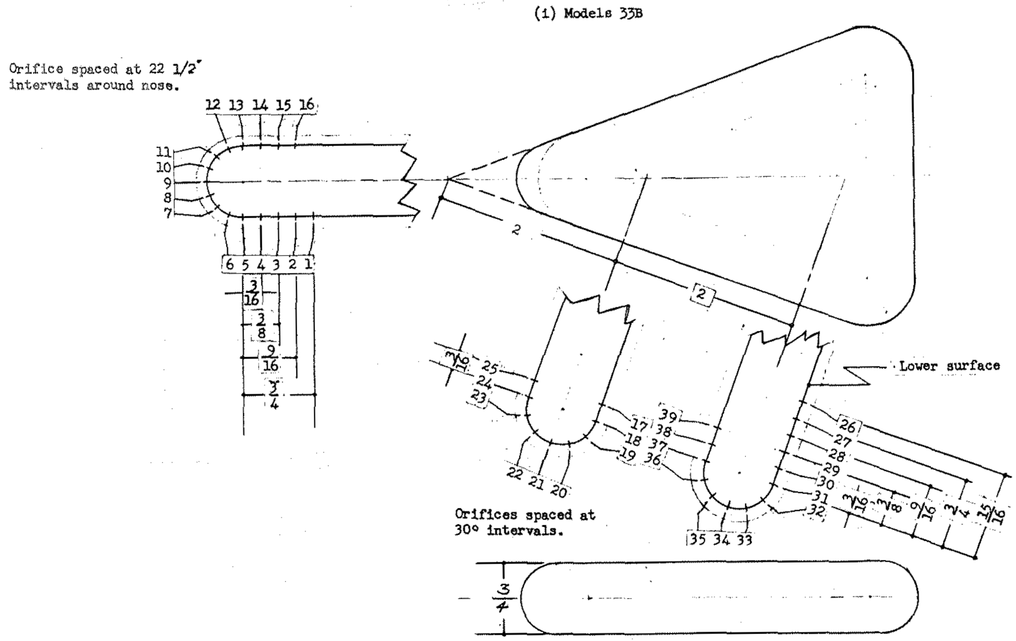

Model 33B

Orifice	Pressure Coefficient, C_p					
	α = 0°	α = 10°	α = 20°	α = 25°	α = 30°	α = 35°
1	0.015	0.122	0.306	0.437	0.603	0.768
2	.015	.126	.314	.440	.606	.772
3	.014	.130	.313	.436	.599	.765
4	.011	.126	.305	.423	.577	.738
5	.014	.139	.322	.435	.579	.721
6	.221	.423	.686	.827	.982	1.151
7	.870	1.174	1.436	1.544	1.661	1.753
8	1.403	1.626	1.731	1.768	1.780	1.717
9	1.743	1.725	1.585	1.519	1.375	1.231
10	1.452	1.187	.914	.772	.624	.494
11	.743	.506	.296	.204	.126	.069
12	.205	.066	-.028	-.059	-.083	-.095
13	.006	-.056	-.100	-.113	-.119	-.123
14	.003	-.051	-.093	-.106	-.114	-.120
15	.013	-.047	-.089	-.102	-.111	-.113
16	.016	-.043	-.077	-.091	-.092	-.090
17	.011	.122	.314	.445	.613	.774
18	-.011	.103	.300	.436	.604	.759
19	.041	.183	.390	.426	.656	.768
20	.134	.230	.346	.407	.468	.508
21	.206	.197	.186	.179	.170	.158
22	.160	.069	-.005	-.029	-.050	-.063
23	.043	-.043	-.101	-.116	-.123	-.129
24	-.014	-.074	-.115	-.127	-.131	-.129
25	.008	-.061	-.115	-.130	-.135	-.136
26	.006	.118	.314	.449	.608	.765
27	.006	.122	.323	.458	.618	.775
28	.010	.124	.327	.466	.621	.783
29	-.040	.123	.334	.472	.628	.787
30	-.040	.119	.341	.483	.635	.791
31	-.043	.096	.335	+476	.629	.780
32	.011	.168	.391	.508	.632	.720
33	.123	.225	.338	.388	.426	.457
34	.192	.178	.164	.156	.146	.131
35	.138	.041	-.028	-.047	-.065	-.077
36	.013	-.076	-.118	-.127	-.131	-.132
37	-.044	-.105	-.129	-.131	-.131	-.131
38	-.038	-.103	-.127	-.130	-.128	-.129
39	-.040	-.110	-.129	-.132	-.132	-.131

L-1552

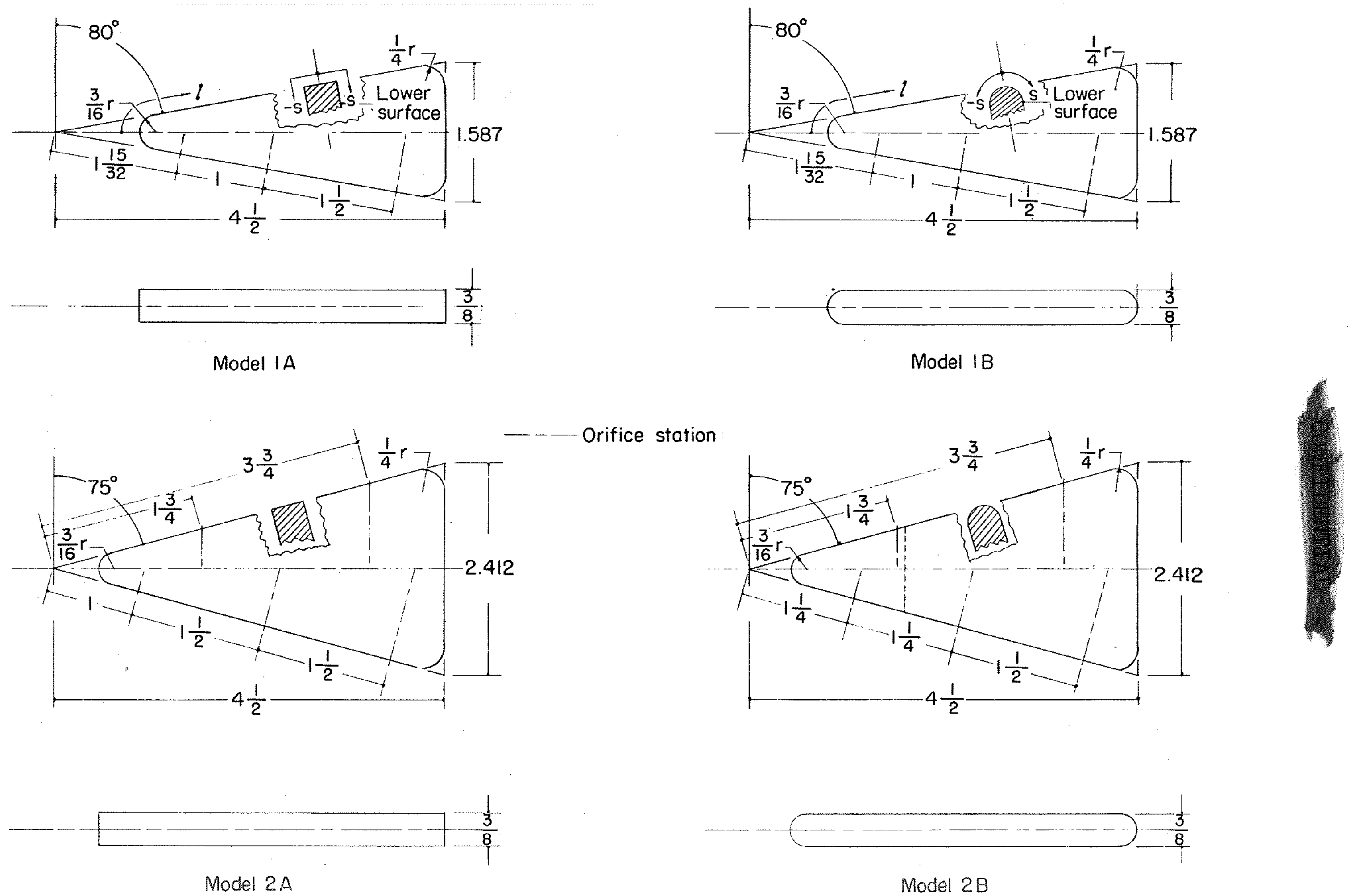

(a) Models 1A, 1B, 2A, and 2B.

Figure 1.- Sketches of models tested in investigation. Dimensions are in inches.

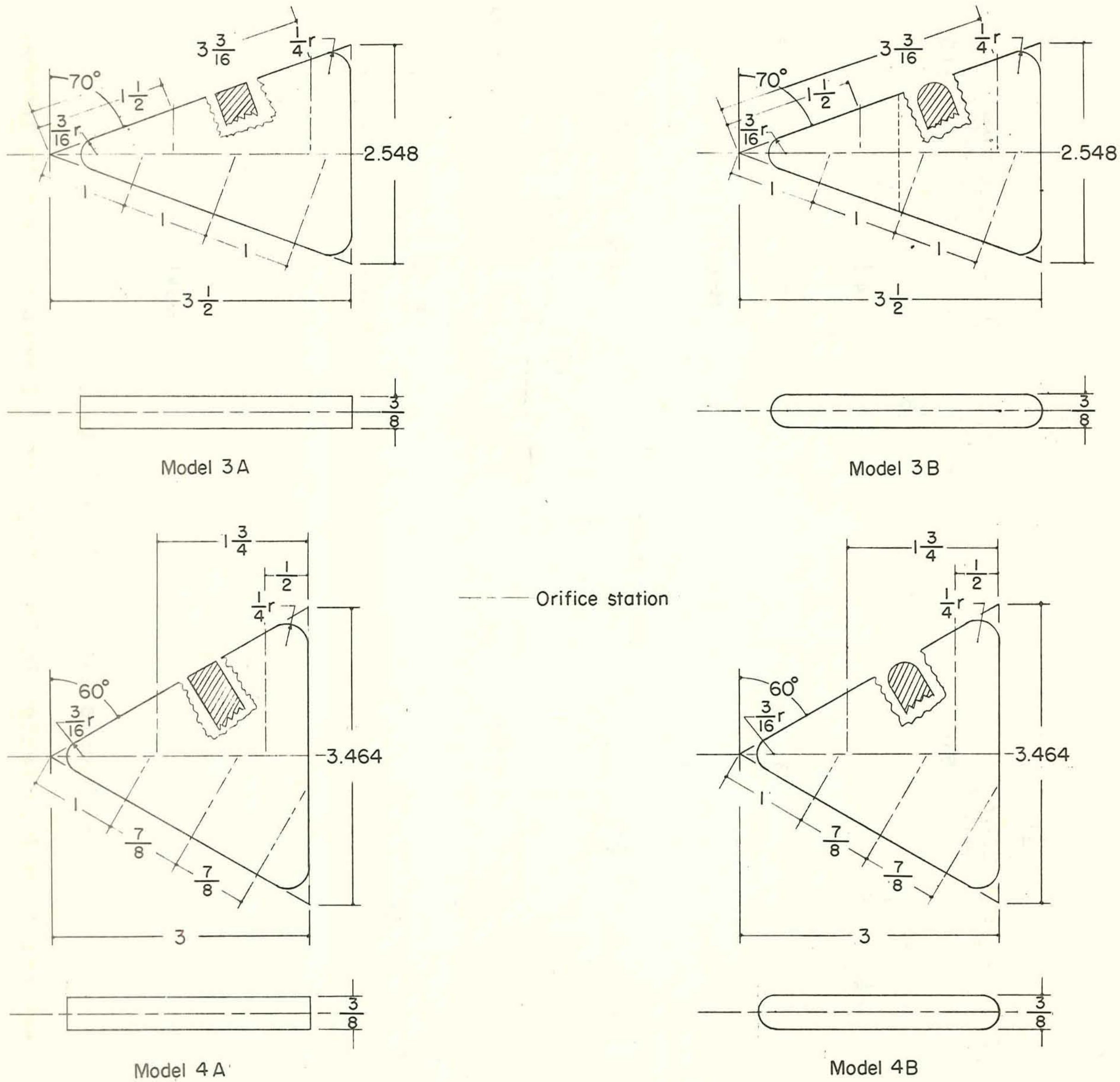

L-1552

(b) Models 3A, 3B, 4A, and 4B.

Figure 1.- Continued.

L-1552

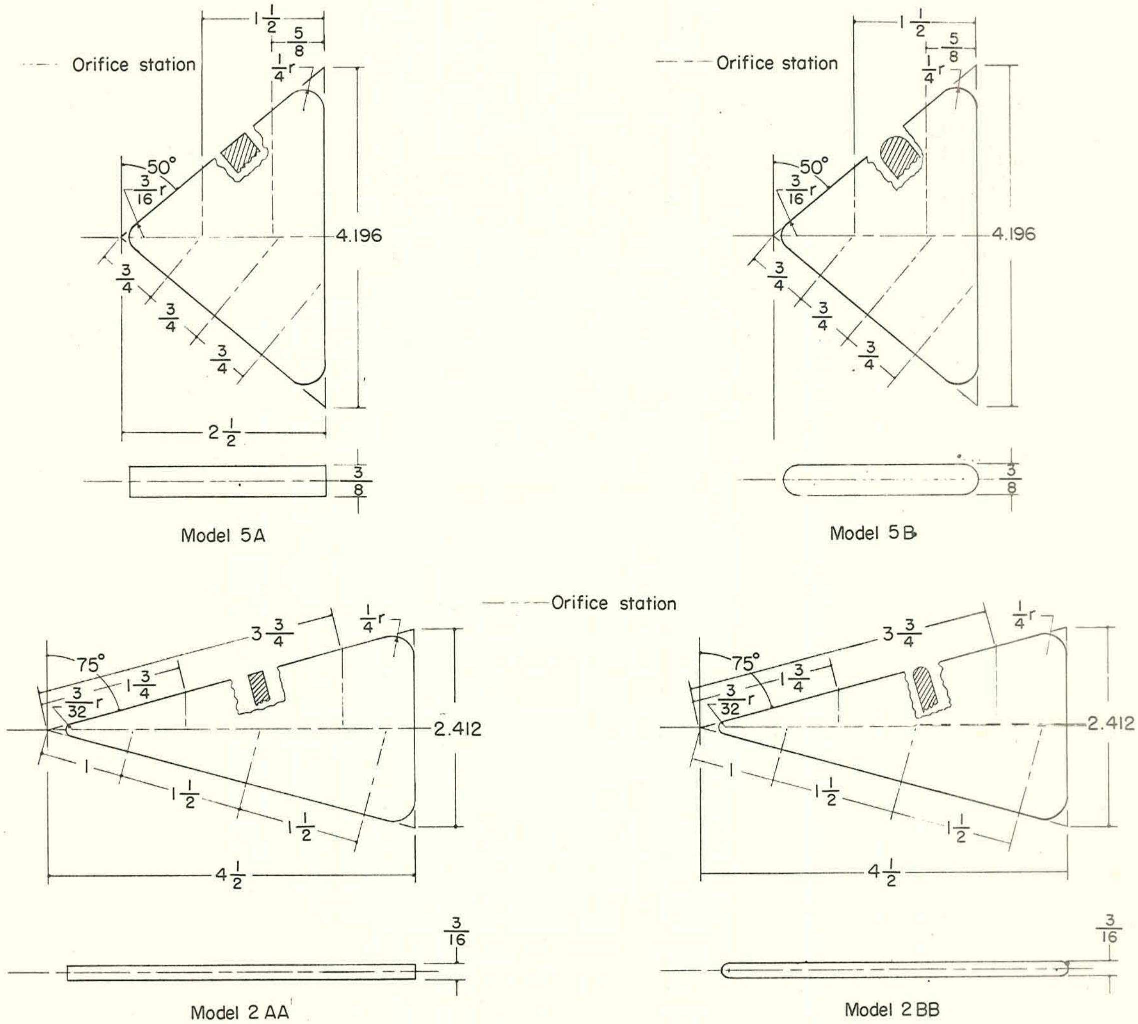

(c) Models 5A, 5B, 2AA, and 2BB.

Figure 1.- Continued.

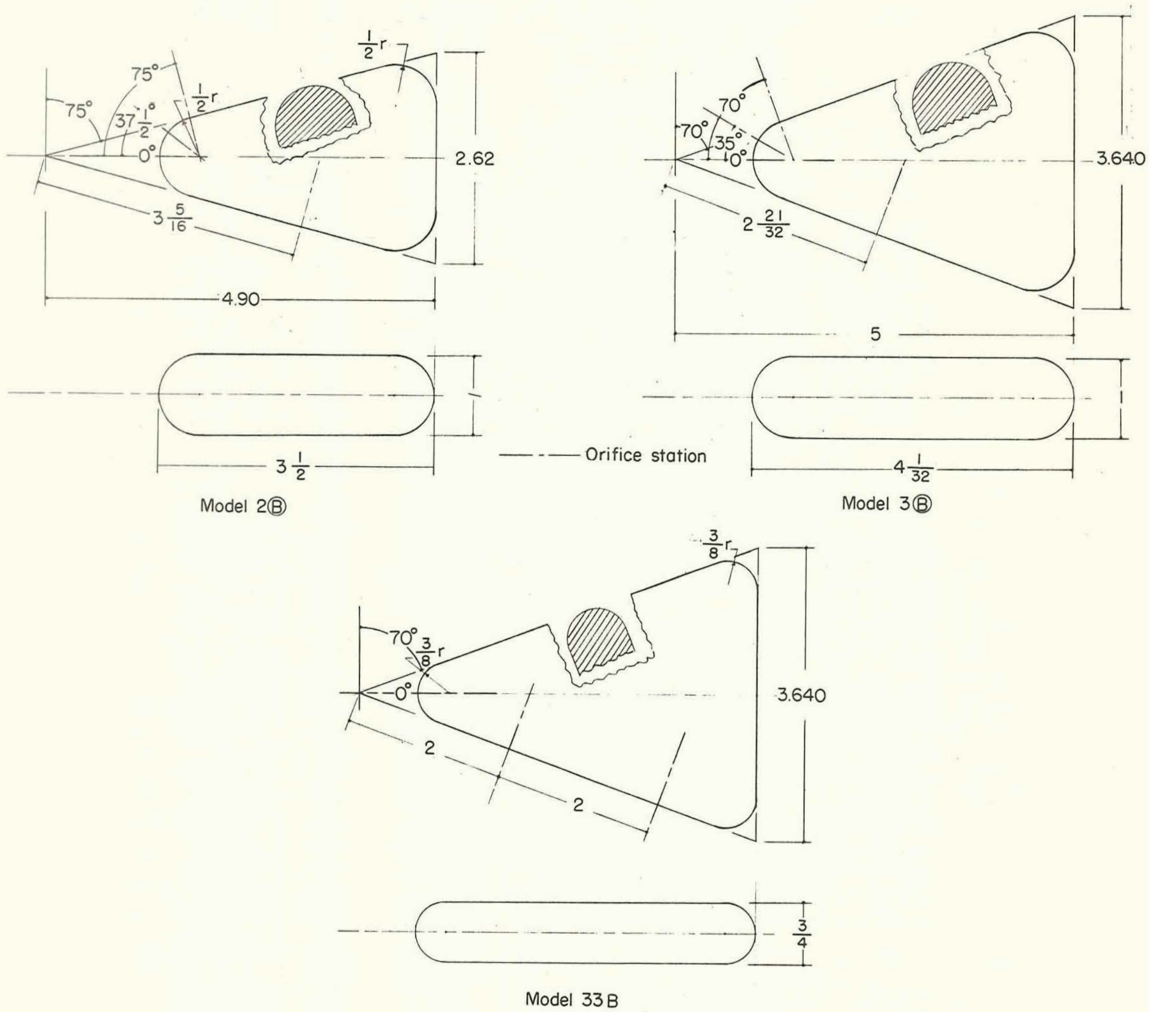

(d) Model 2 Ⓑ , 3 Ⓑ , and 33B.

Figure 1.- Concluded.

L-1552

[redacted]

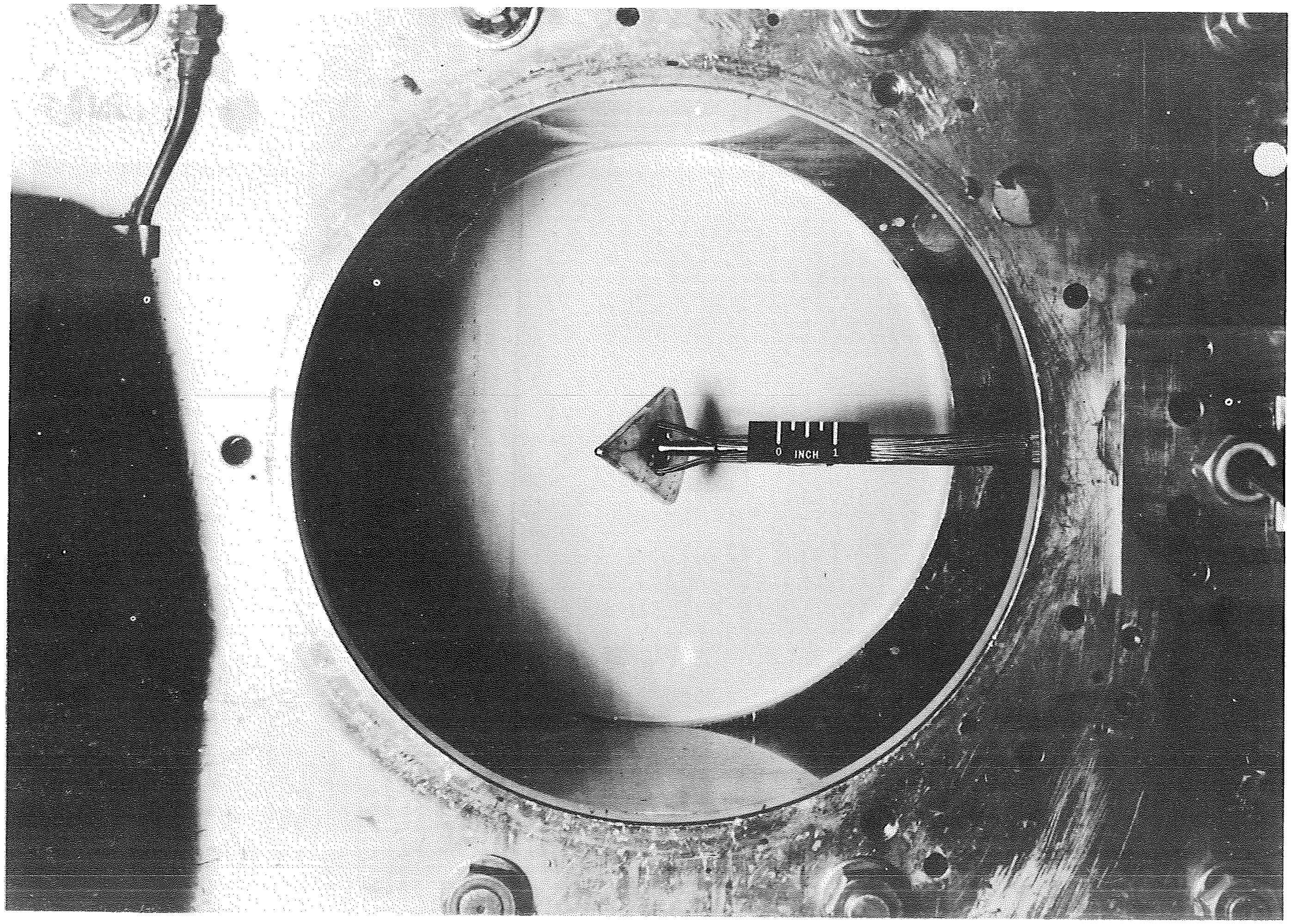

(a) Overall view showing model mounted in test section of wind tunnel. L-59-2617

Figure 2.- Model installed in wind tunnel.

[redacted]

~~CONFIDENTIAL~~

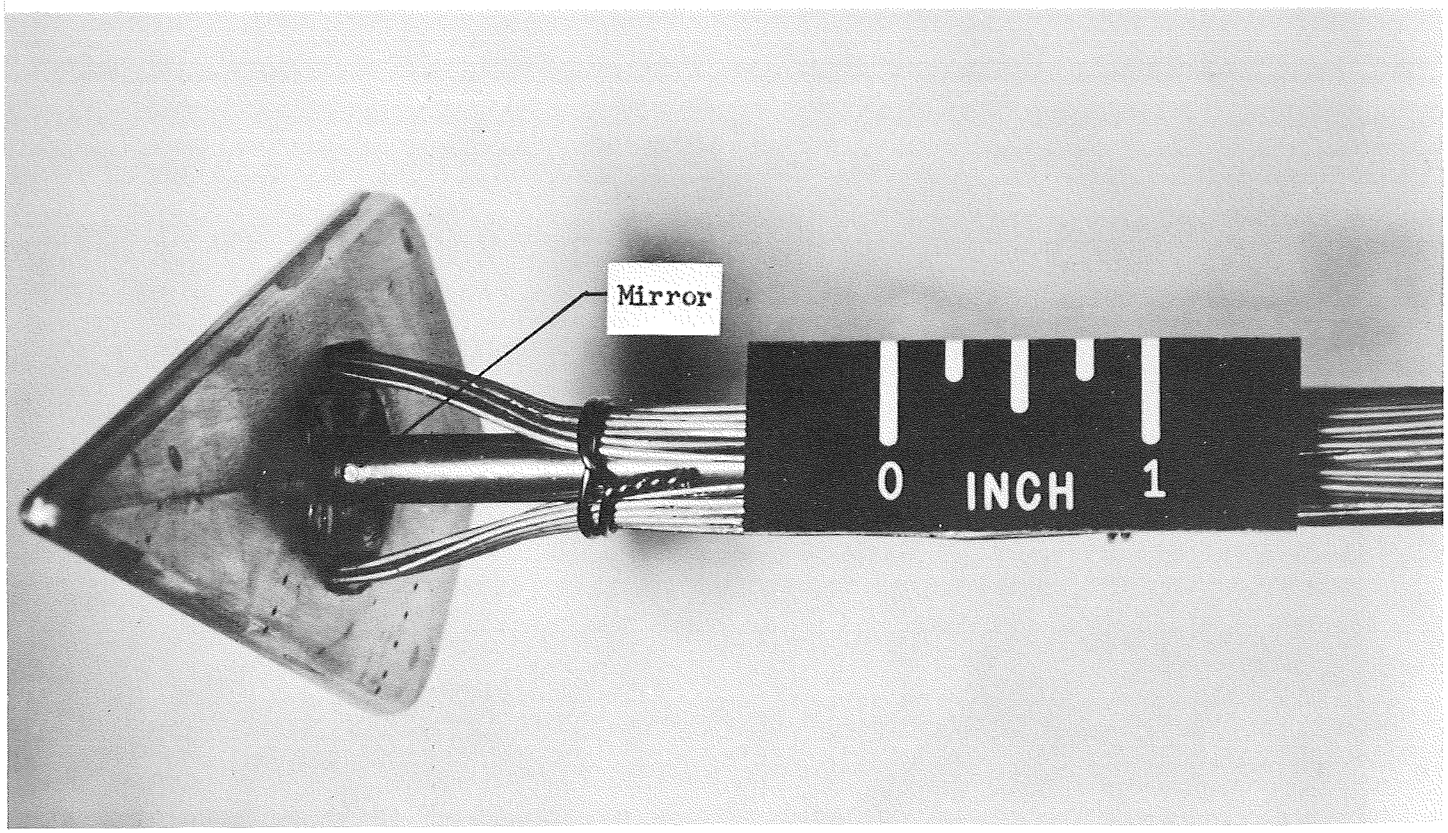

(b) Closeup view of model. L-59-2616.1

Figure 2.- Concluded.

L-1552

~~CONFIDENTIAL~~

L-1552

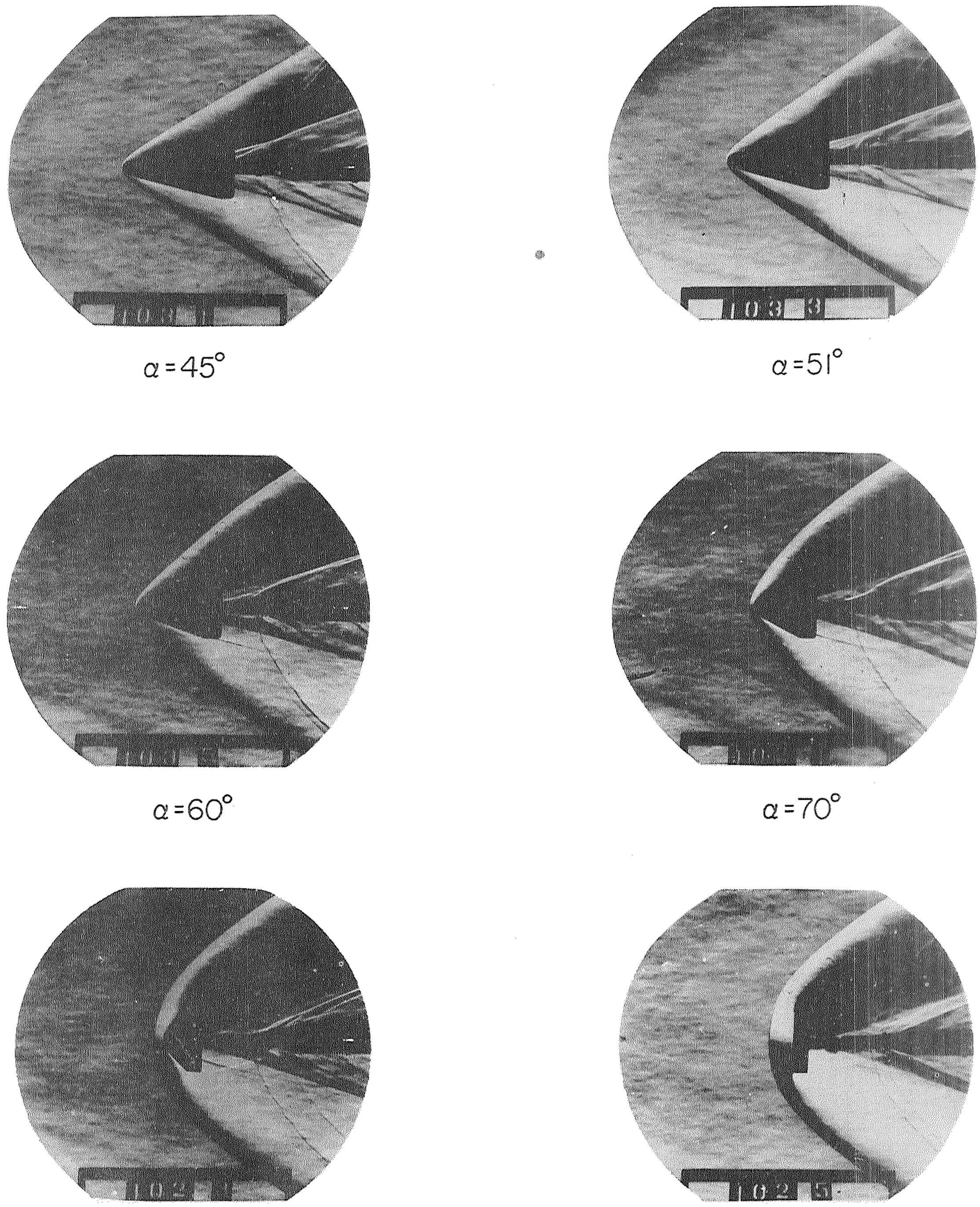

(a) Model 1A.

L-61-7713

Figure 3.- Schlieren photographs of models.

[redacted]

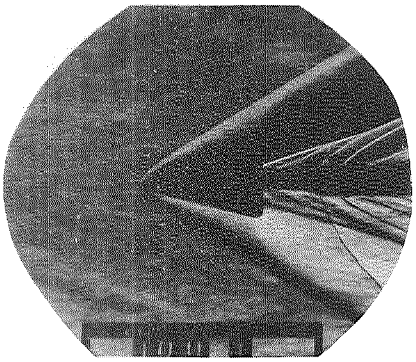

$\alpha = 45°$

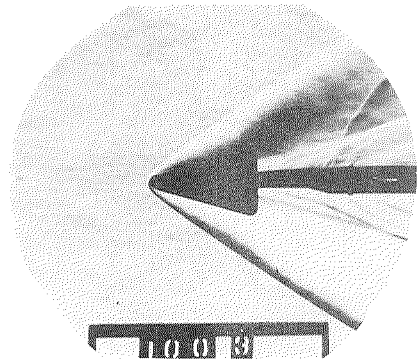

$\alpha = 51°$

L-1552

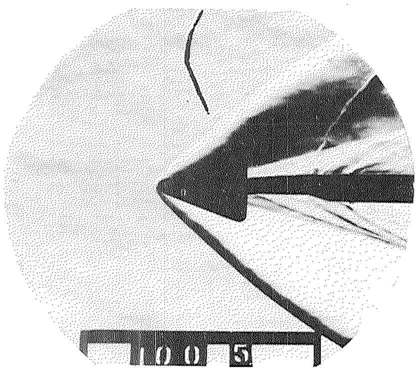

$\alpha = 60°$

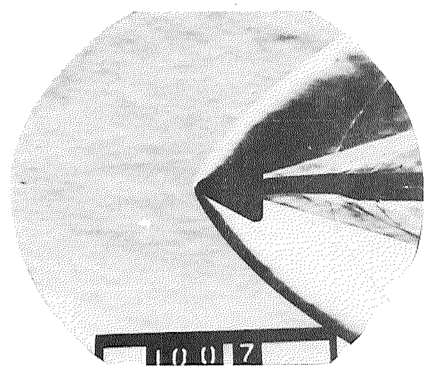

$\alpha = 70°$

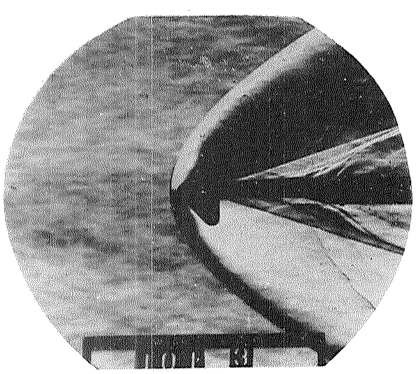

$\alpha = 80°$

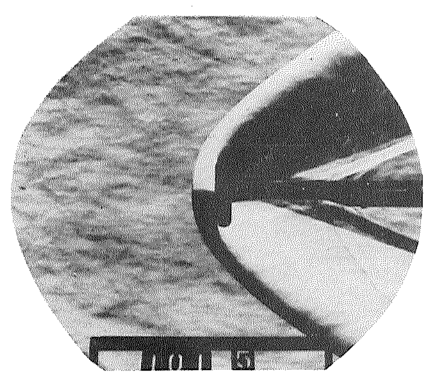

$\alpha = 90°$

(b) Model 1B. L-61-7714

Figure 3.- Continued.

[redacted]

L-1552

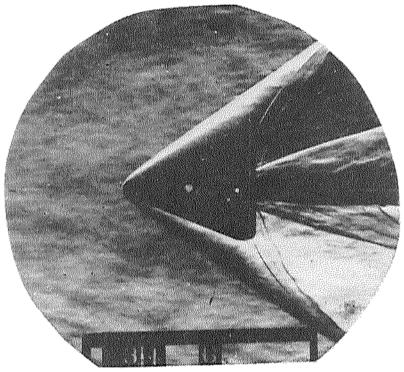

$\alpha = 45°$

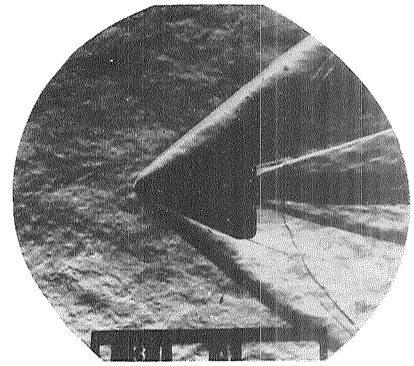

$\alpha = 51°$

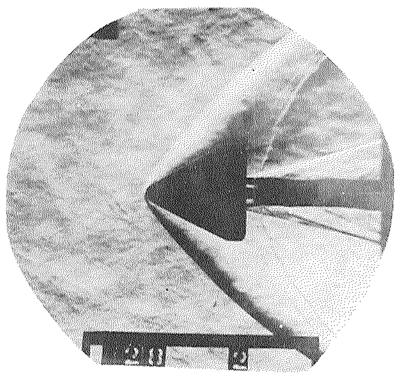

$\alpha = 60°$

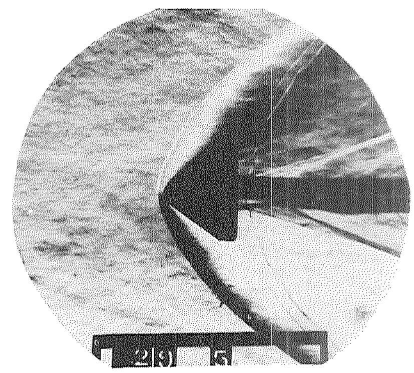

$\alpha = 70°$

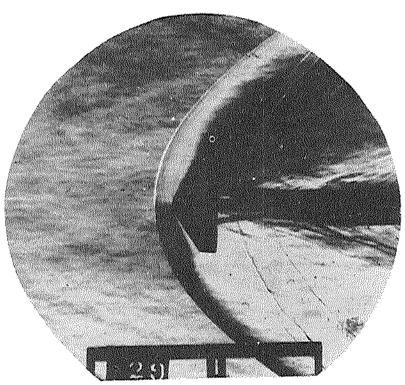

$\alpha = 80°$

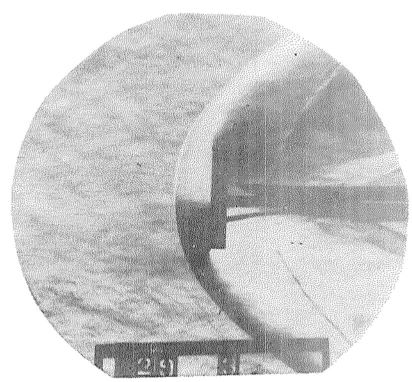

$\alpha = 90°$

(c) Model 2A.

L-61-7715

Figure 3.- Continued.

[redacted]

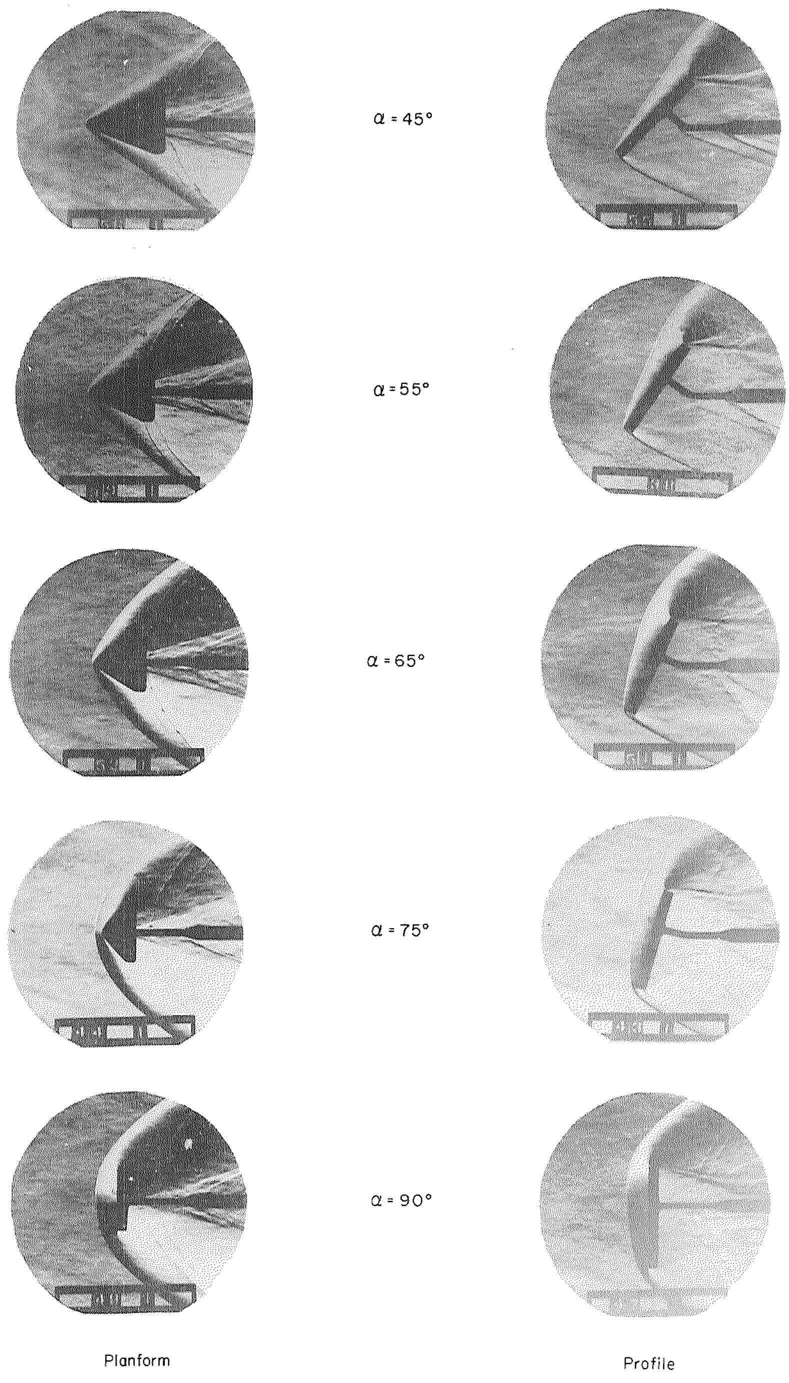

L-1552

(c) Model 2A - Concluded. L-61-7716

Figure 3.- Continued.

[redacted]

L-1552

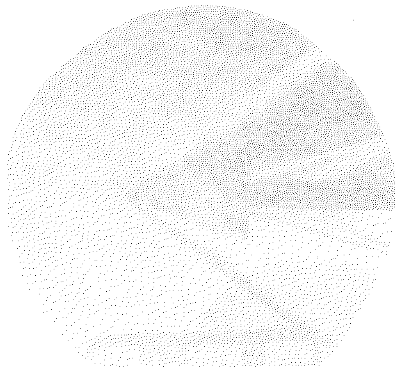

$\alpha = 48°$

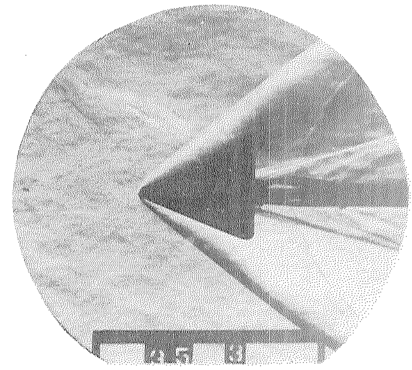

$\alpha = 51°$

$\alpha = 60°$

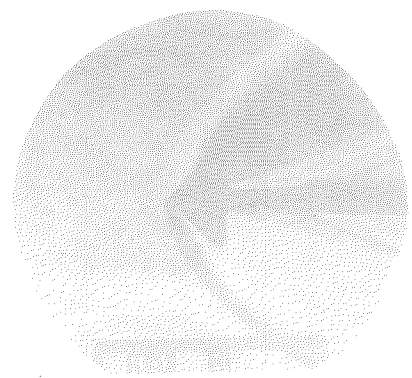

$\alpha = 75°$

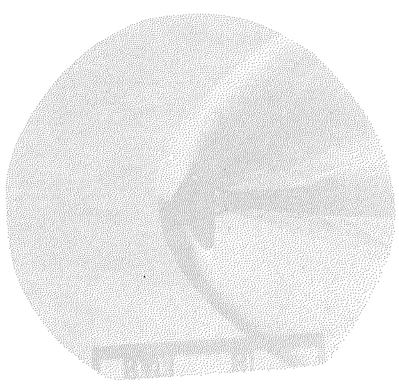

$\alpha = 80°$

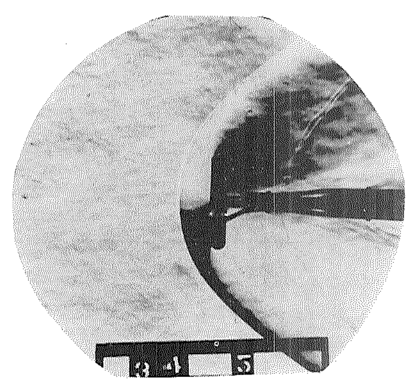

$\alpha = 90°$

(d) Model 2B.

L-61-7717

Figure 3.- Continued.

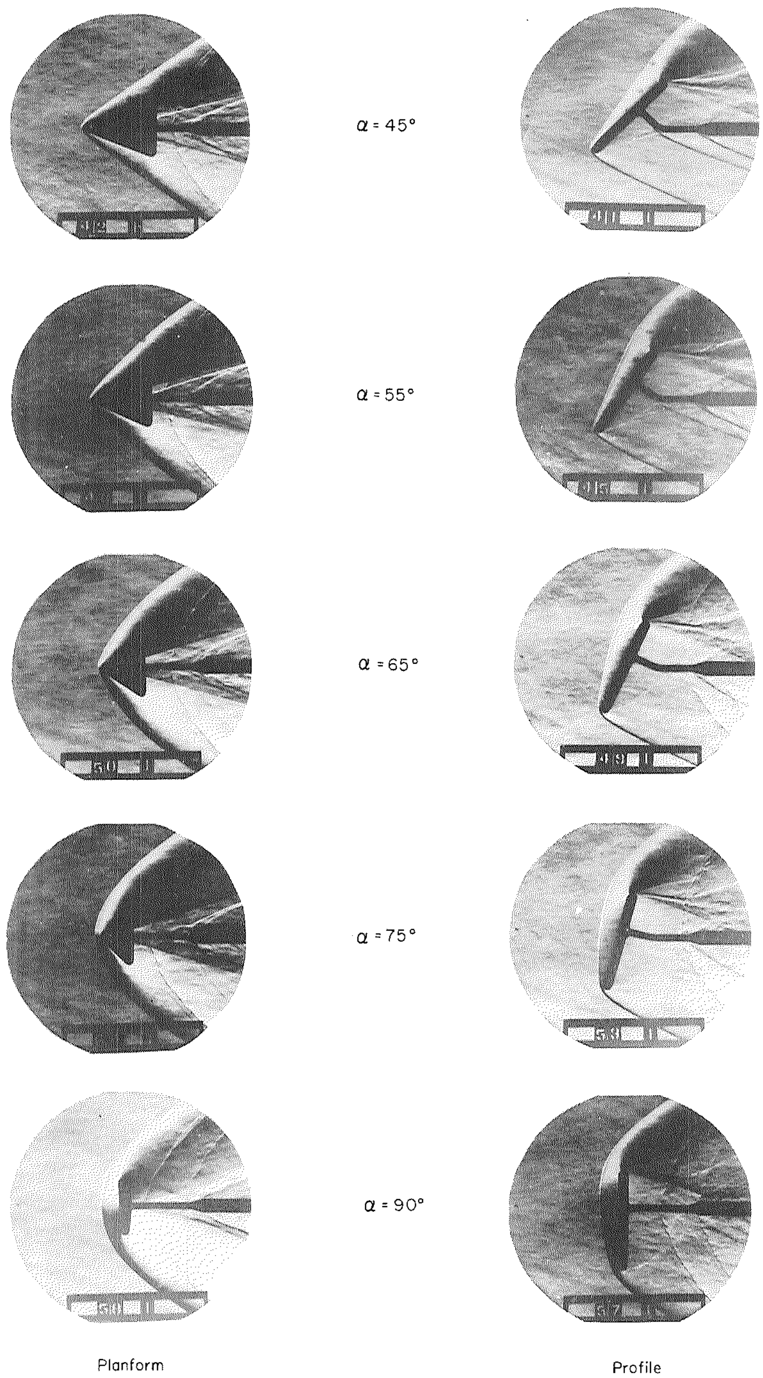

L-1552

(d) Model 2B - Concluded. L-61-7718

Figure 3.- Continued.

L-1552

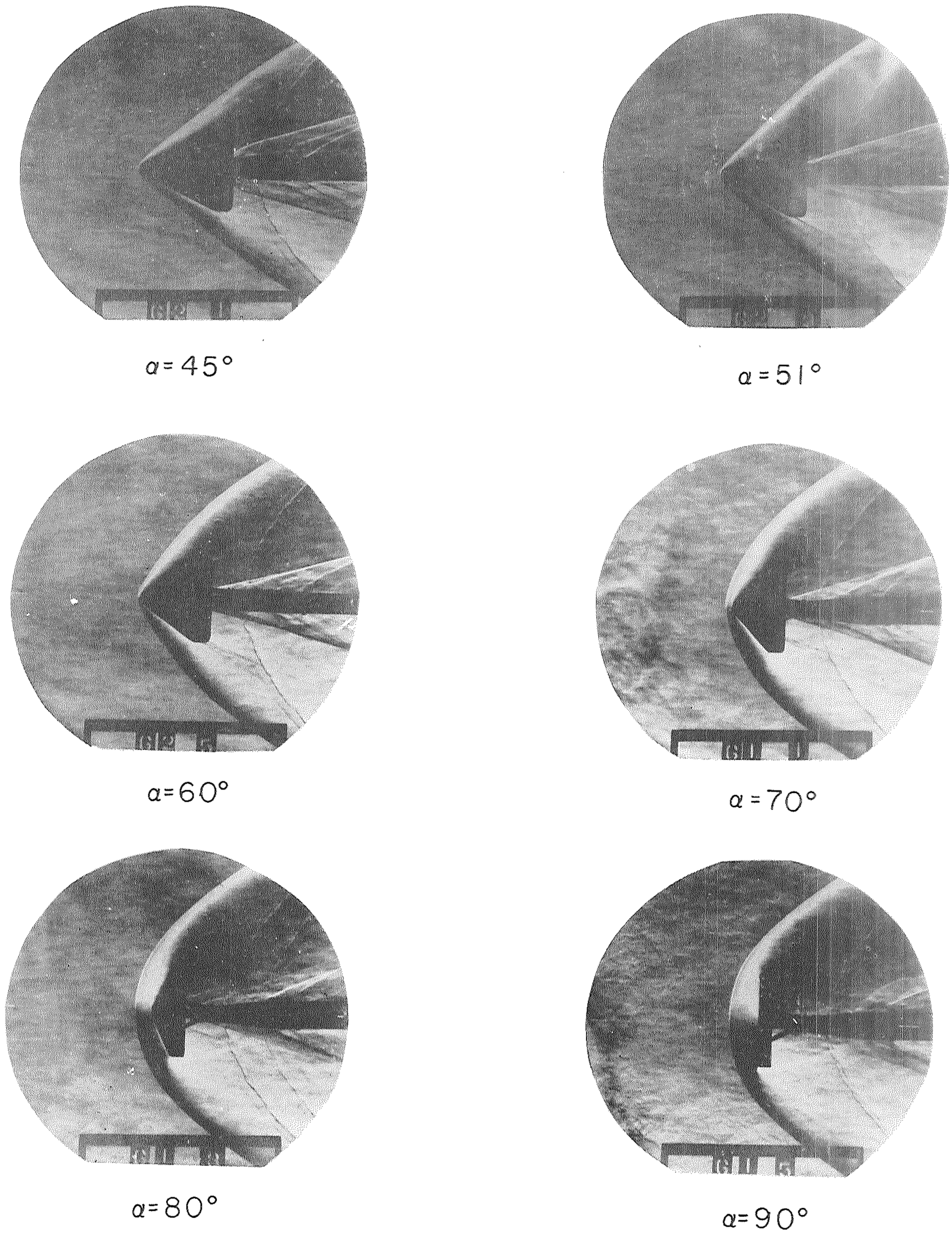

(e) Model 3A. L-61-7719

Figure 3.- Continued.

[redacted]

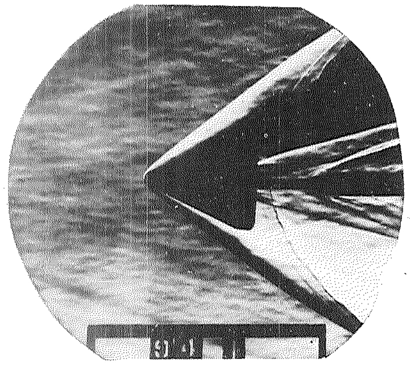

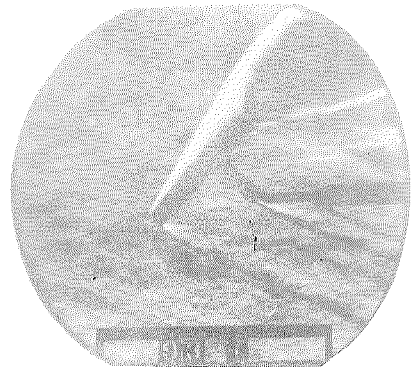

Planform α=45° Profile

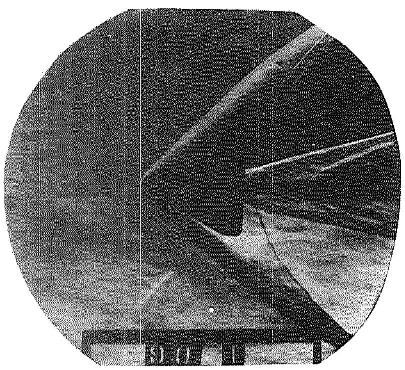

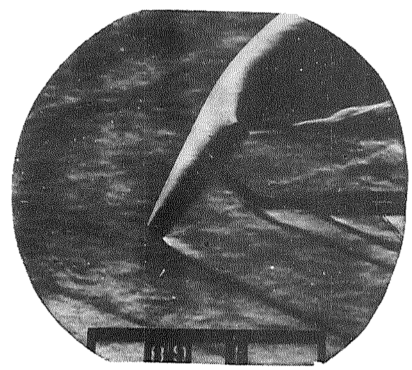

Planform α=51° Profile

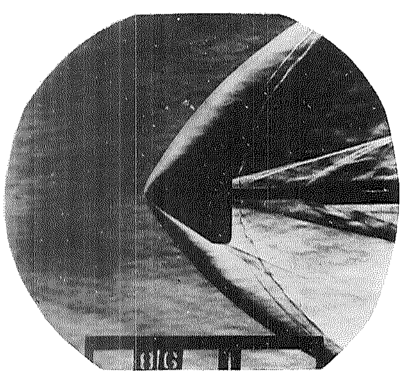

Planform α=60° Profile

Schlieren Model

(e) Model 3A - Continued. L-61-7720

Figure 3.- Continued.

L-1552

[redacted]

L-1552

Planform

Profile

$\alpha = 70°$

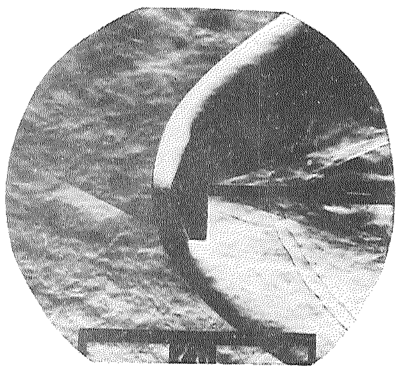

Planform

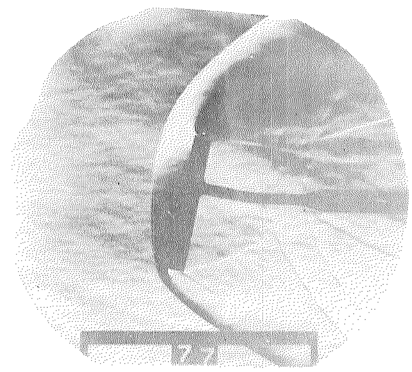

Profile

$\alpha = 80°$

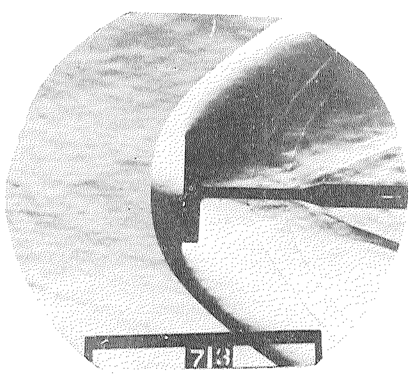

Planform

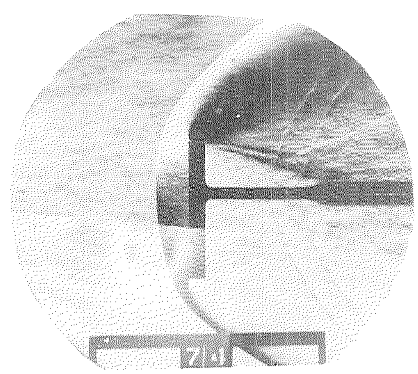

Profile

$\alpha = 90°$

Schlieren Model

(e) Model 3A - Concluded.

L-61-7721

Figure 3.- Continued.

[redacted]

$\alpha = 45°$

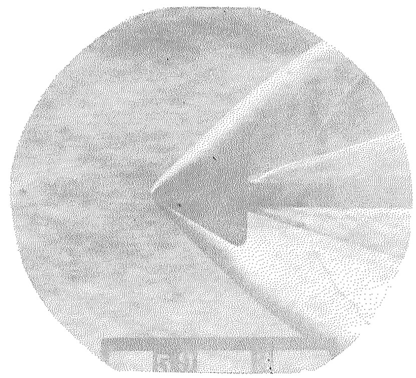

$\alpha = 51°$

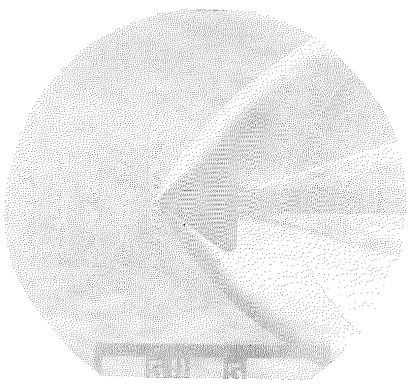

$\alpha = 60°$

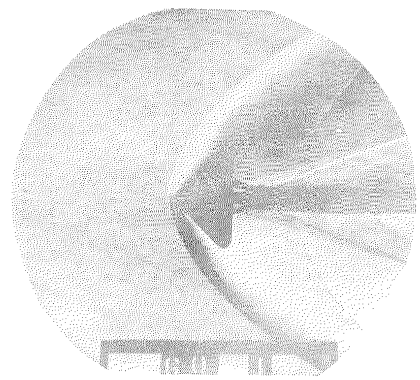

$\alpha = 70°$

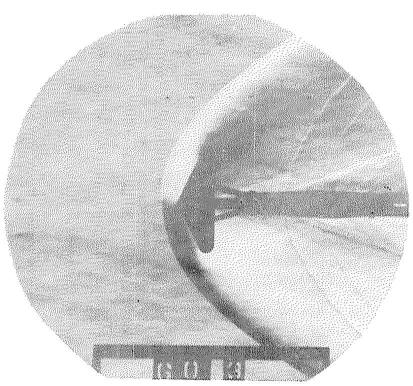

$\alpha = 80°$

$\alpha = 90°$

(f) Model 3B. L-61-7722

Figure 3.- Continued.

L-1552

[redacted]

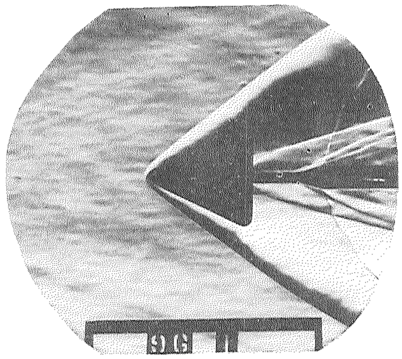
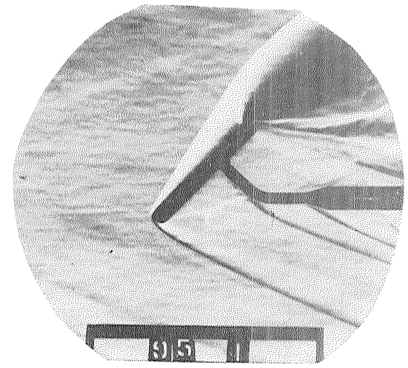

Planform $\alpha = 45°$ Profile

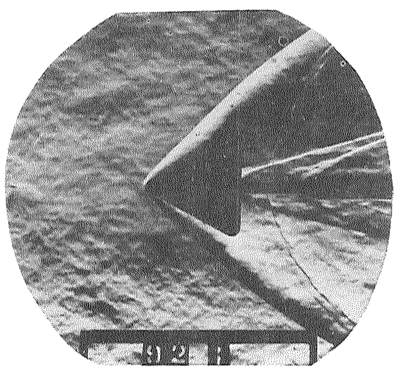
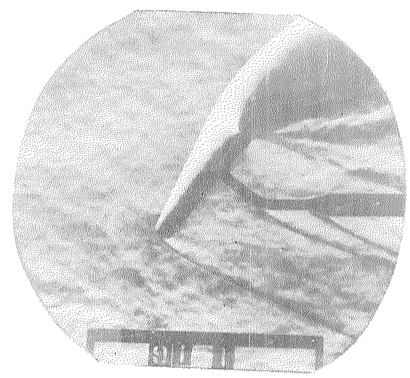

Planform $\alpha = 51°$ Profile

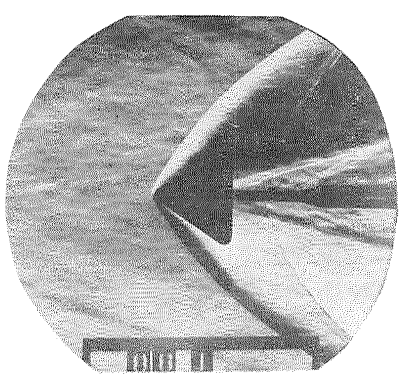
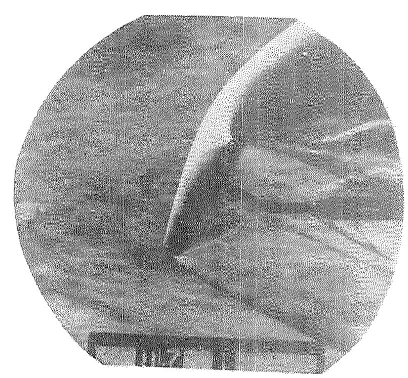

Planform $\alpha = 60°$ Profile

Schlieren Model

(f) Model 3B - Continued. L-61-7723

Figure 3.- Continued.

[redacted]

Planform

$\alpha = 70°$

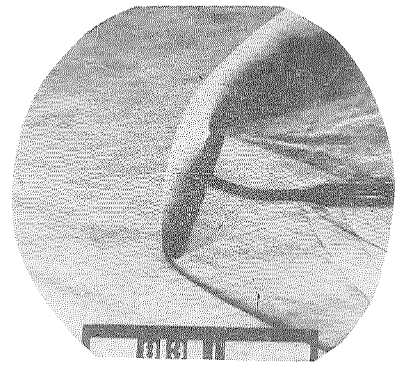

Profile

L-1552

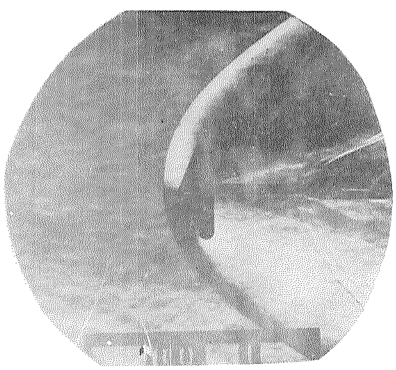

Planform

$\alpha = 80°$

Profile

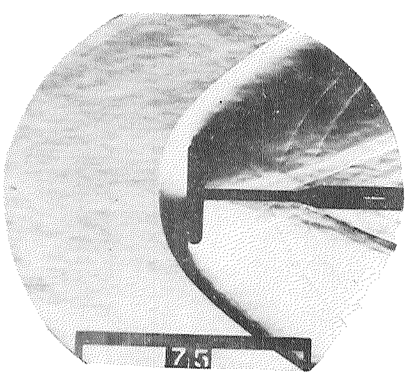

Planform

$\alpha = 90°$

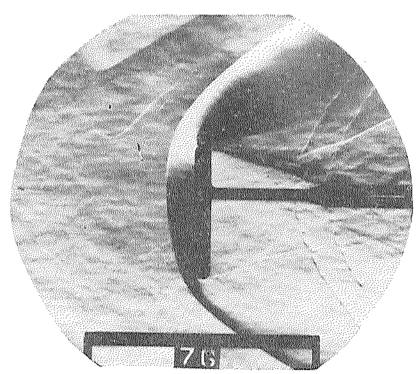

Profile

Schlieren Model

(f) Model 3B - Concluded. L-61-7724

Figure 3.- Continued.

[redacted]

L-1552

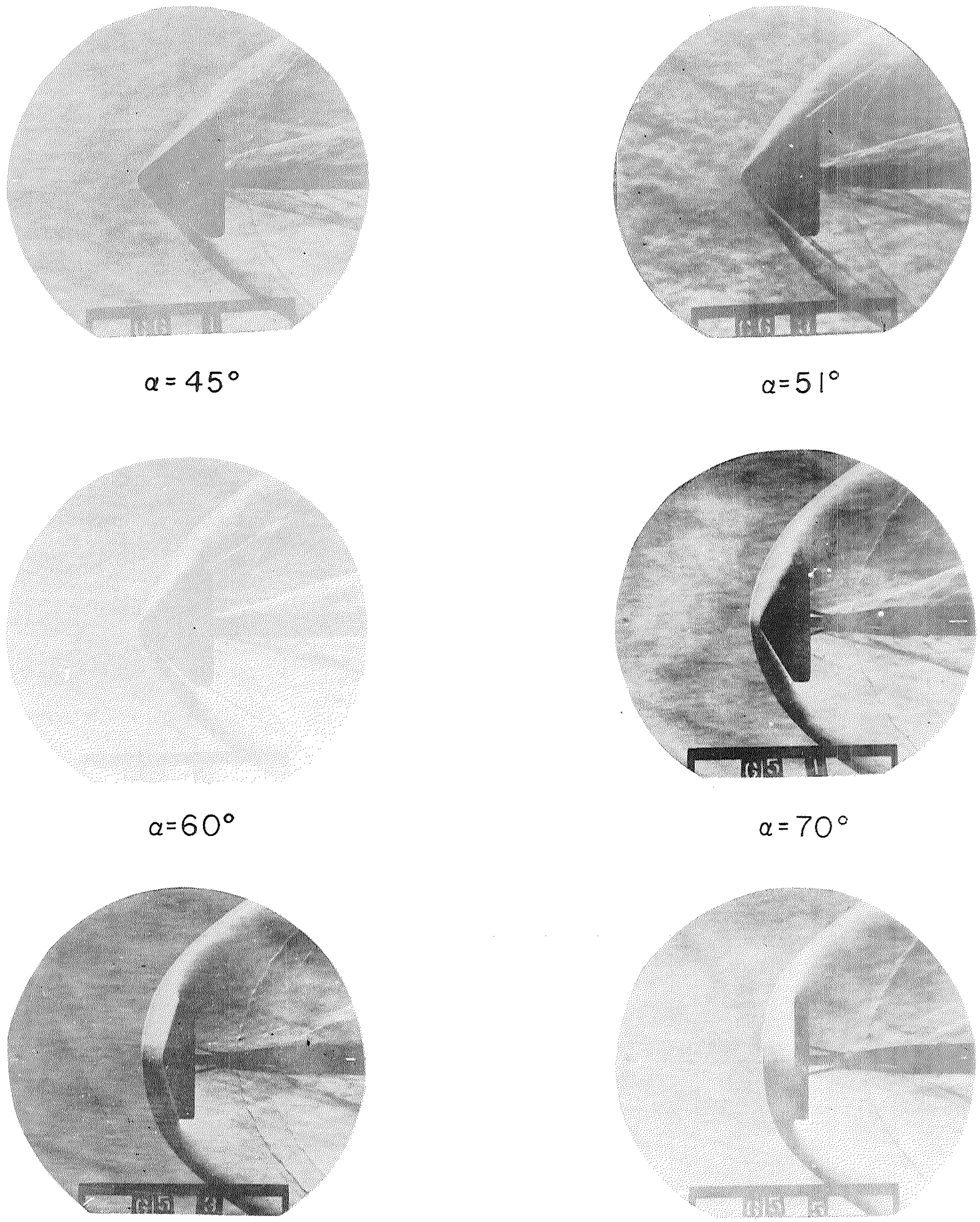

α = 45°

α = 51°

α = 60°

α = 70°

α = 80°

α = 90°

(g) Model 4A. L-61-7725

Figure 3.- Continued.

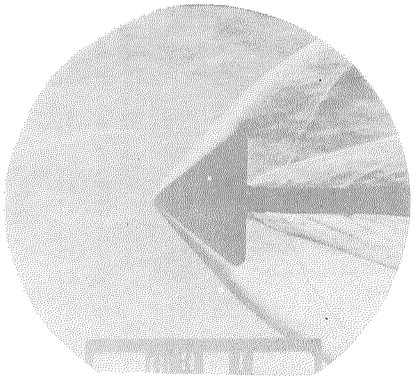

$\alpha = 45°$

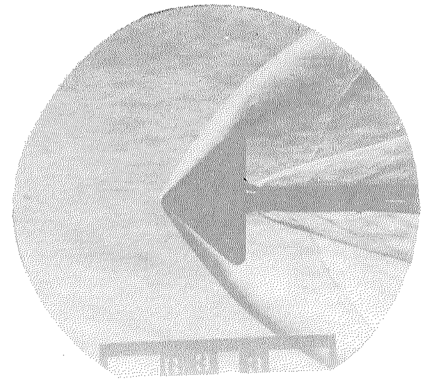

$\alpha = 51°$

L-1552

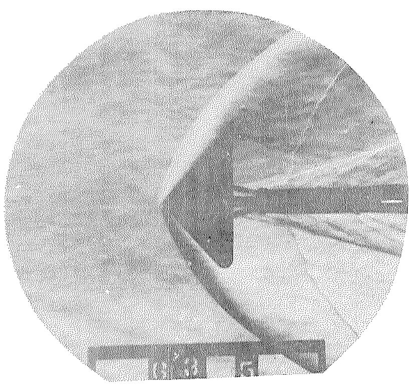

$\alpha = 60°$

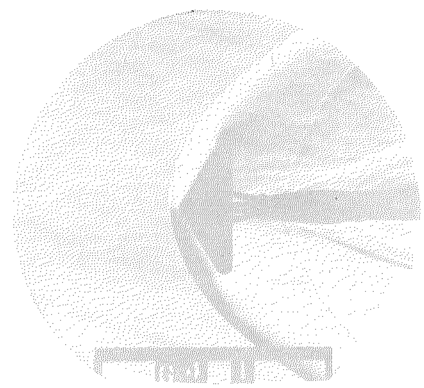

$\alpha = 70°$

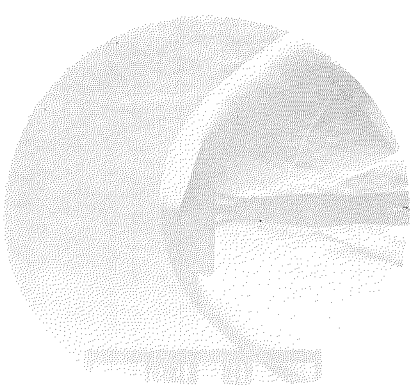

$\alpha = 80°$

$\alpha = 90°$

(h) Model 4B. L-61-7726

Figure 3.- Continued.

L-1552

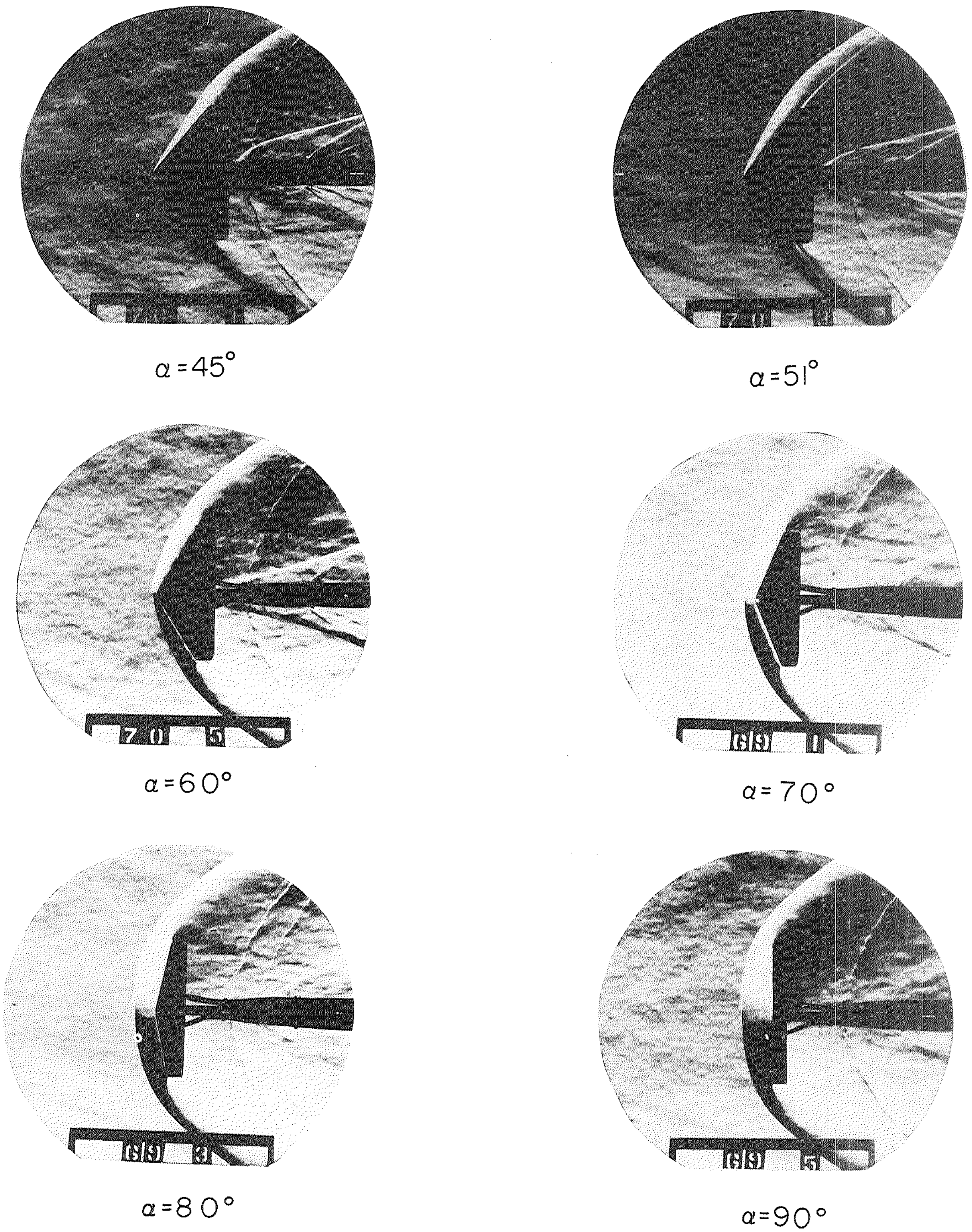

(i) Model 5A. L-61-7727

Figure 3.- Continued.

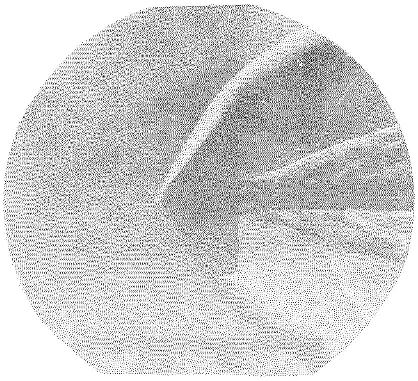

α = 45°

α = 51°

L-1552

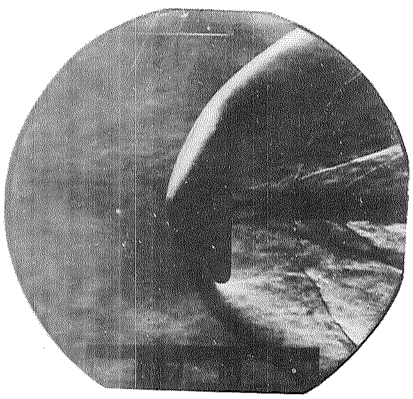

α = 60°

α = 70°

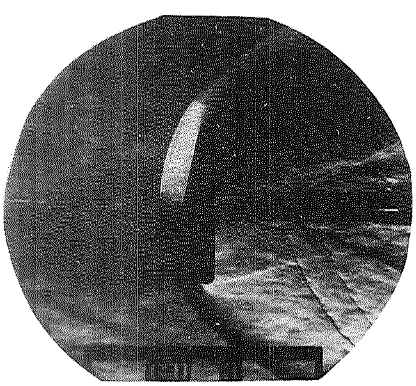

α = 80°

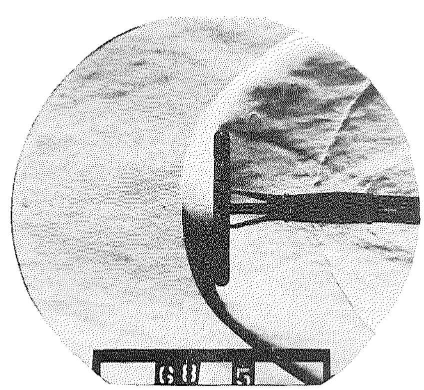

α = 90°

(j) Model 5B.

L-61-7728

Figure 3.- Continued.

L-1552

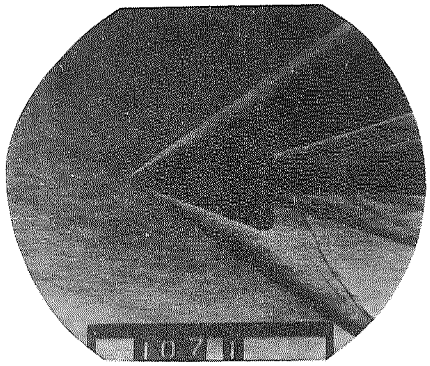

$\alpha = 45°$

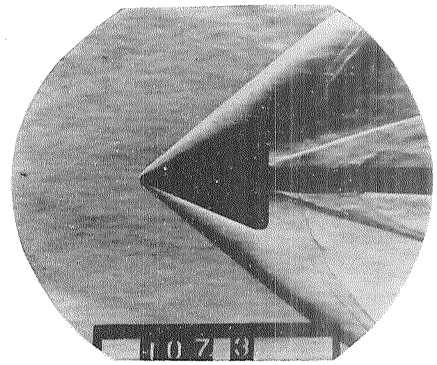

$\alpha = 51°$

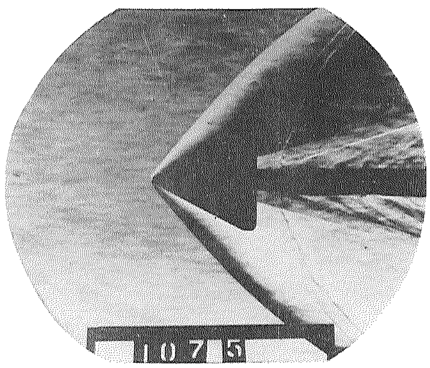

$\alpha = 60°$

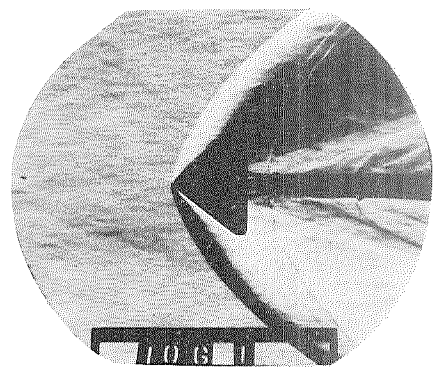

$\alpha = 70°$

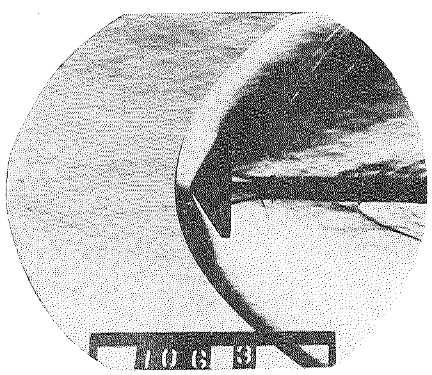

$\alpha = 80°$

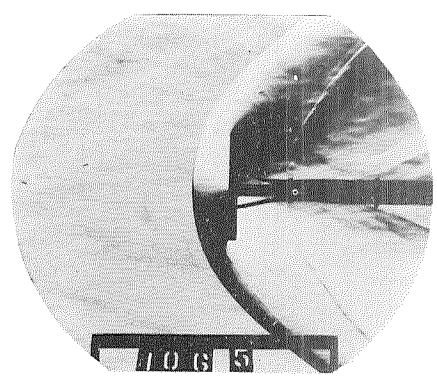

$\alpha = 90°$

(k) Model 2AA.

L-61-7729

Figure 3.- Continued.

[redacted]

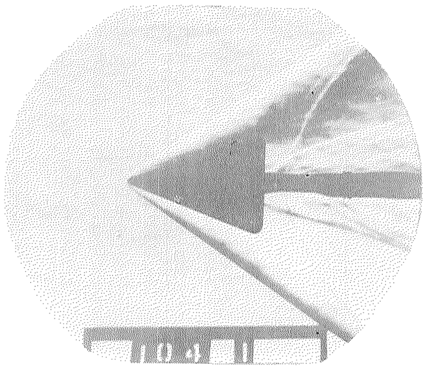

$\alpha = 45°$

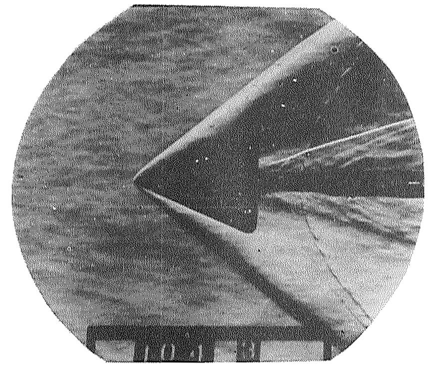

$\alpha = 51°$

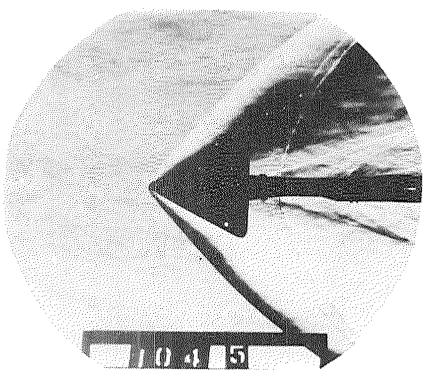

$\alpha = 60°$

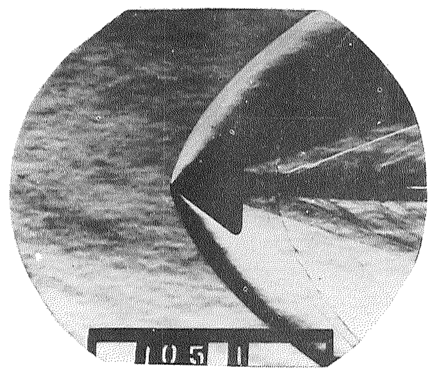

$\alpha = 70°$

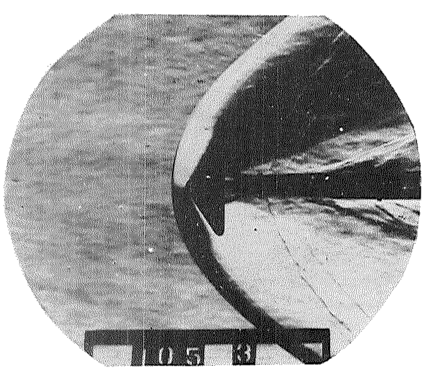

$\alpha = 80°$

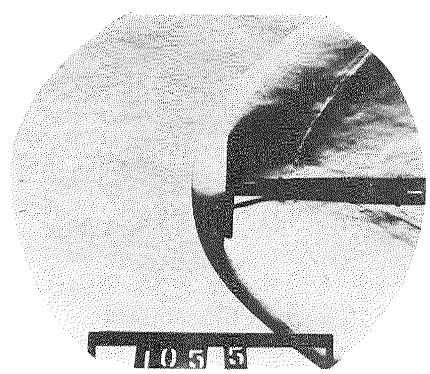

$\alpha = 90°$

(l) Model 2BB.

L-61-7730

Figure 3.- Continued.

L-1552

[redacted]

L-1552

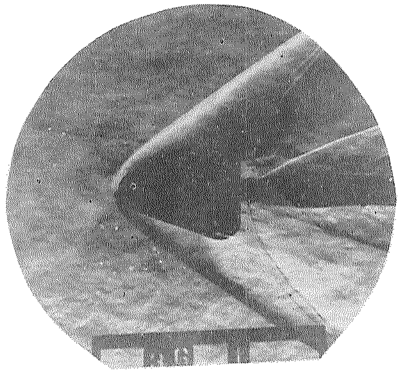

$\alpha = 45°$

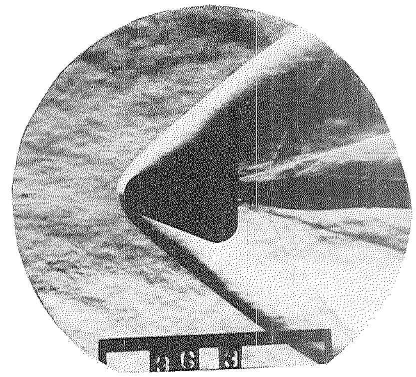

$\alpha = 51°$

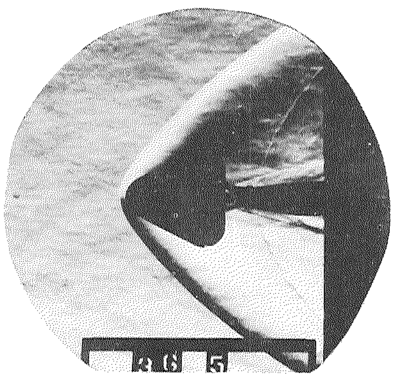

$\alpha = 60°$

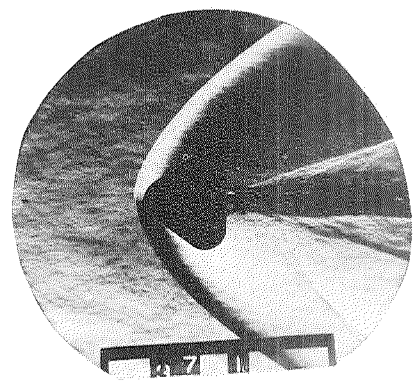

$\alpha = 70°$

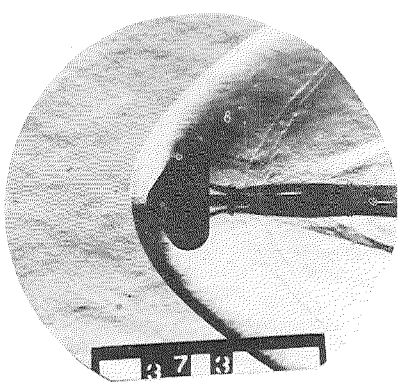

$\alpha = 80°$

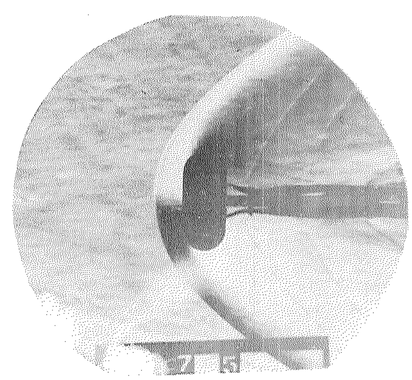

$\alpha = 90°$

(m) Model 2 B . L-61-7731

Figure 3.- Continued.

[redacted]

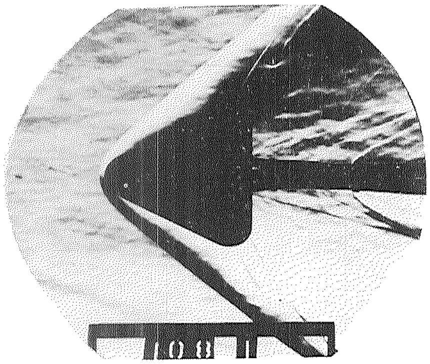

α = 45°

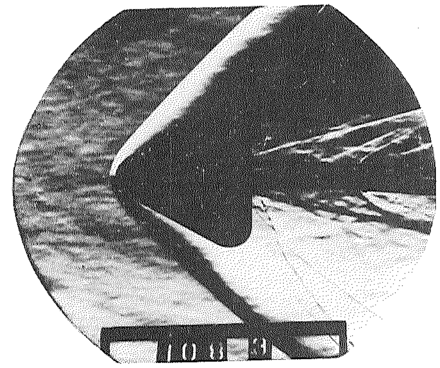

α = 51°

L-1552

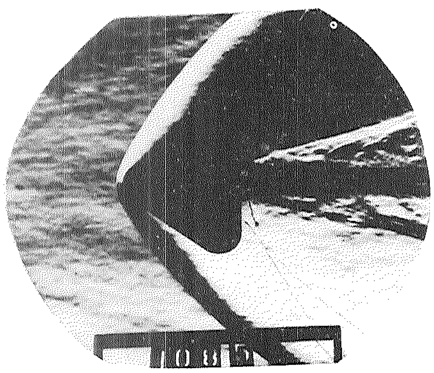

α = 60°

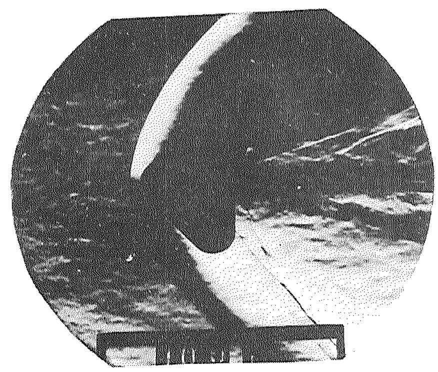

α = 70°

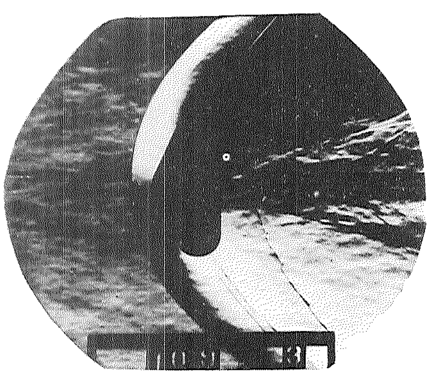

α = 80°

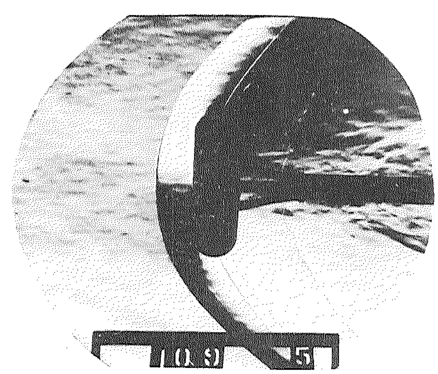

α = 90°

(n) Model 3Ⓑ. L-61-7732

Figure 3.- Continued.

[redacted]

L-1552

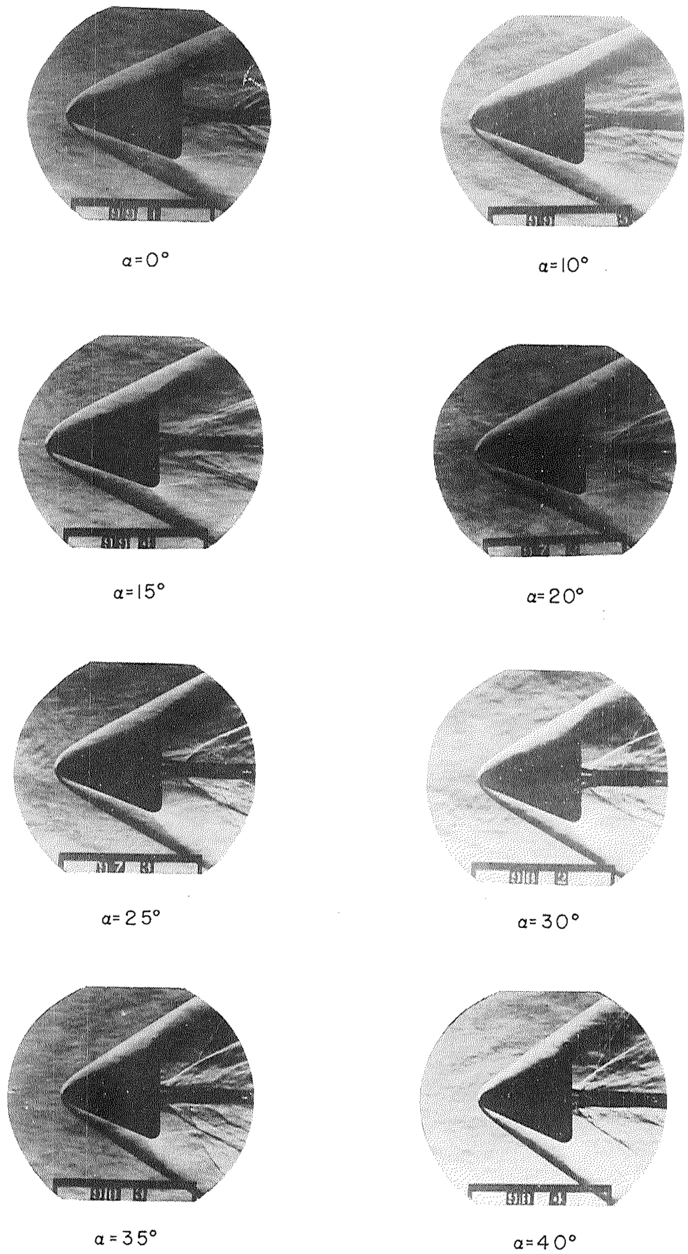

(o) Model 33B. L-61-7733 A

Figure 3.- Concluded.

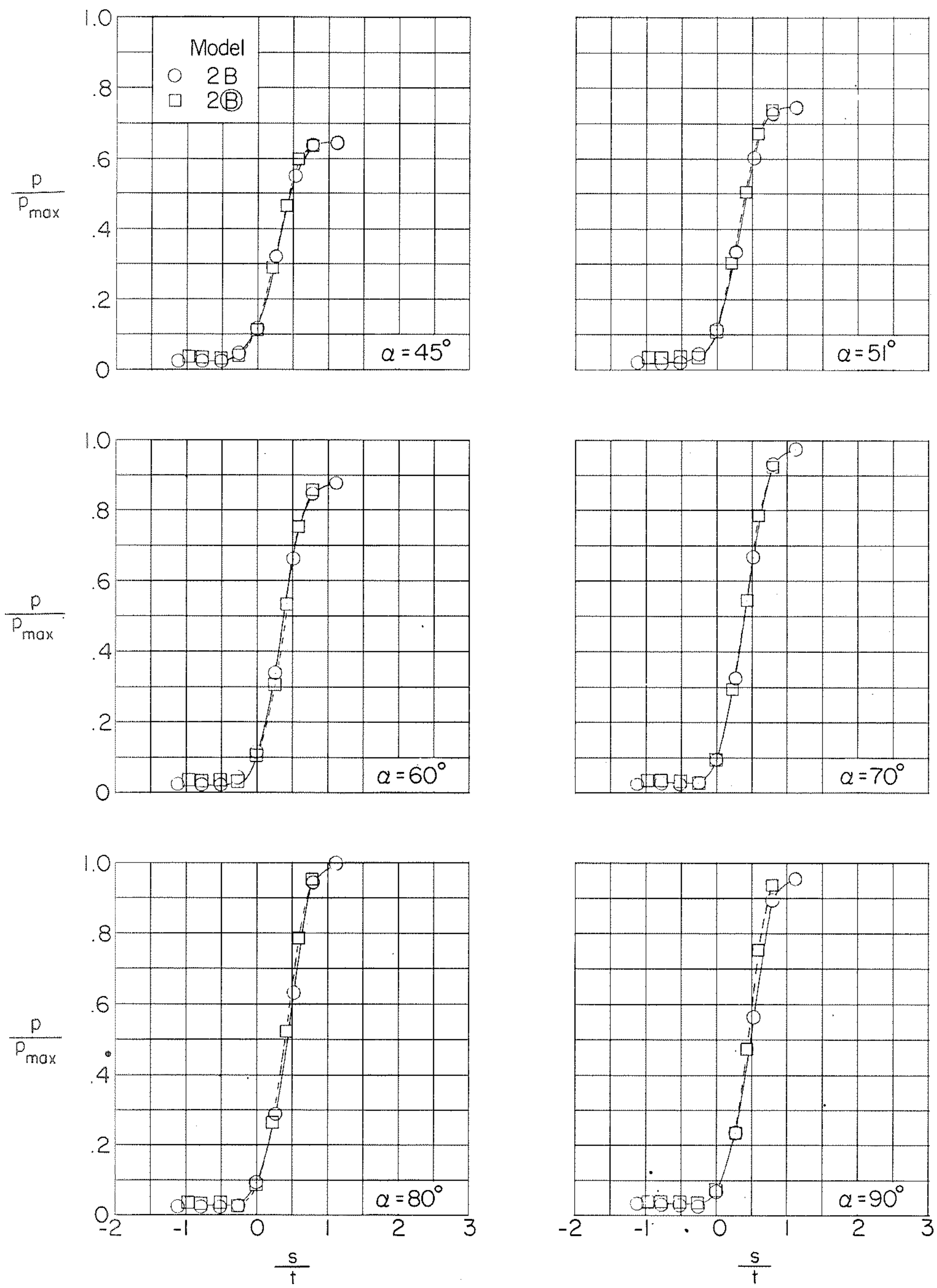

(a) Models 2B and 2Ⓑ; $l/t = 2.1$.

Figure 4.- Comparison of the pressure distributions obtained on two of the round-leading-edge models of different sizes.

L-1552

L-1552

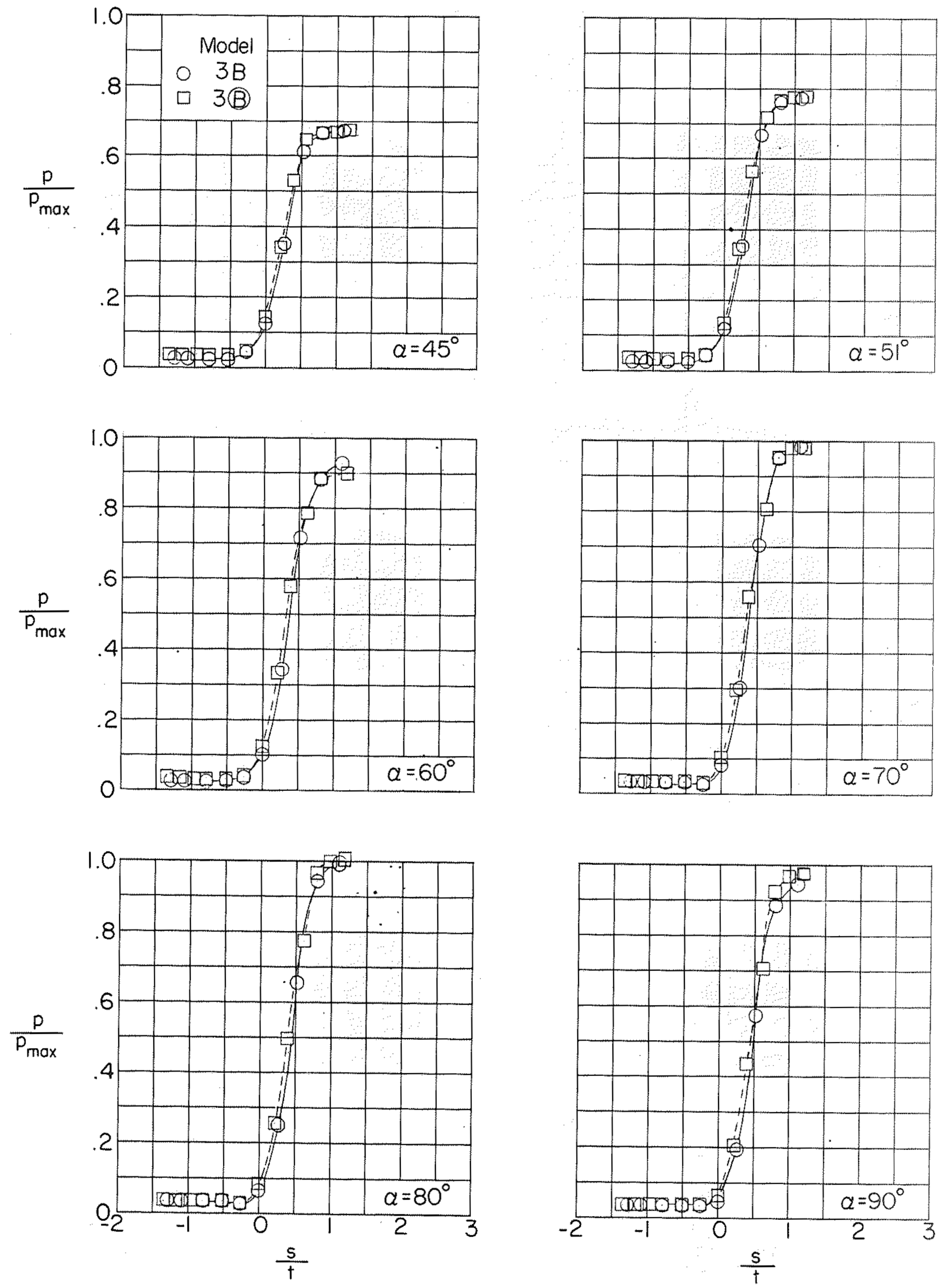

(b) Models 3B and 3Ⓑ; $l/t = 1.9$.

Figure 4.- Concluded.

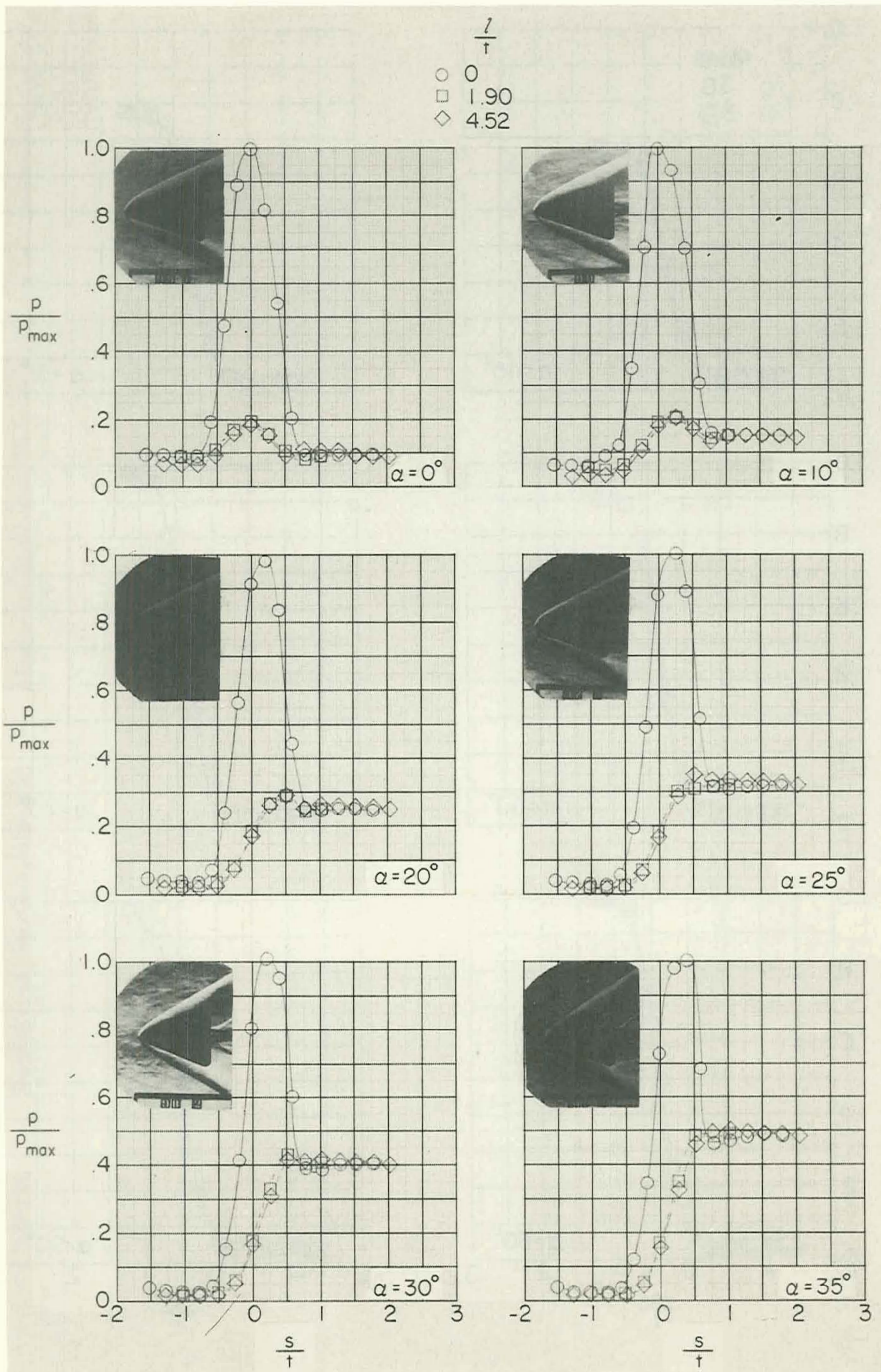

L-1552

Figure 5.- Pressure distributions obtained on a typical round-leading-edge model in the angle-of-attack range from 0° to 35°. Model 33B; $\Lambda = 70^{\circ}$.

L-1552

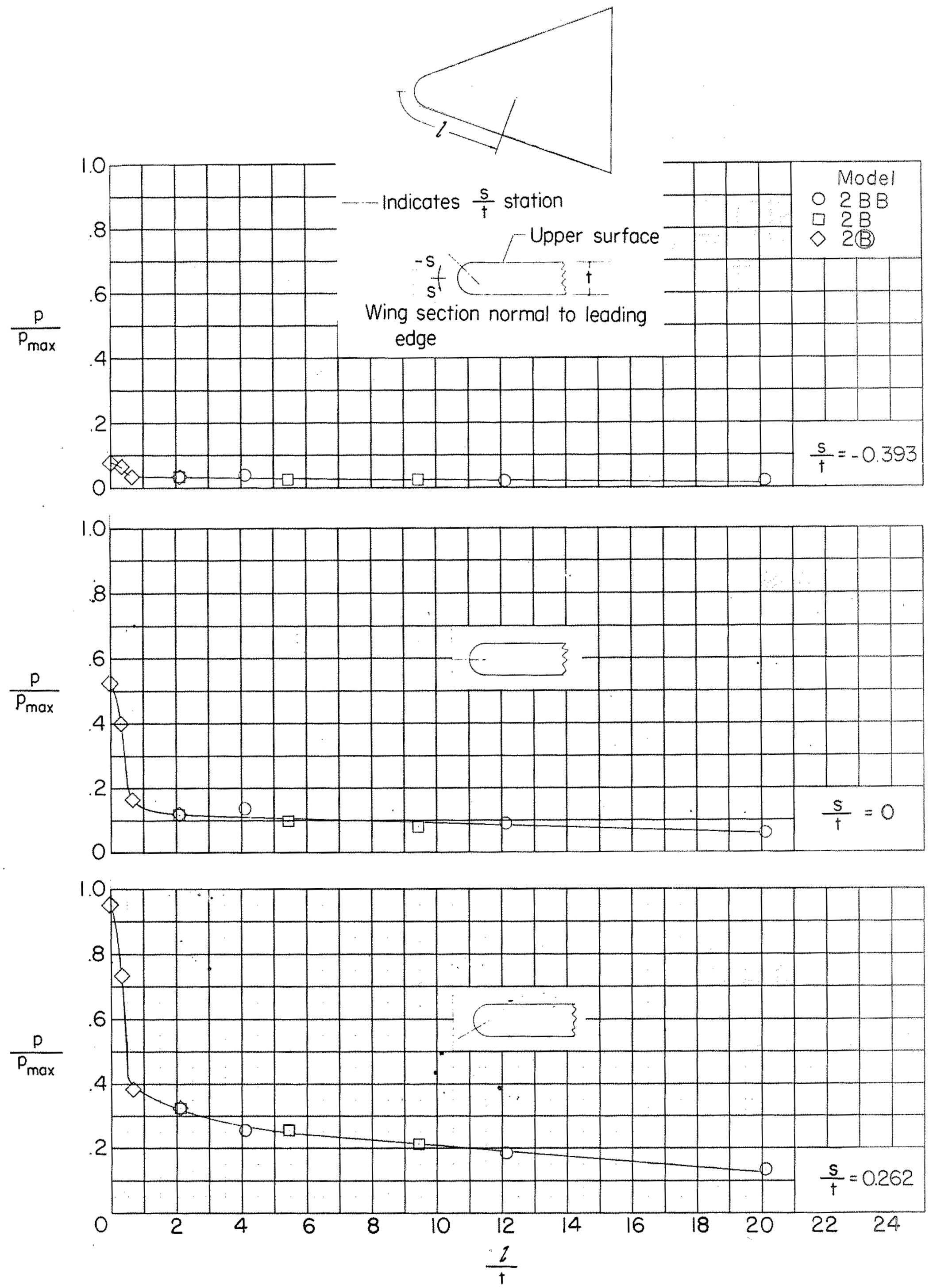

(a) $\alpha = 45^{\circ}$.

Figure 6.- Pressure distributions obtained on round-leading-edge wings showing the general effects of l/t location on wing pressure at high angles of attack. $\Lambda = 75^{\circ}$.

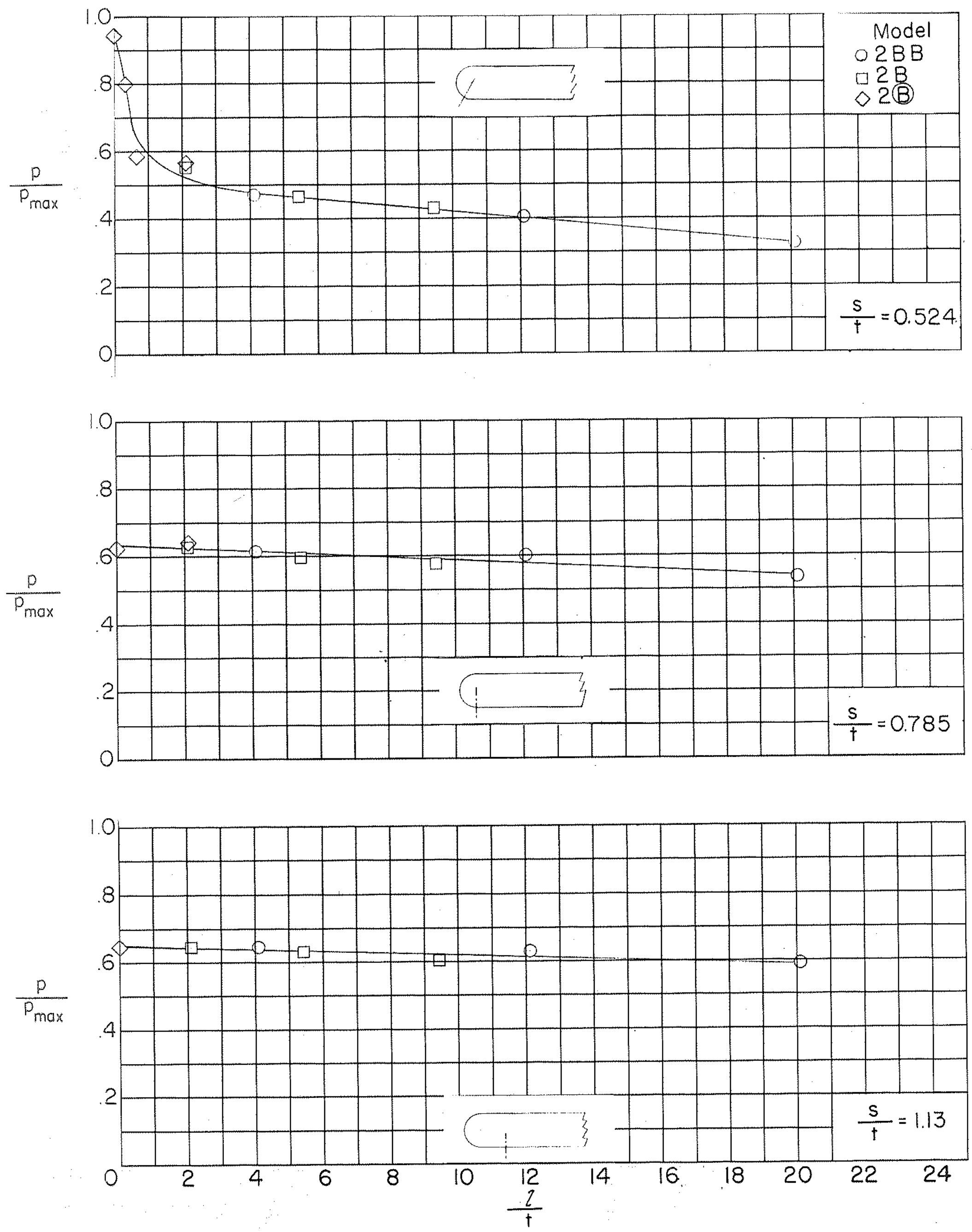

(a) Concluded.

Figure 6.- Continued.

L-1552

L-1552

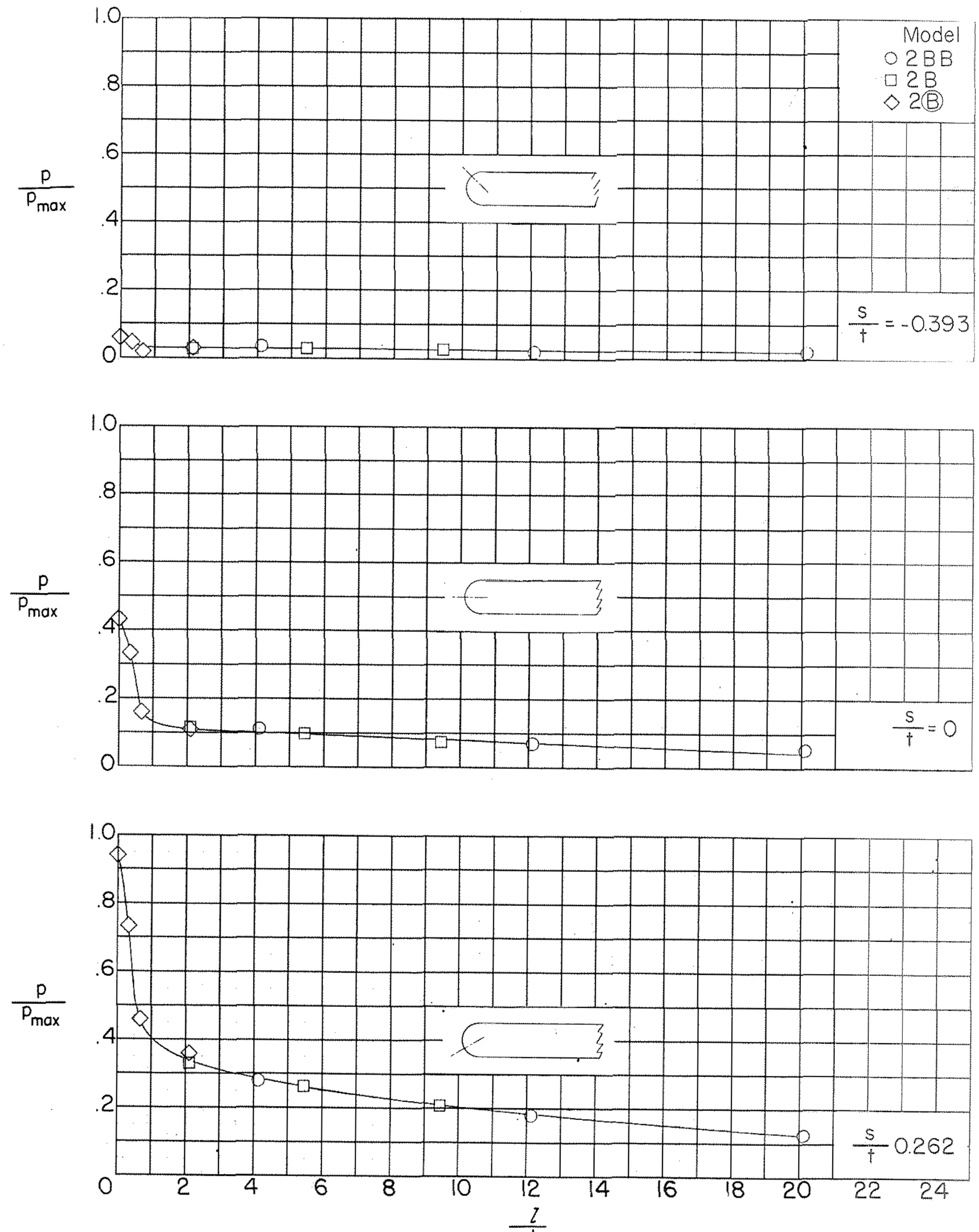

(b) $\alpha = 51^\circ$.

Figure 6.- Continued.

CONFIDENTIAL

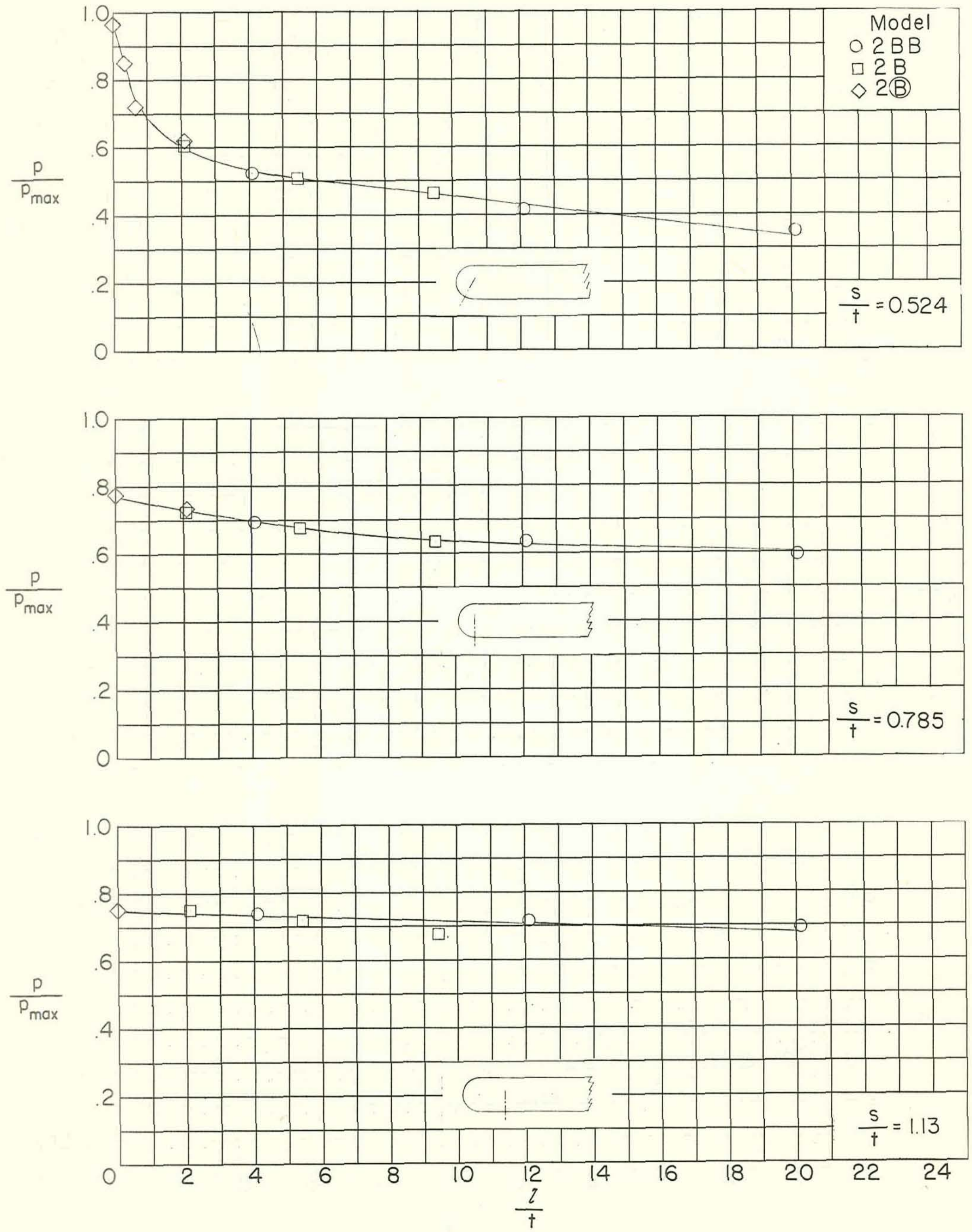

(b) Concluded.

Figure 6.- Continued.

L-1552

CONFIDENTIAL

L-1552

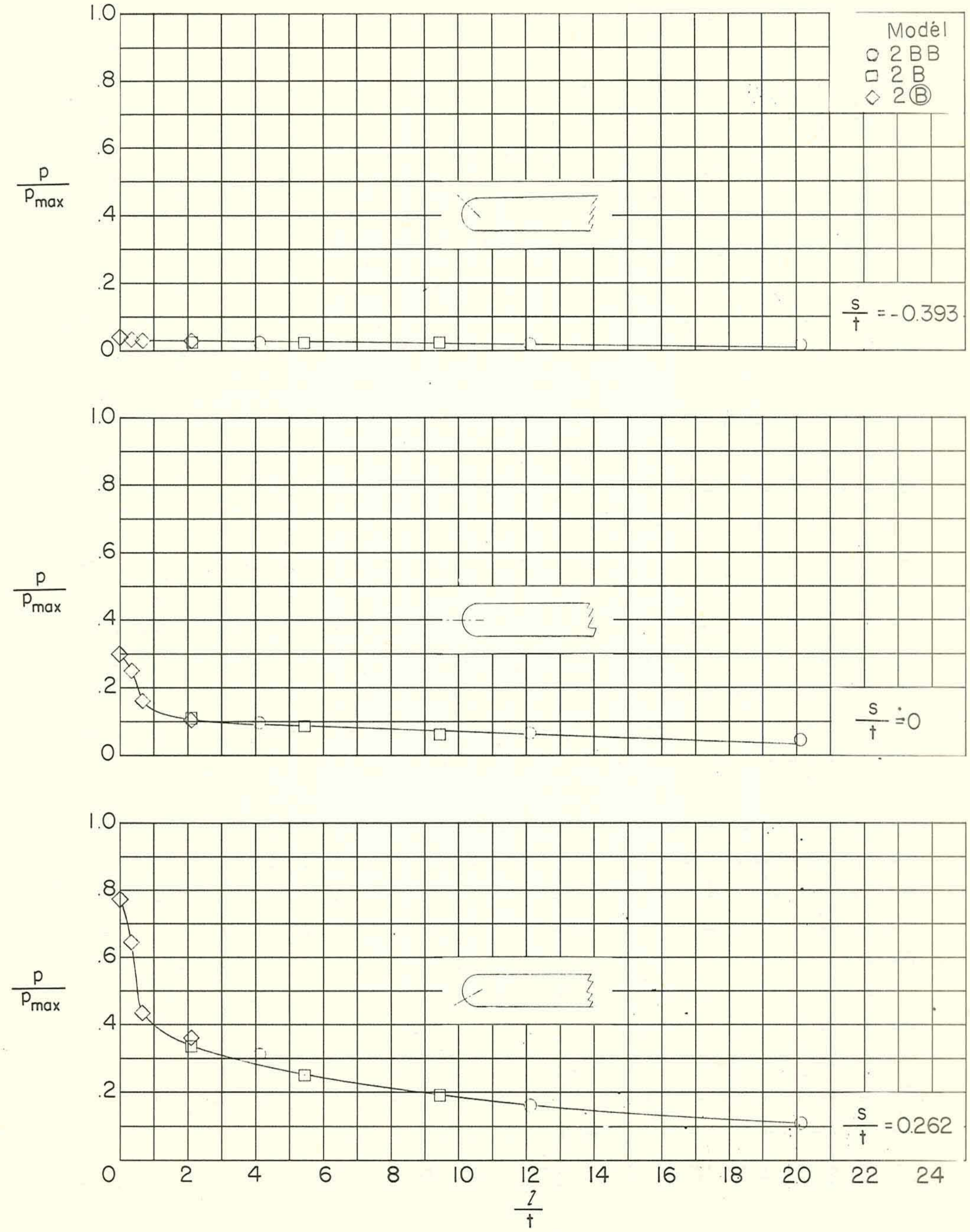

(c) $\alpha = 60^{\circ}$.

Figure 6.- Continued.

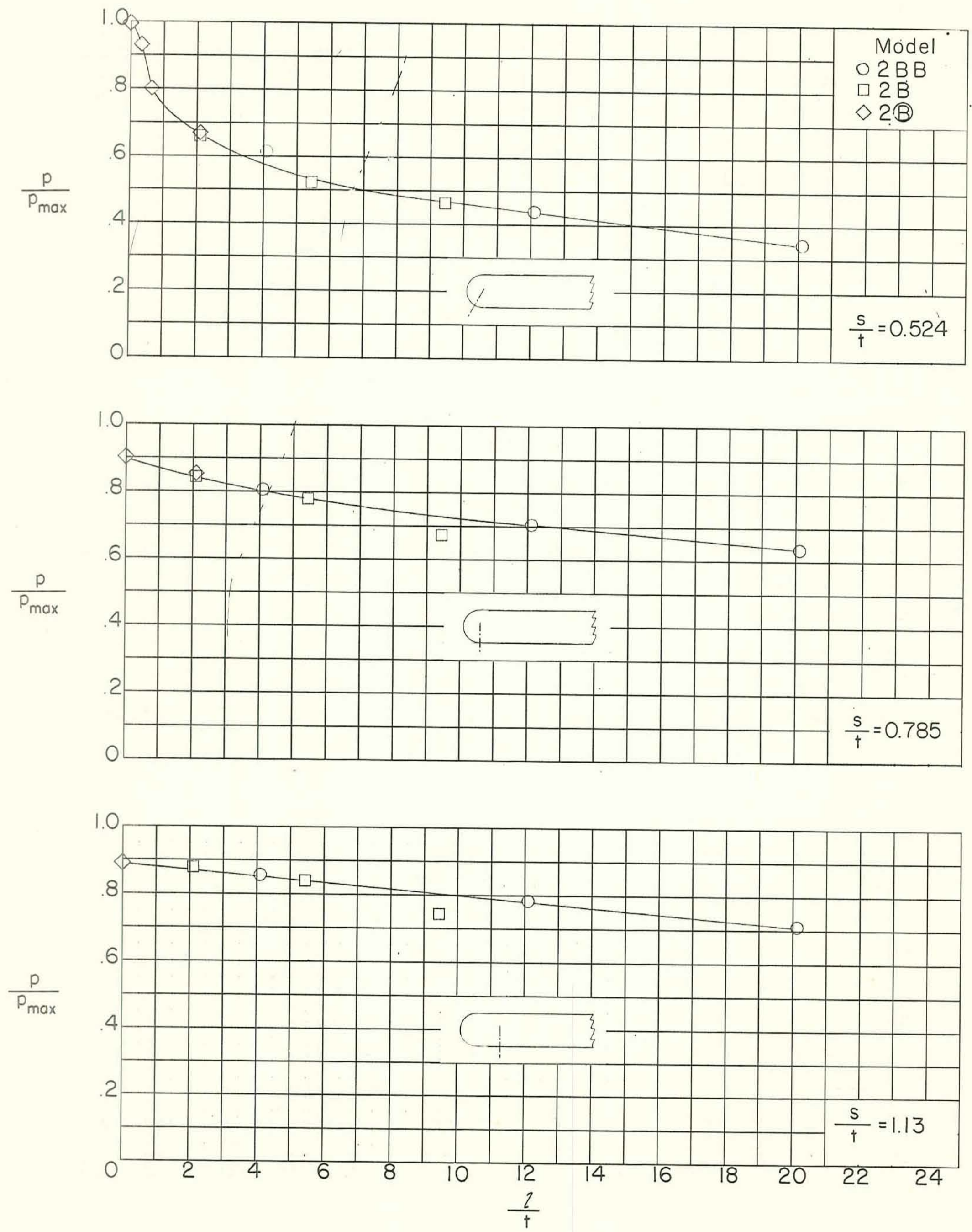

(c) Concluded.

Figure 6.- Continued.

L-1552

L-1552

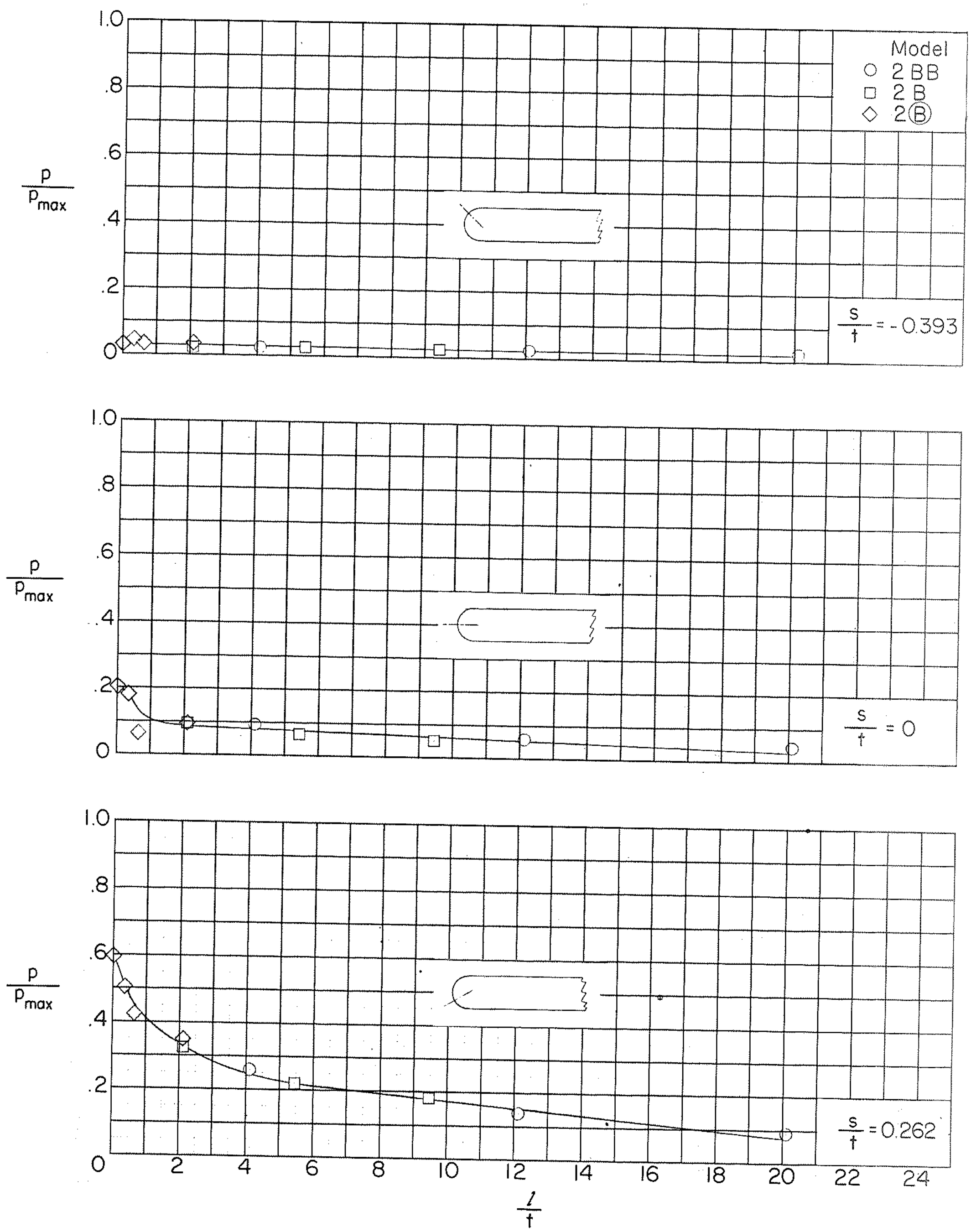

(d) $\alpha = 70^{\circ}$.

Figure 6.- Continued.

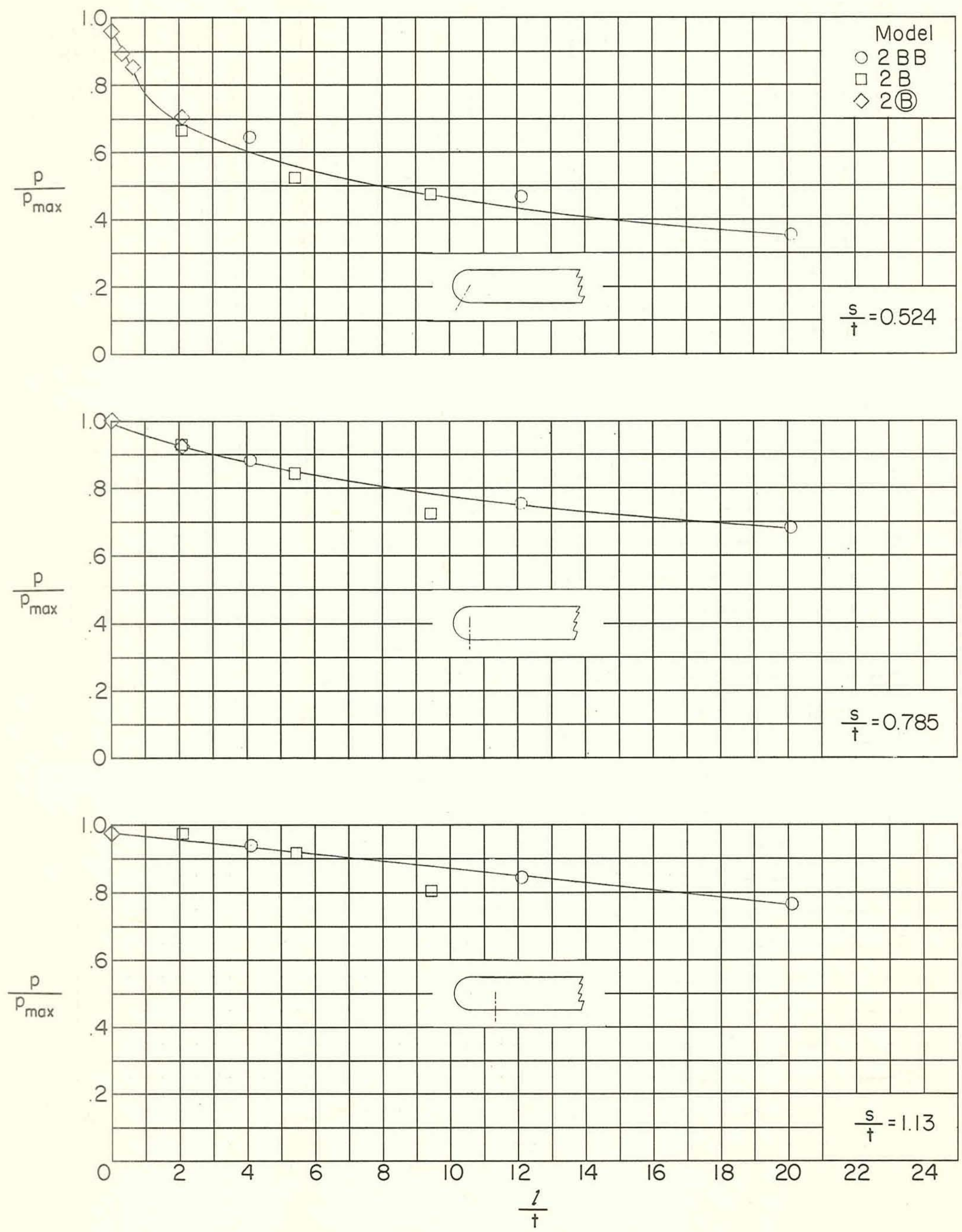

(d) Concluded.

Figure 6.- Continued.

L-1552

L-1552

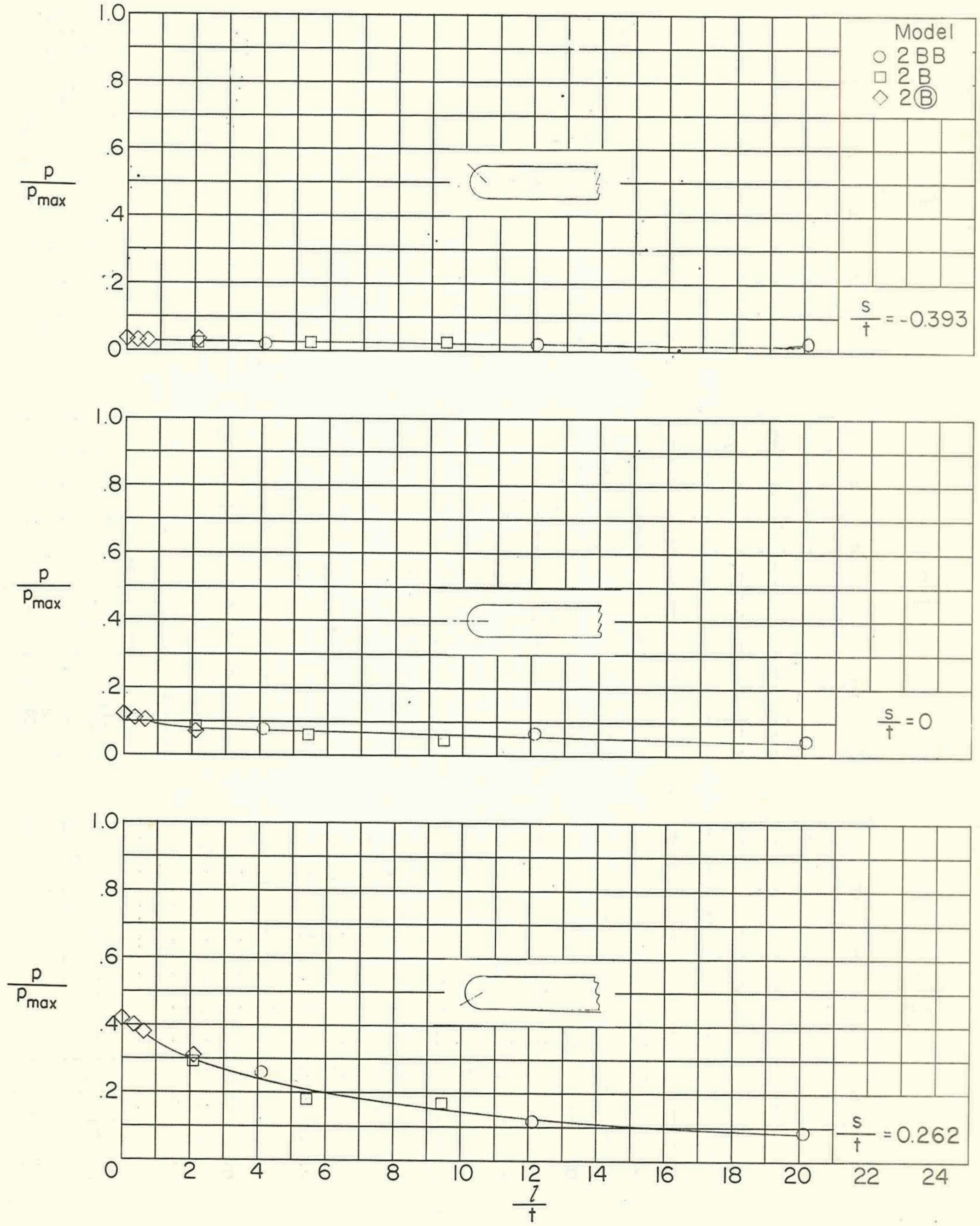

(e) $\alpha = 80°$.

Figure 6.- Continued.

[redacted]

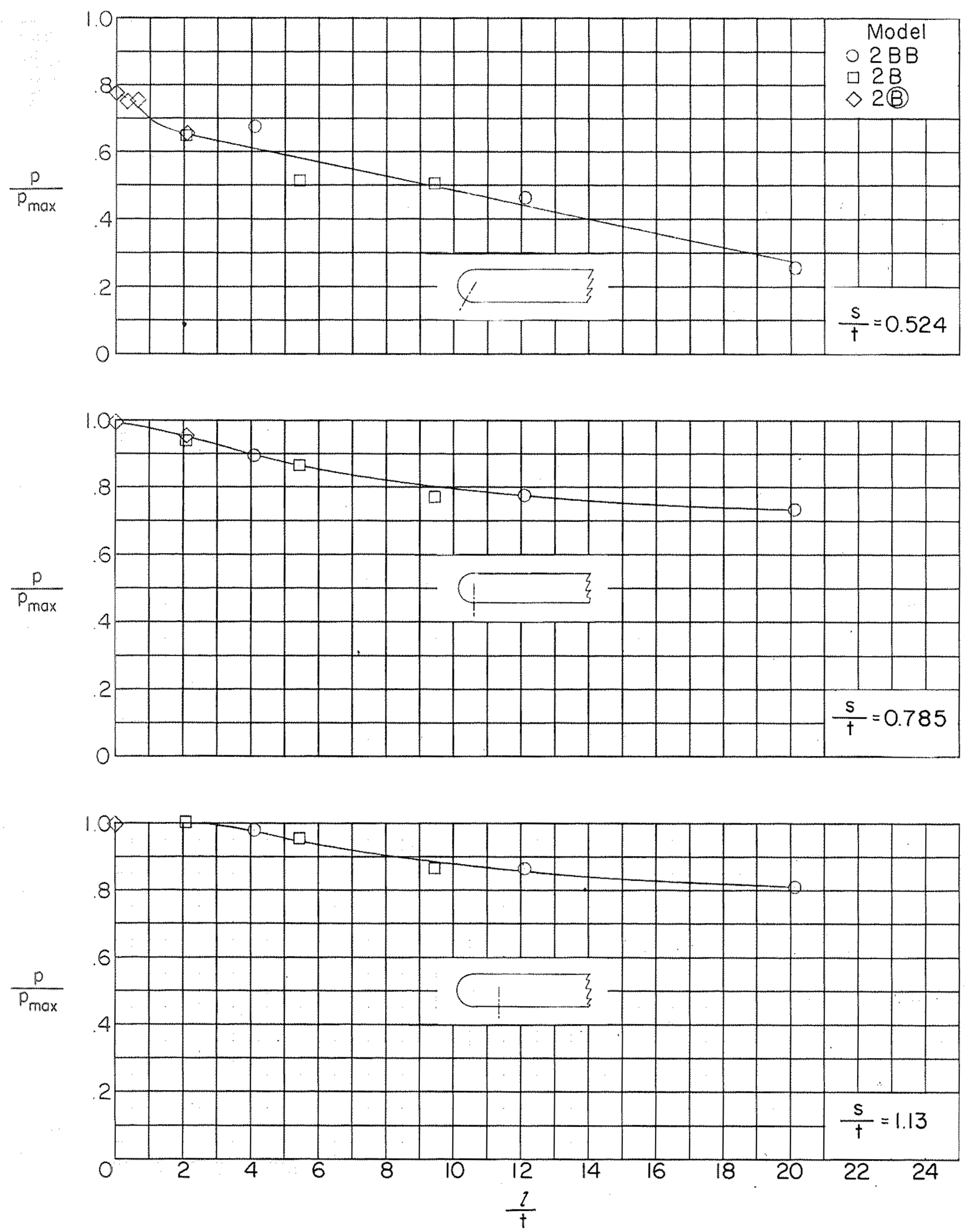

L-1552

(e) Concluded.

Figure 6.- Continued.

[redacted]

L-1552

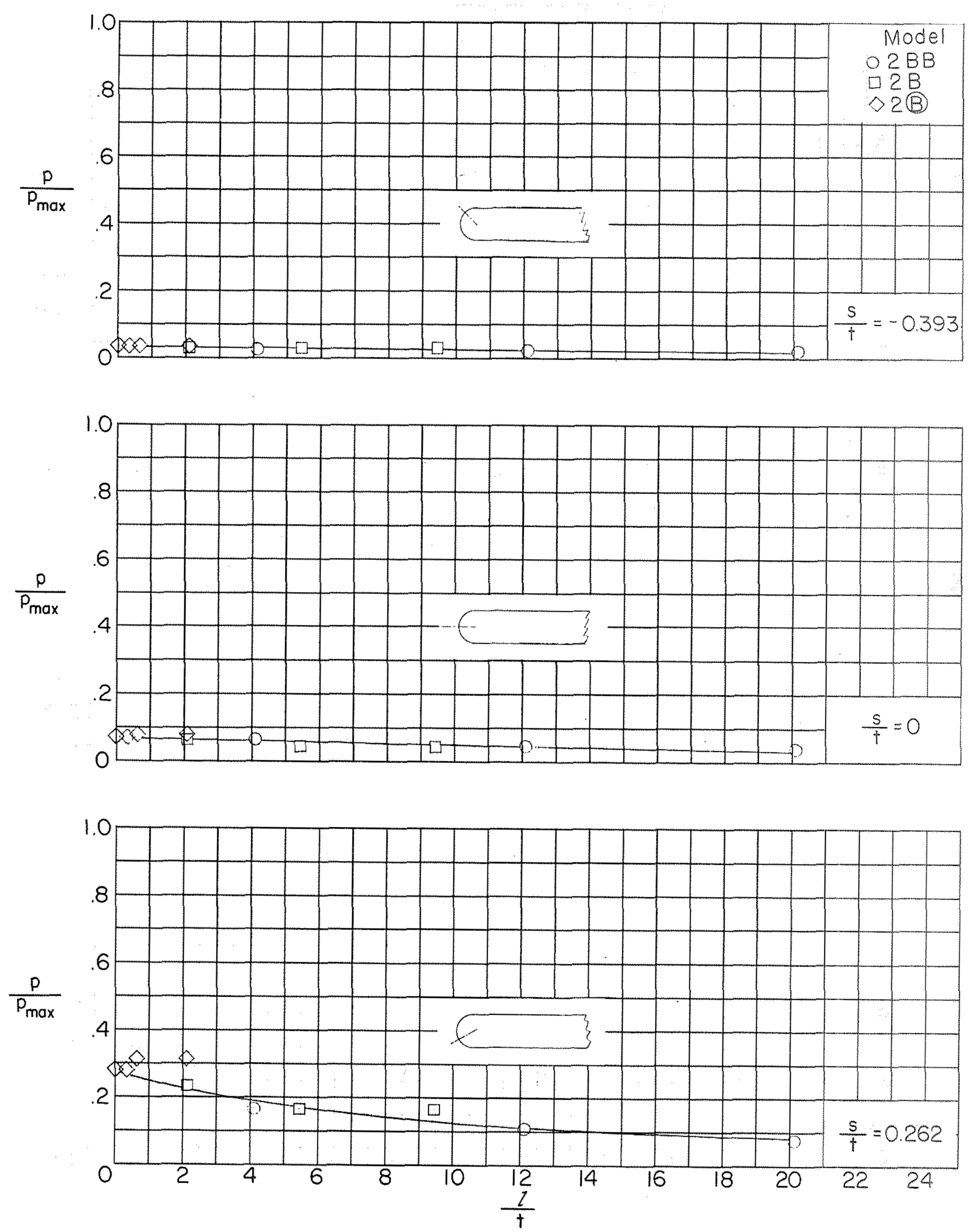

(f) $\alpha = 90^{\circ}$.

Figure 6.- Continued.

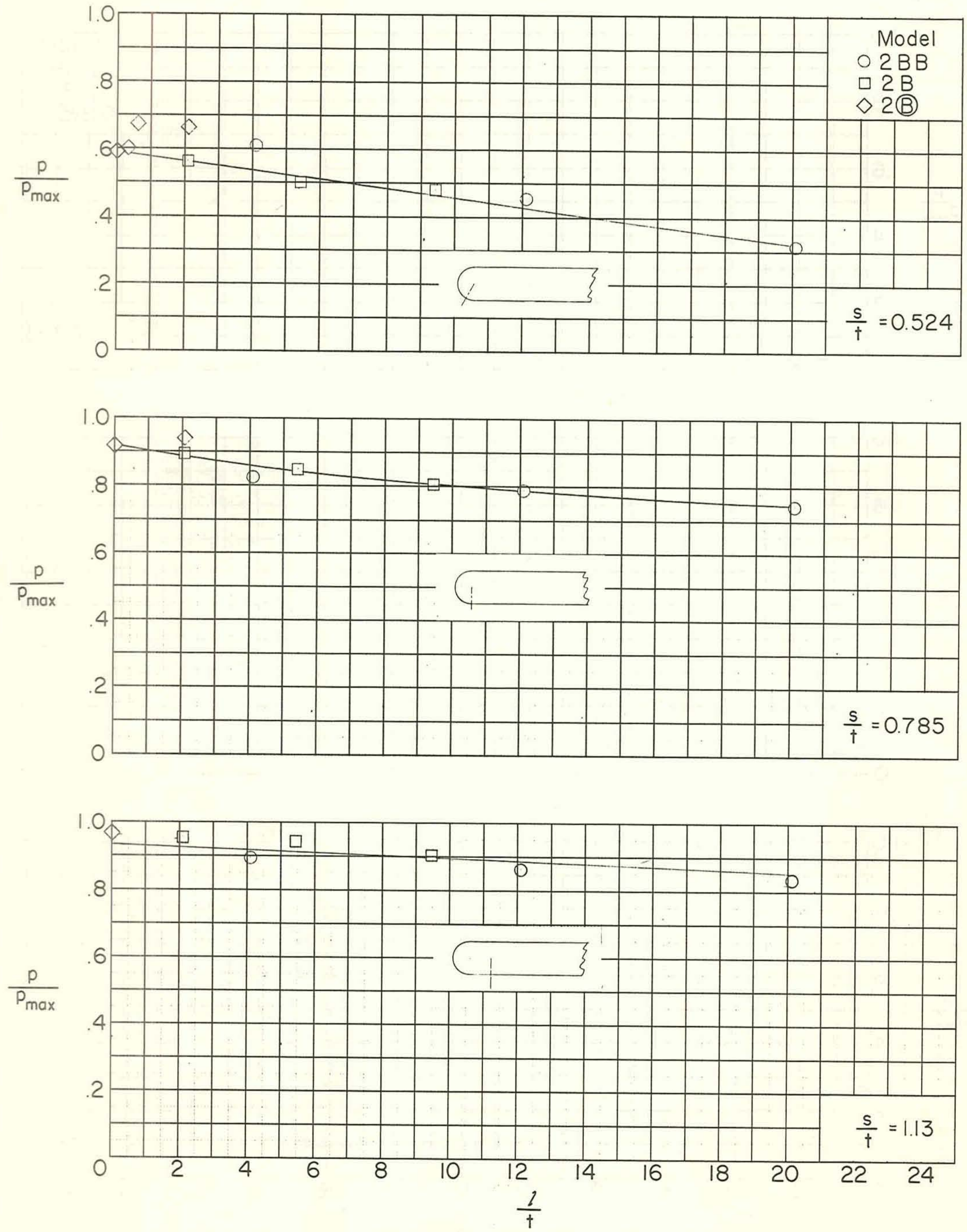

(f) Concluded.

Figure 6.- Concluded.

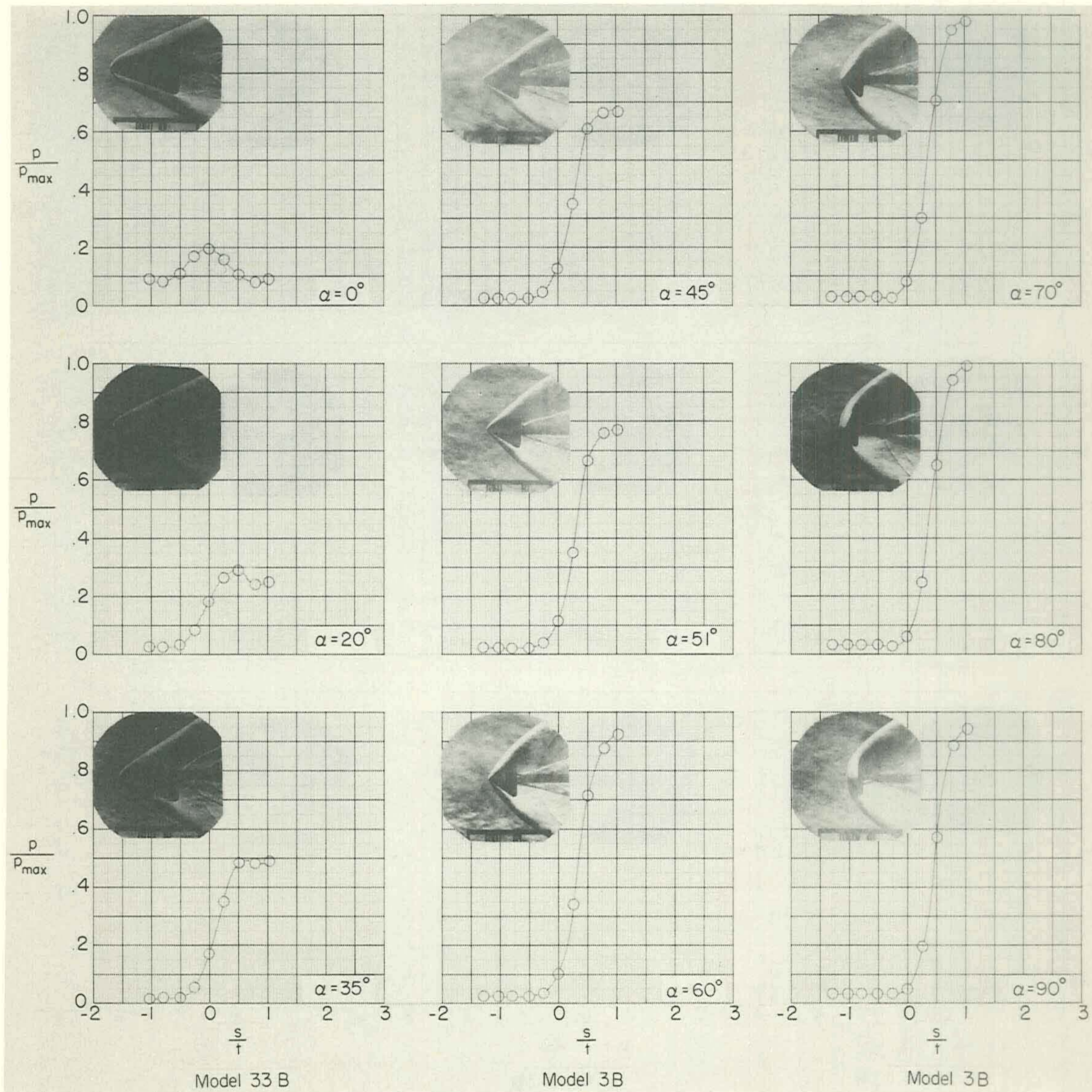

(a) $l/t = 1.90$.

Figure 7.- Pressure distributions obtained over an angle-of-attack range from 0° to 90° on two round-leading-edge models. Models 33B and 3B; $\Lambda = 70^{\circ}$.

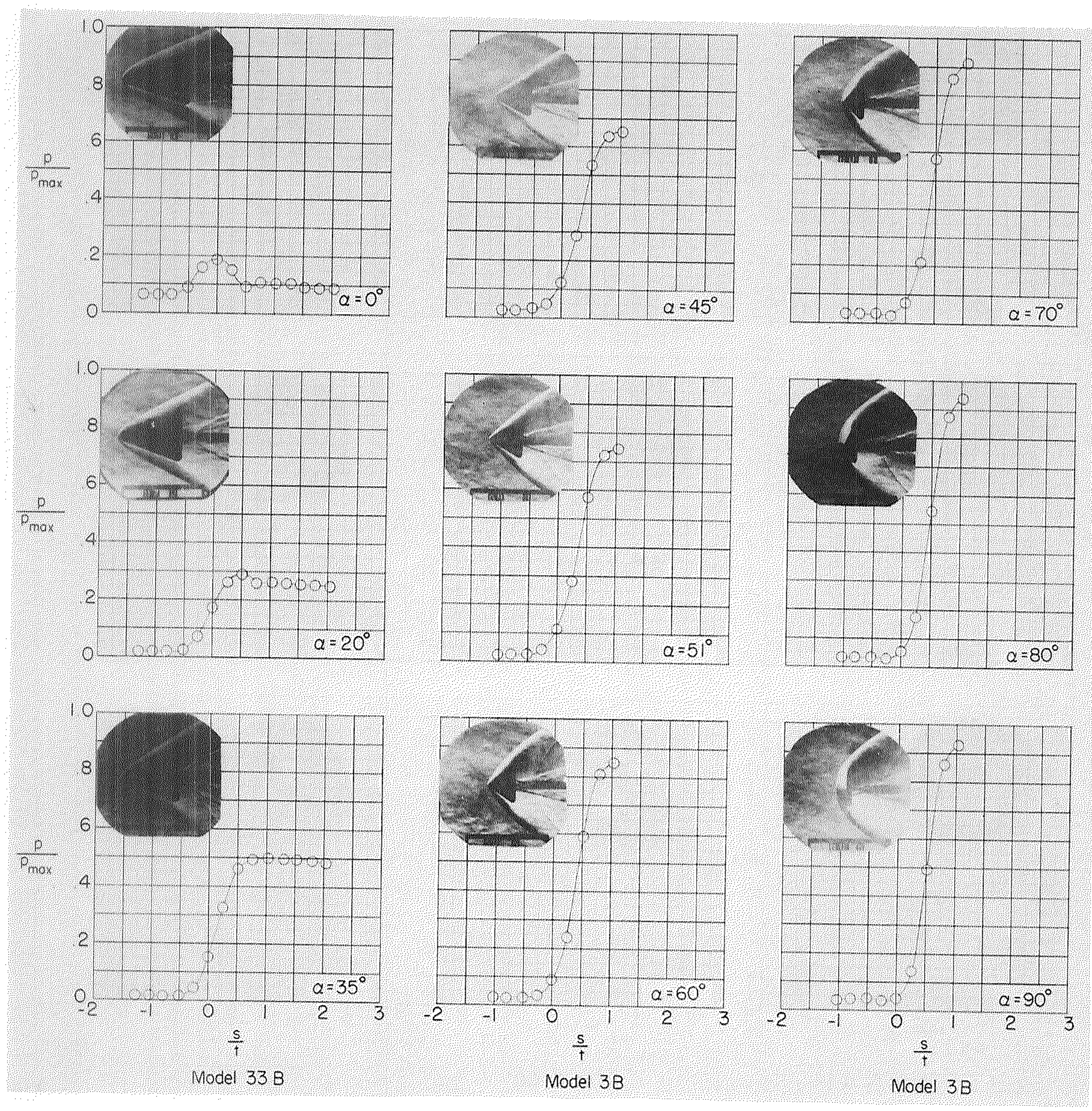

(b) $l/t = 4.56$.

Figure 7.- Concluded.

L-1552

L-1552

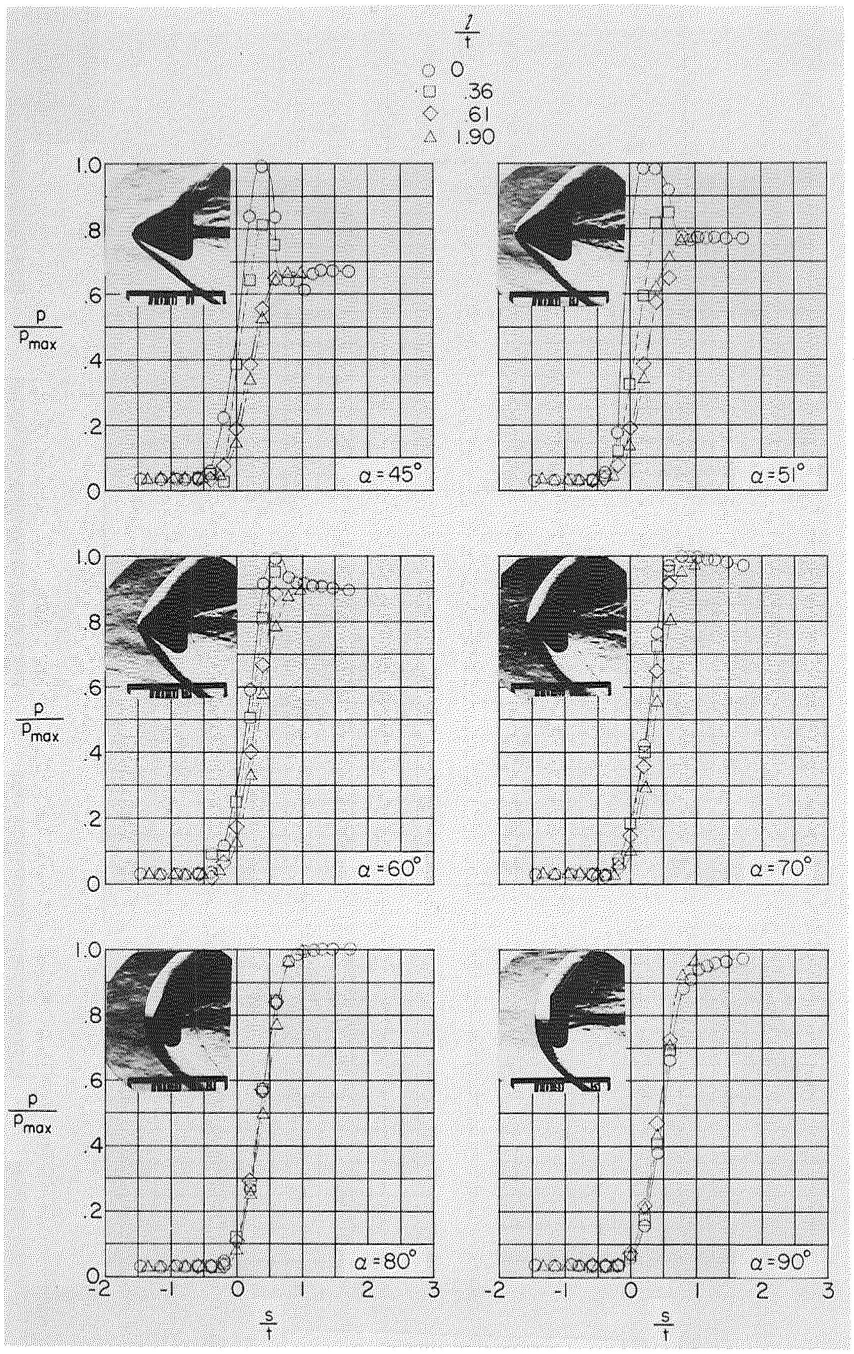

(a) Model 3 (B) ; Λ = 70°.

Figure 8.- Pressure distributions obtained around the nose section of two round-leading-edge models of different sweep angles.

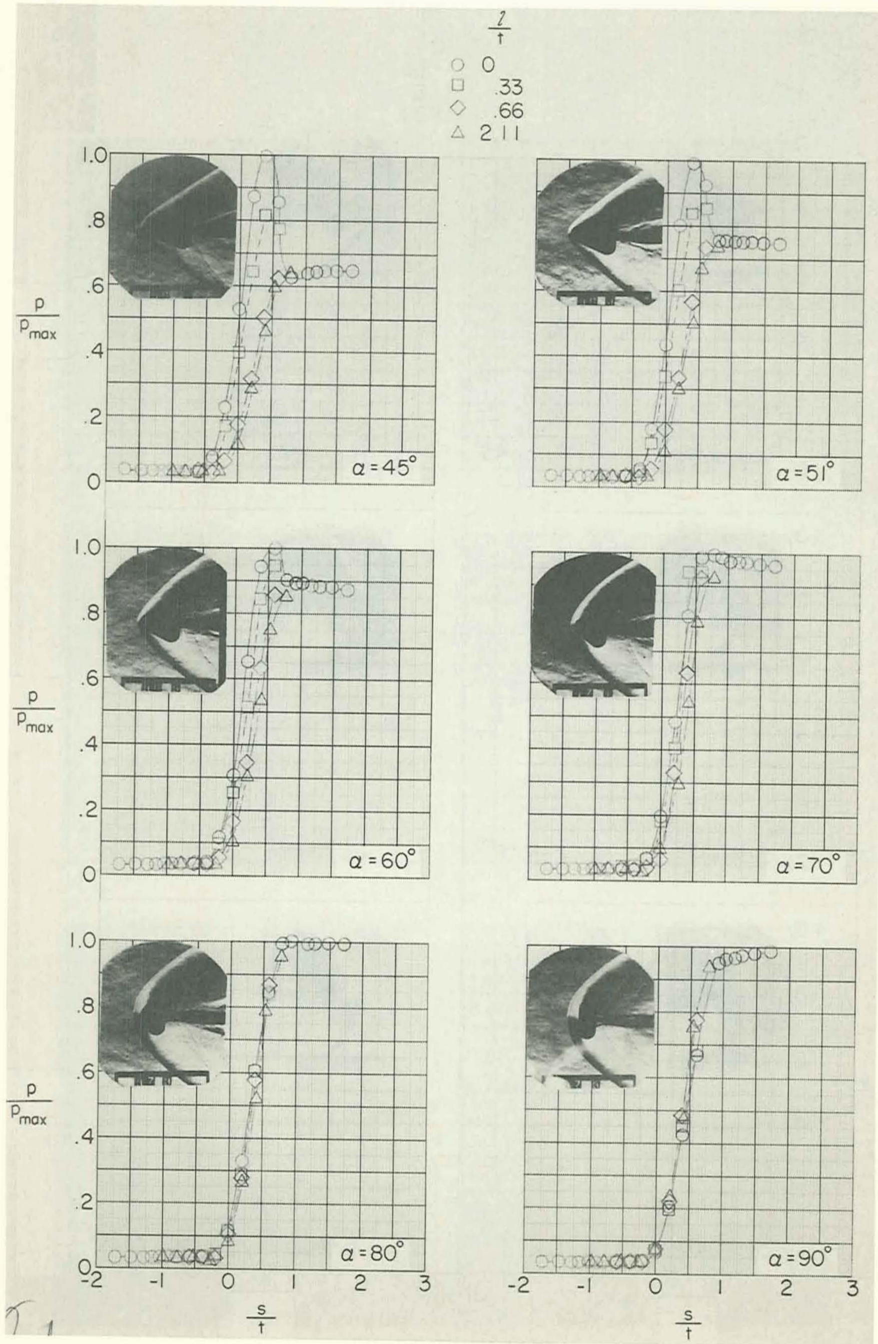

(b) Model 2 (B); Λ = 75°.

Figure 8.- Concluded.

L-1552

L-1552

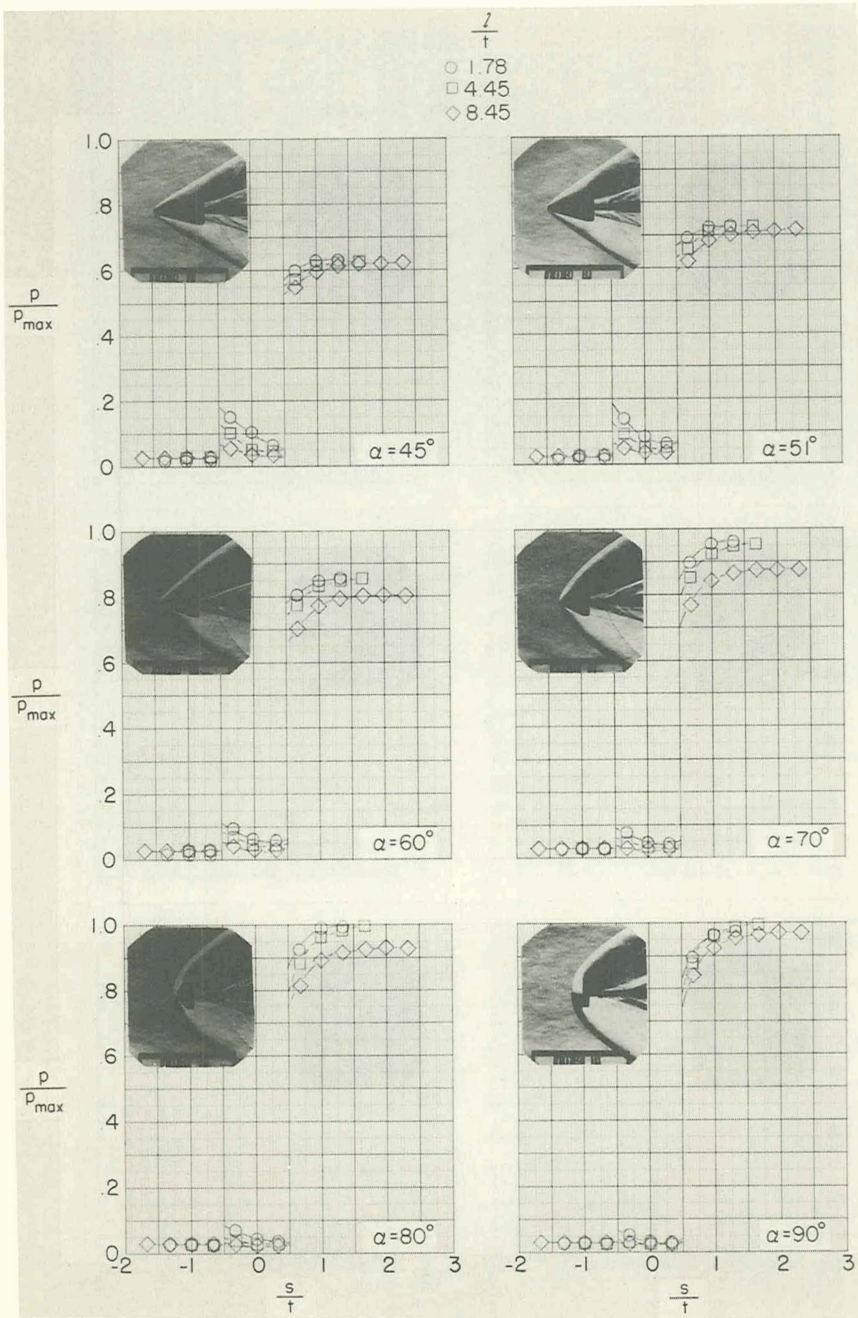

(a) Model 1A; Λ = 80°.

Figure 9.- Pressure distributions obtained on the basic A-series models (square leading edge).

CONFIDENTIAL

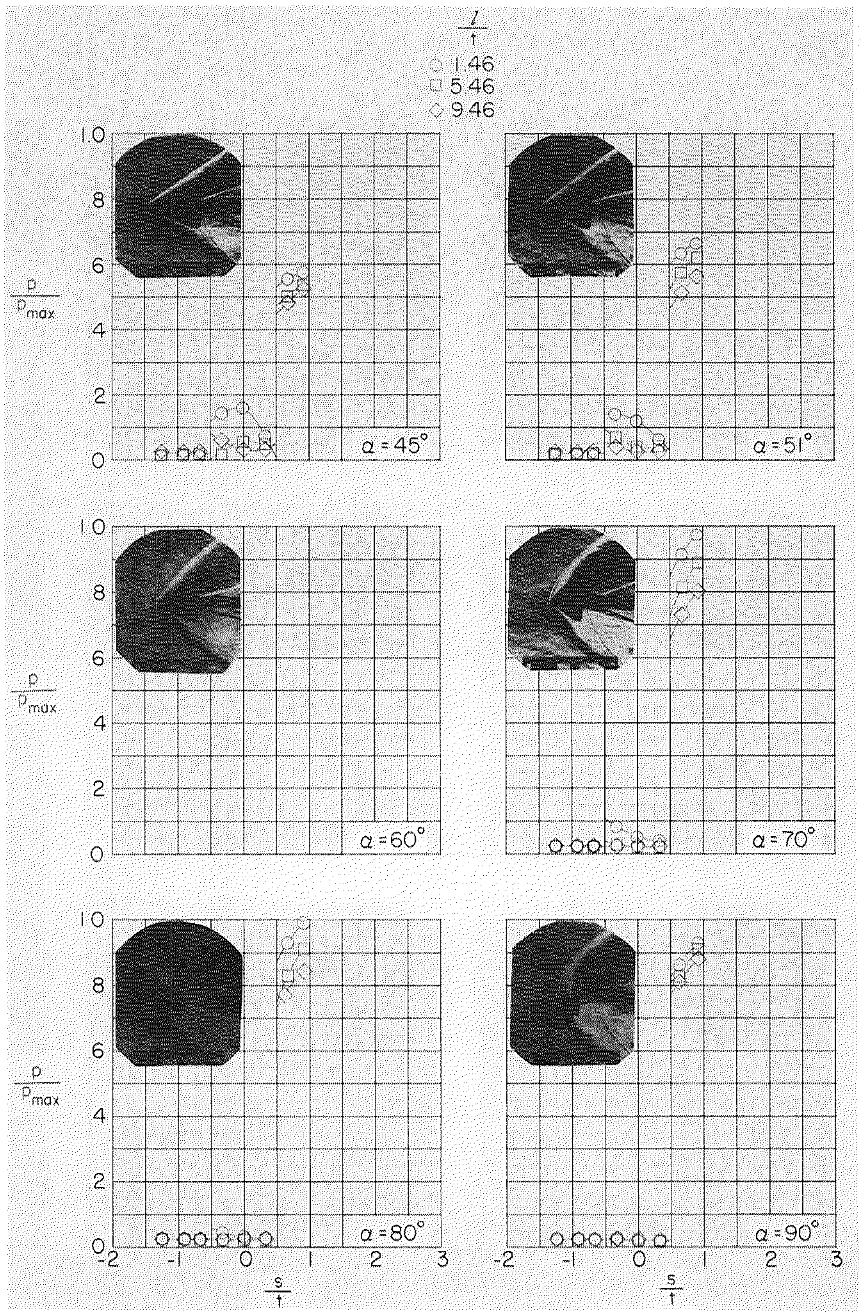

(b) Model 2A; $\Lambda = 75^{\circ}$.

Figure 9.- Continued.

L-1552

L-1552

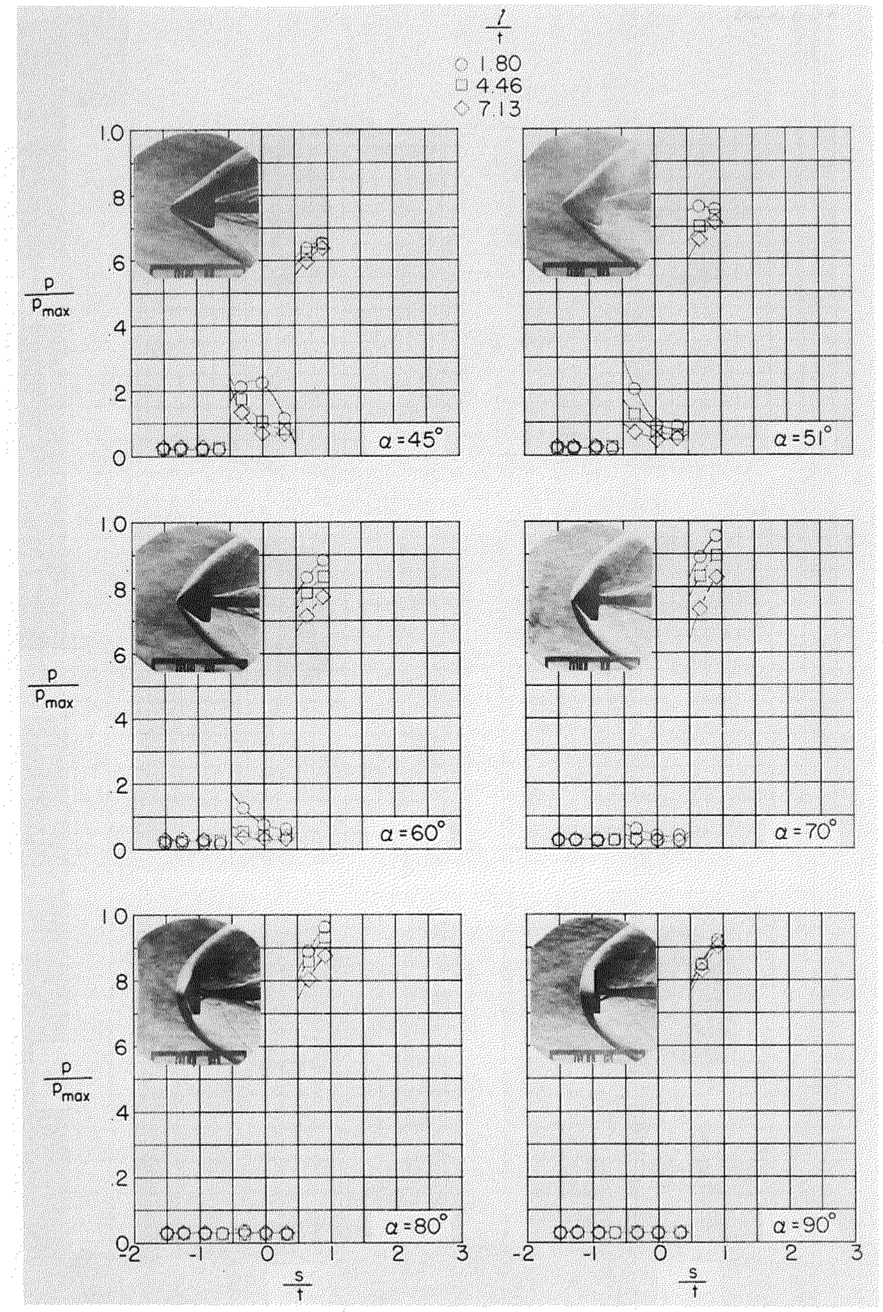

(c) Model 3A; $\Lambda = 70^{\circ}$.

Figure 9.- Continued.

CONFIDENTIAL

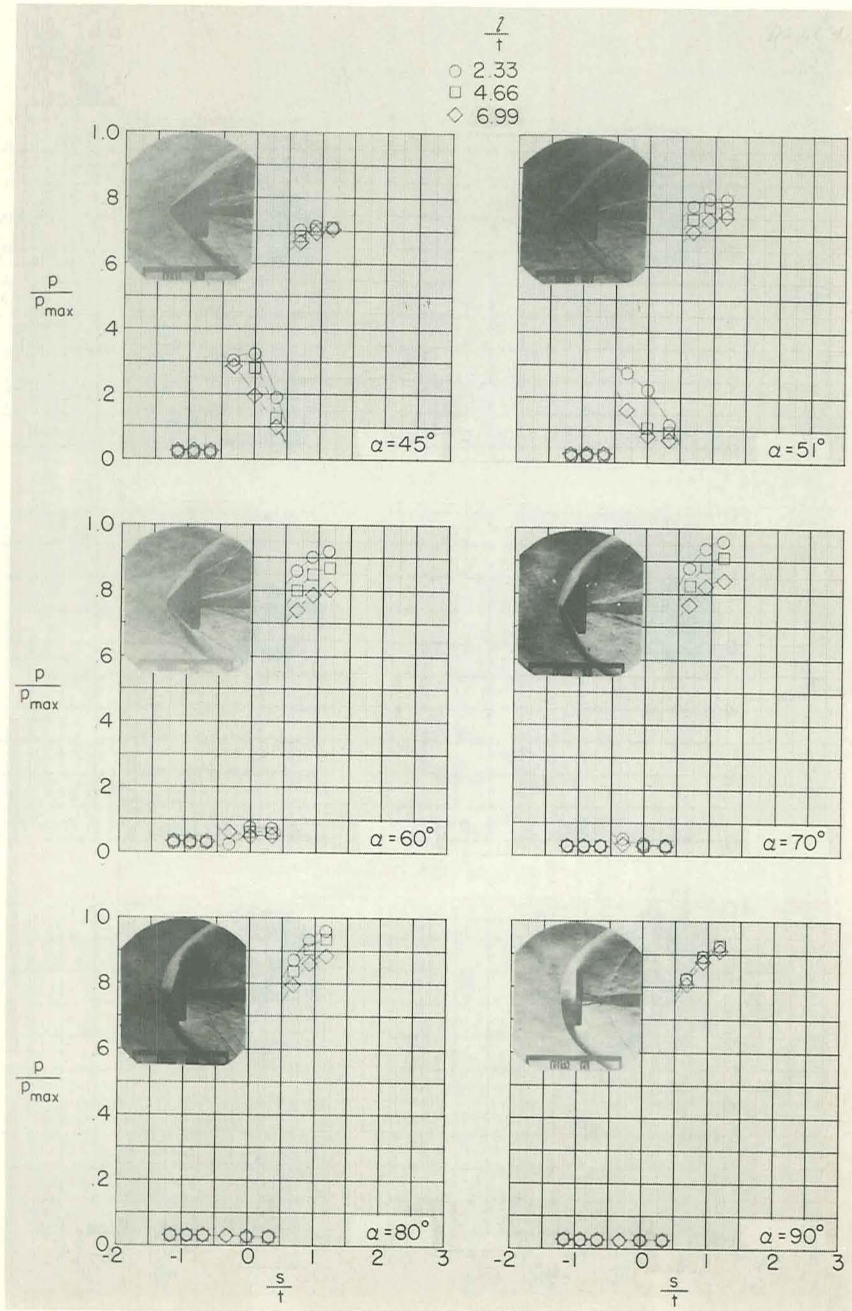

(d) Model 4A; Λ = 60°.

Figure 9.- Continued.

L-1552

CONFIDENTIAL

L-1552

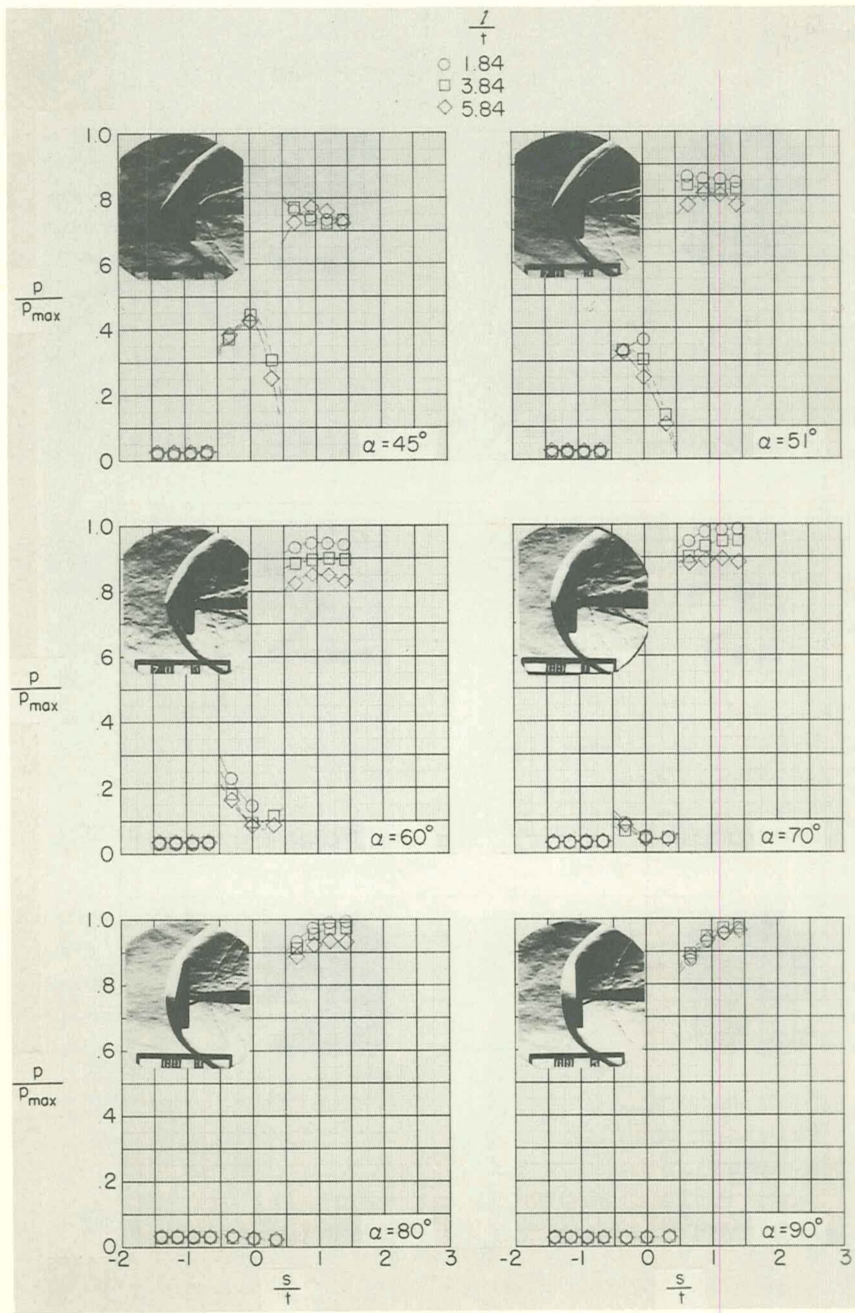

(e) Model 5A; Λ = 50°.

Figure 9.- Concluded.

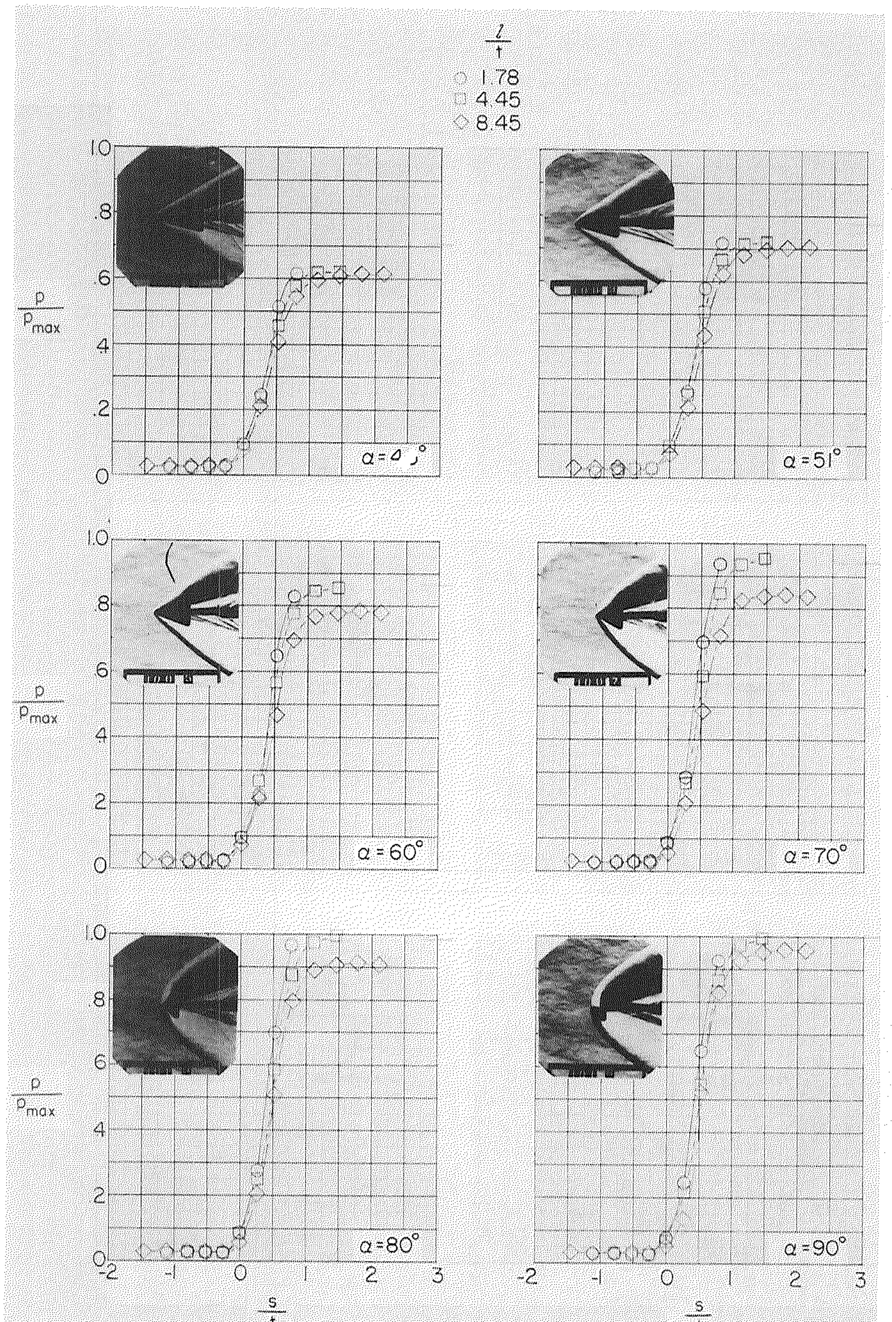

(a) Model 1B; $\Lambda = 80^{\circ}$.

Figure 10.- Pressure distributions obtained on the basic B-series models (round leading edge).

L-1552

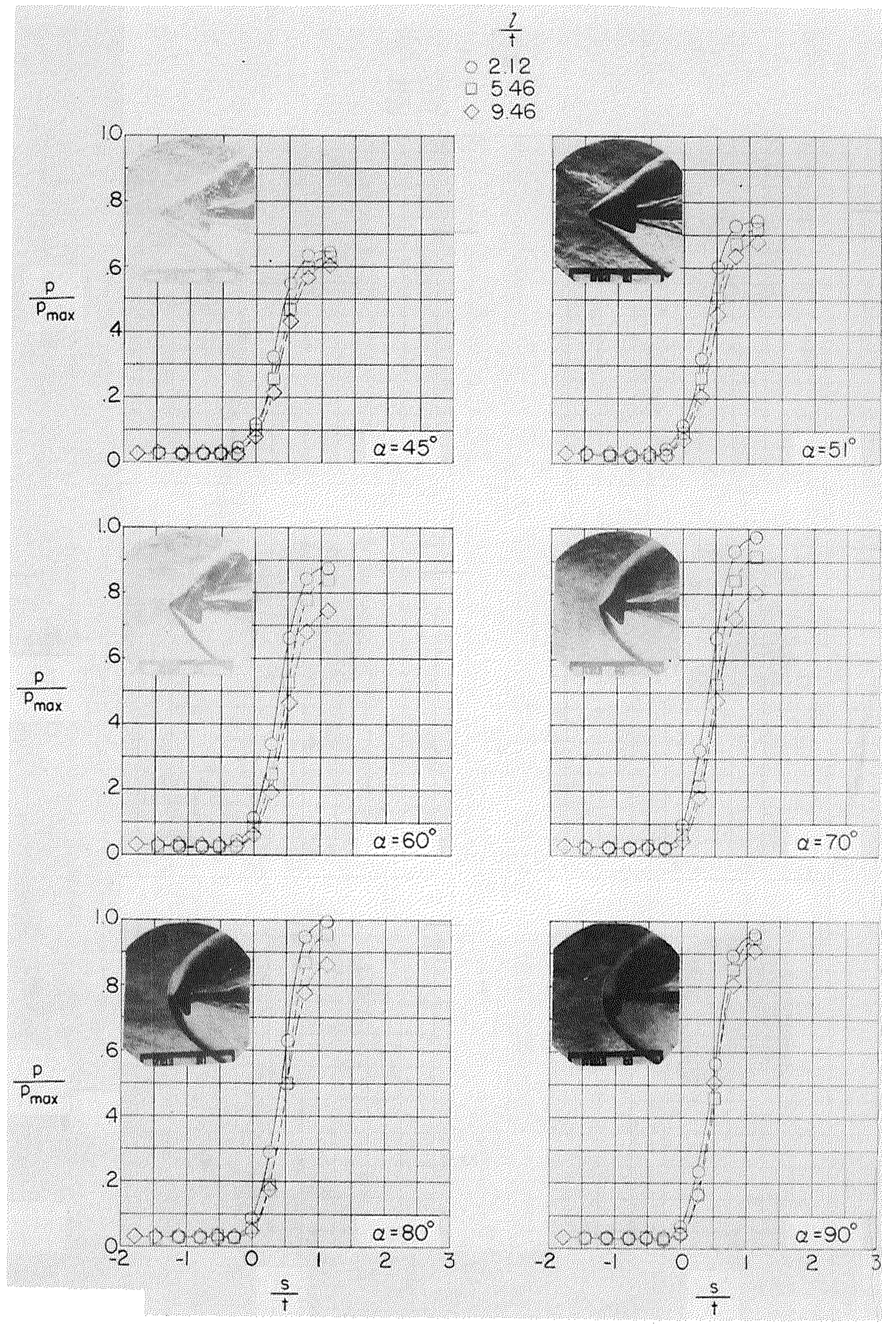

(b) Model 2B; $\Lambda = 75^{\circ}$.

Figure 10.- Continued.

CONFIDENTIAL

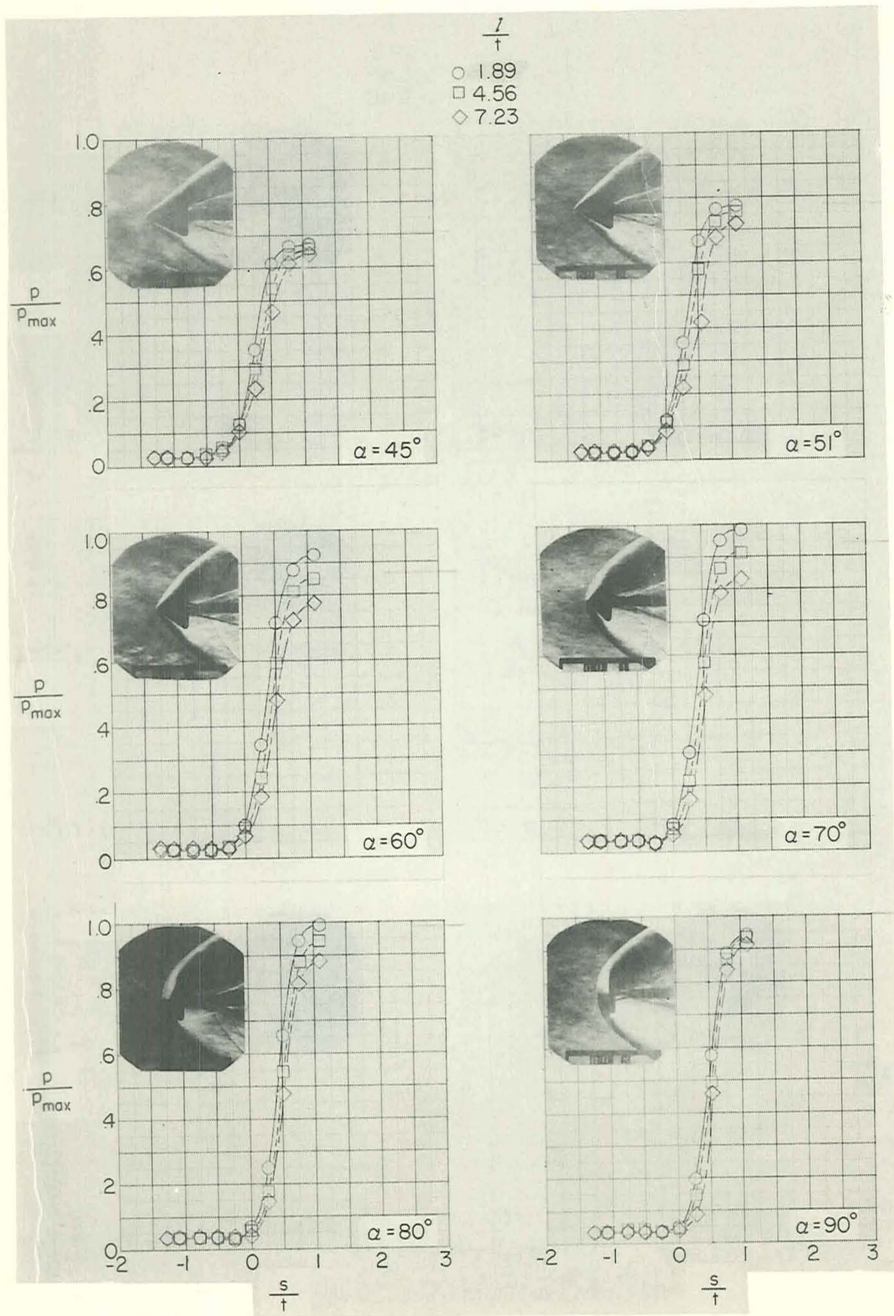

(c) Model 3B; Λ = 70°.

Figure 10.- Continued.

L-1552

CONFIDENTIAL

L-1552

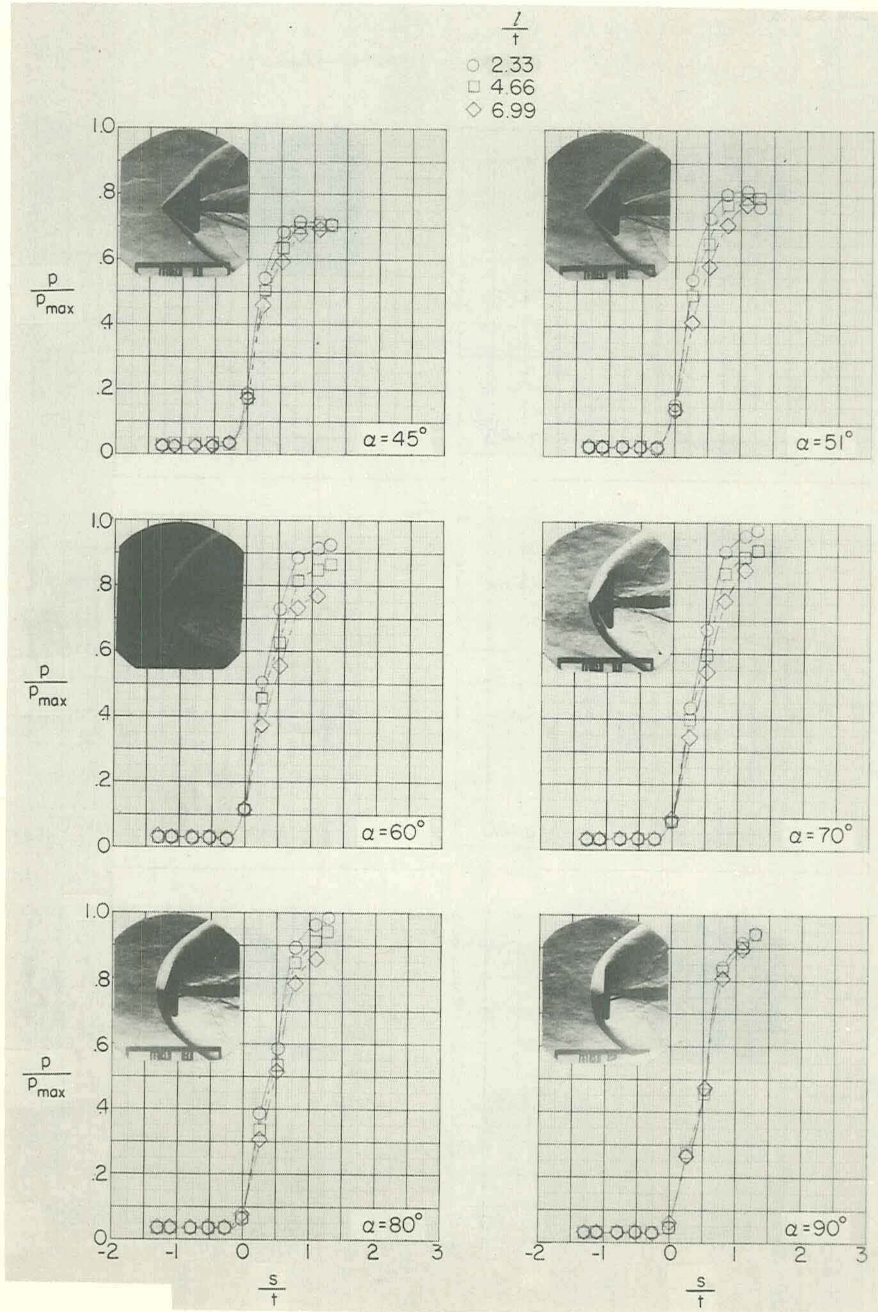

(d) Model 4B; Λ = 60°.

Figure 10.- Continued.

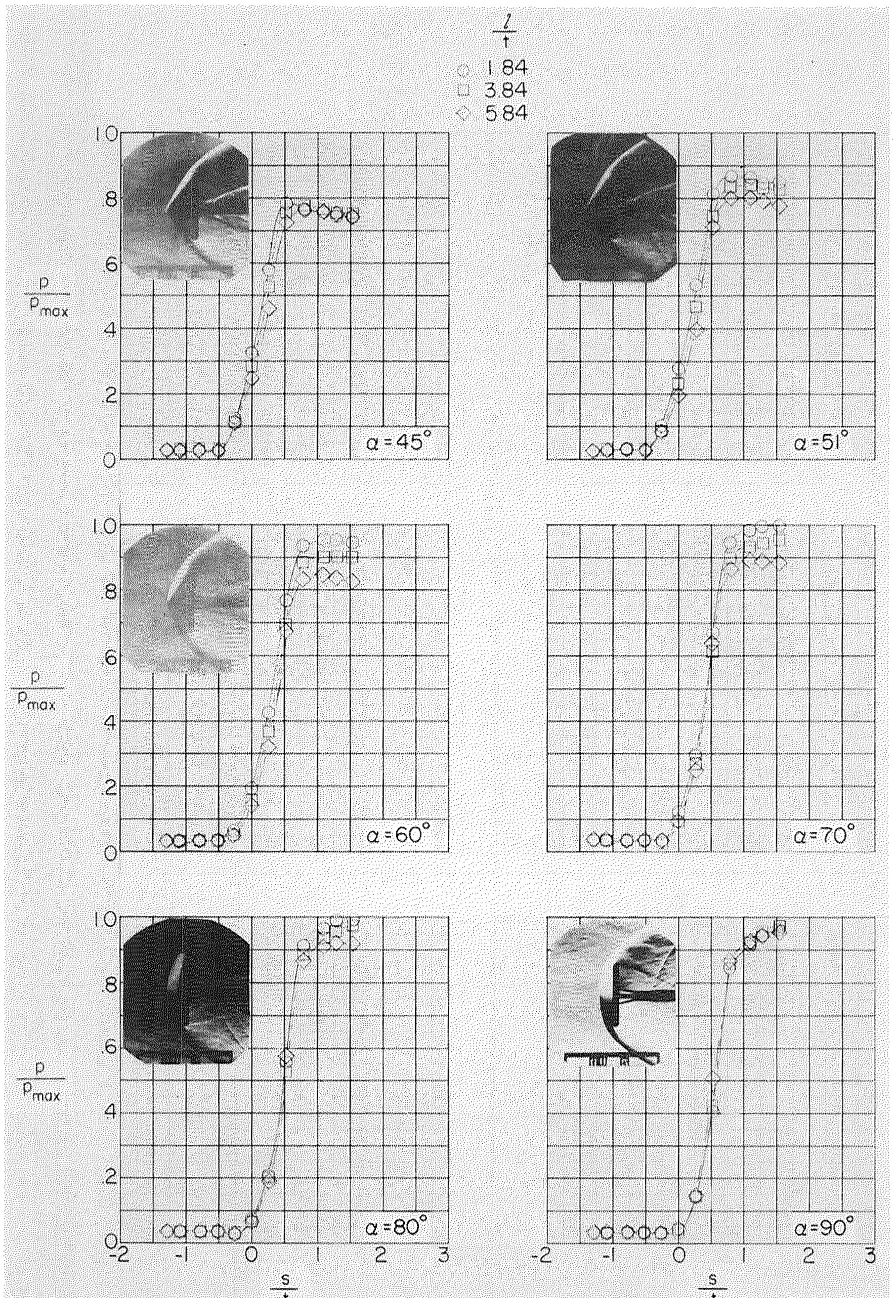

(e) Model 5B; $\Lambda = 50^{\circ}$.

Figure 10.- Concluded.

L-1552

L-1552

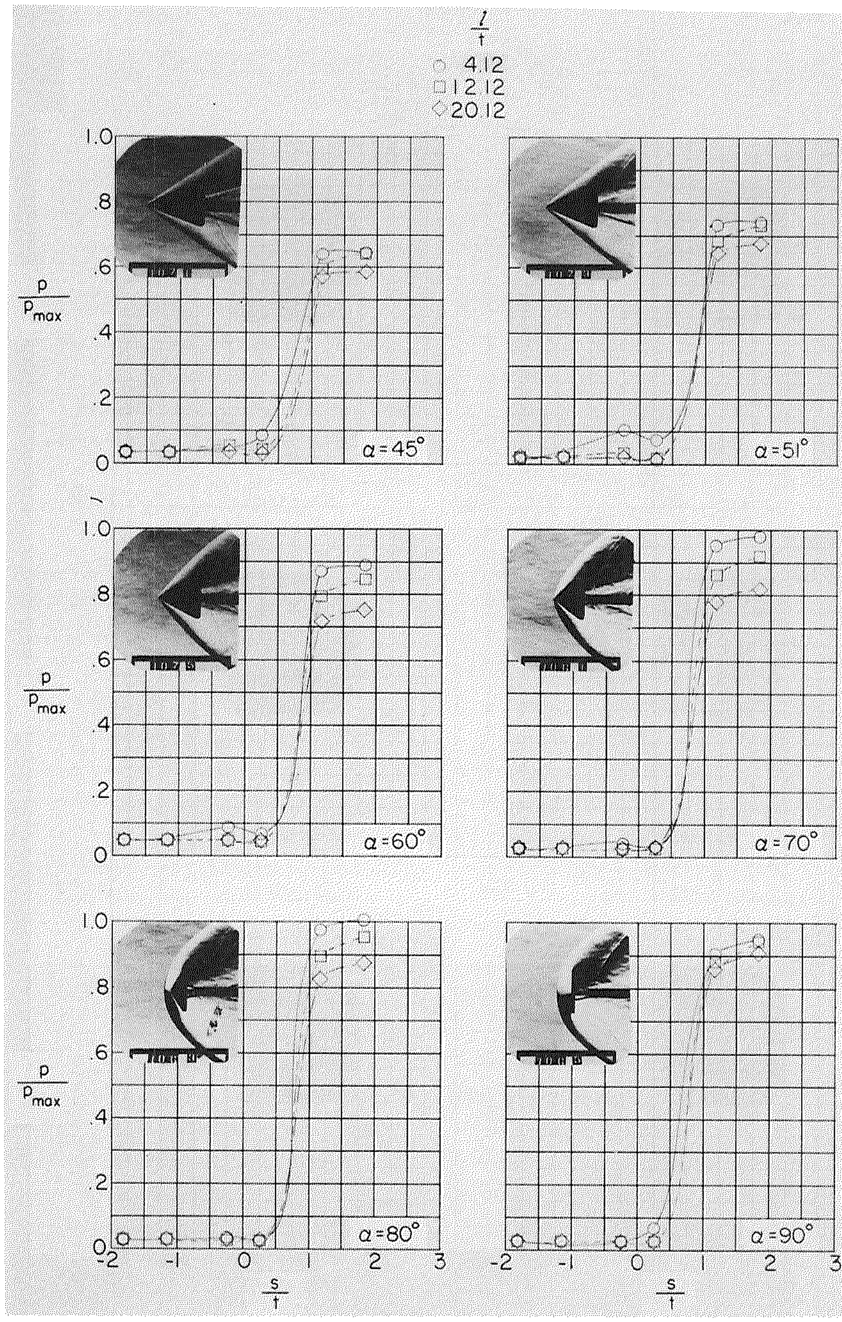

(a) Model 2AA; $\Lambda = 75^{\circ}$.

Figure 11.- Supplementary pressure distributions obtained on a square- and a round-leading-edge model designed to extend the range of l/t and s/t.

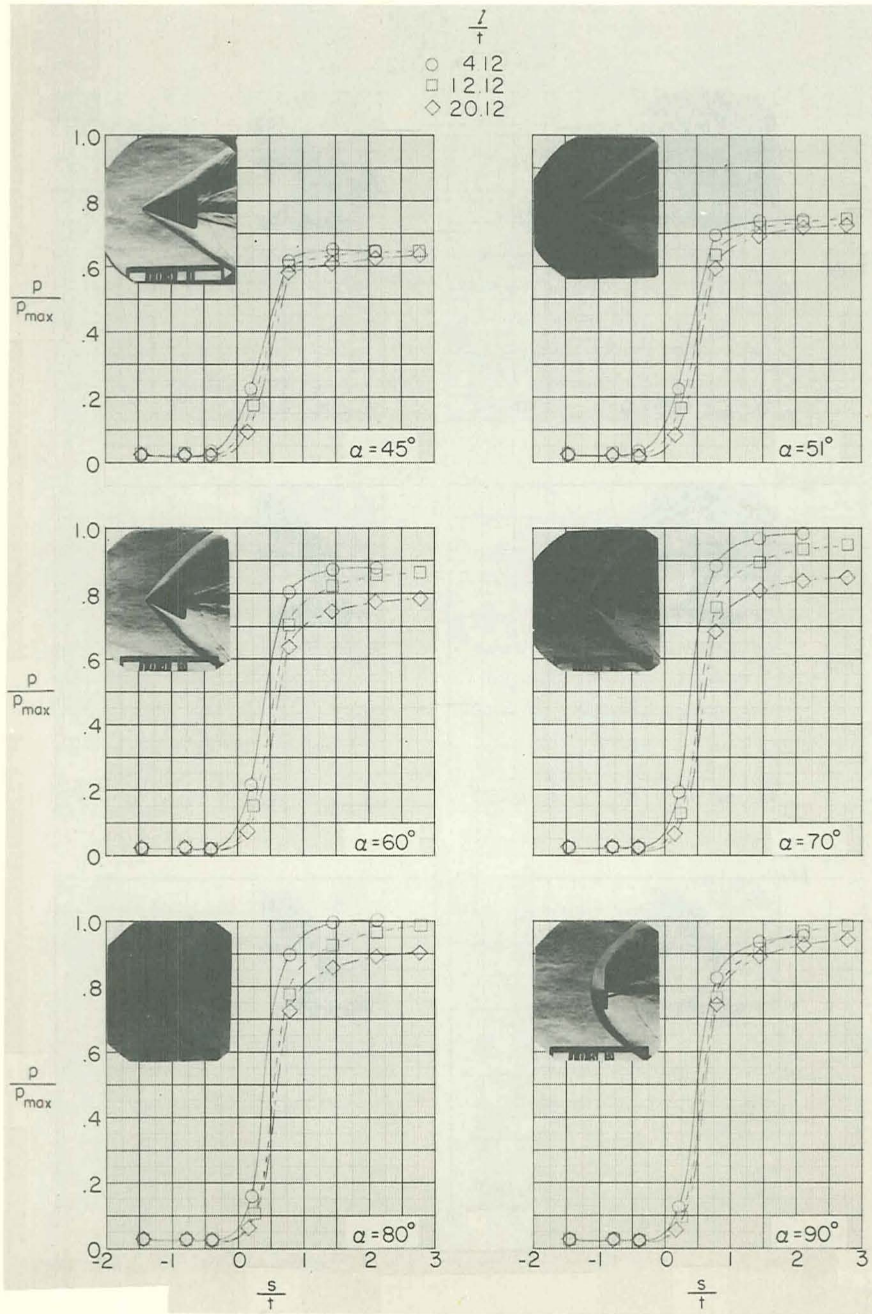

(b) Model 2BB; $\Lambda = 75^{\circ}$.

Figure 11.- Concluded.

L-1552

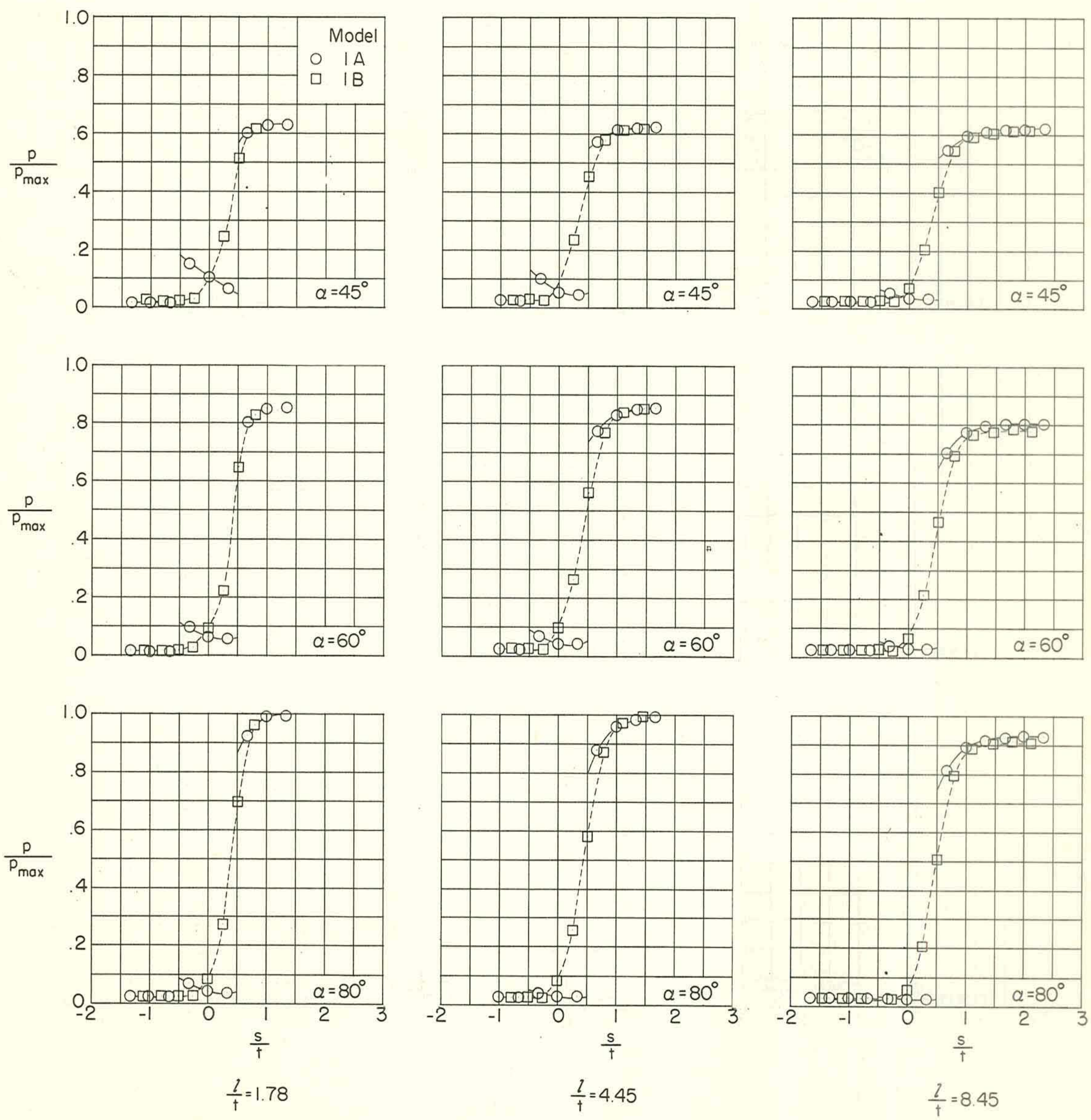

(a) Models 1A and 1B; Λ = 80°.

Figure 12.- Effect of leading-edge shape on the pressure distributions over the basic models for various sweep angles.

L-1552

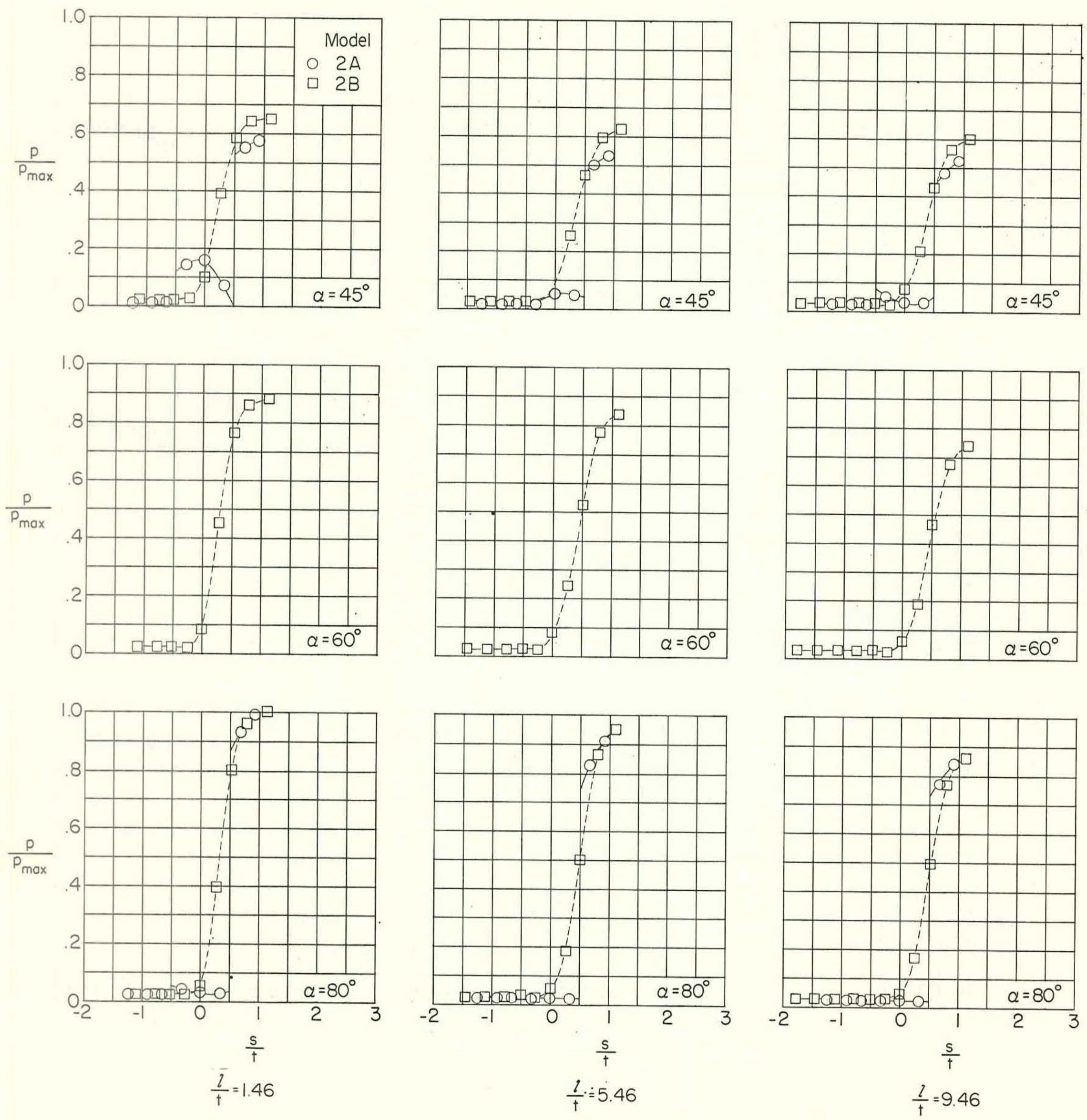

(b) Models 2A and 2B; $\Lambda = 75^{\circ}$.

Figure 12.- Continued.

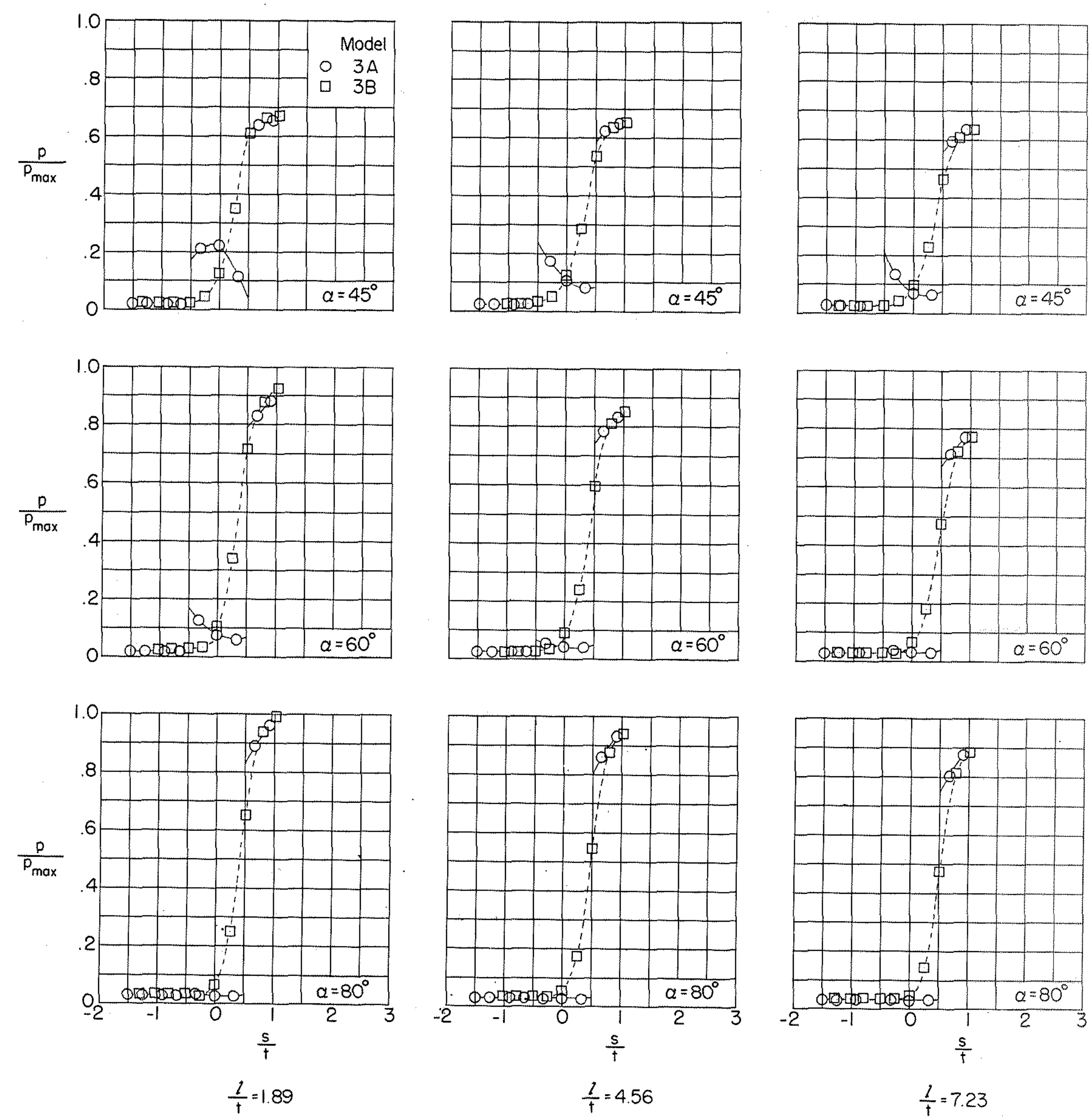

(c) Models 3A and 3B; $\Lambda = 70^\circ$.

Figure 12.- Continued.

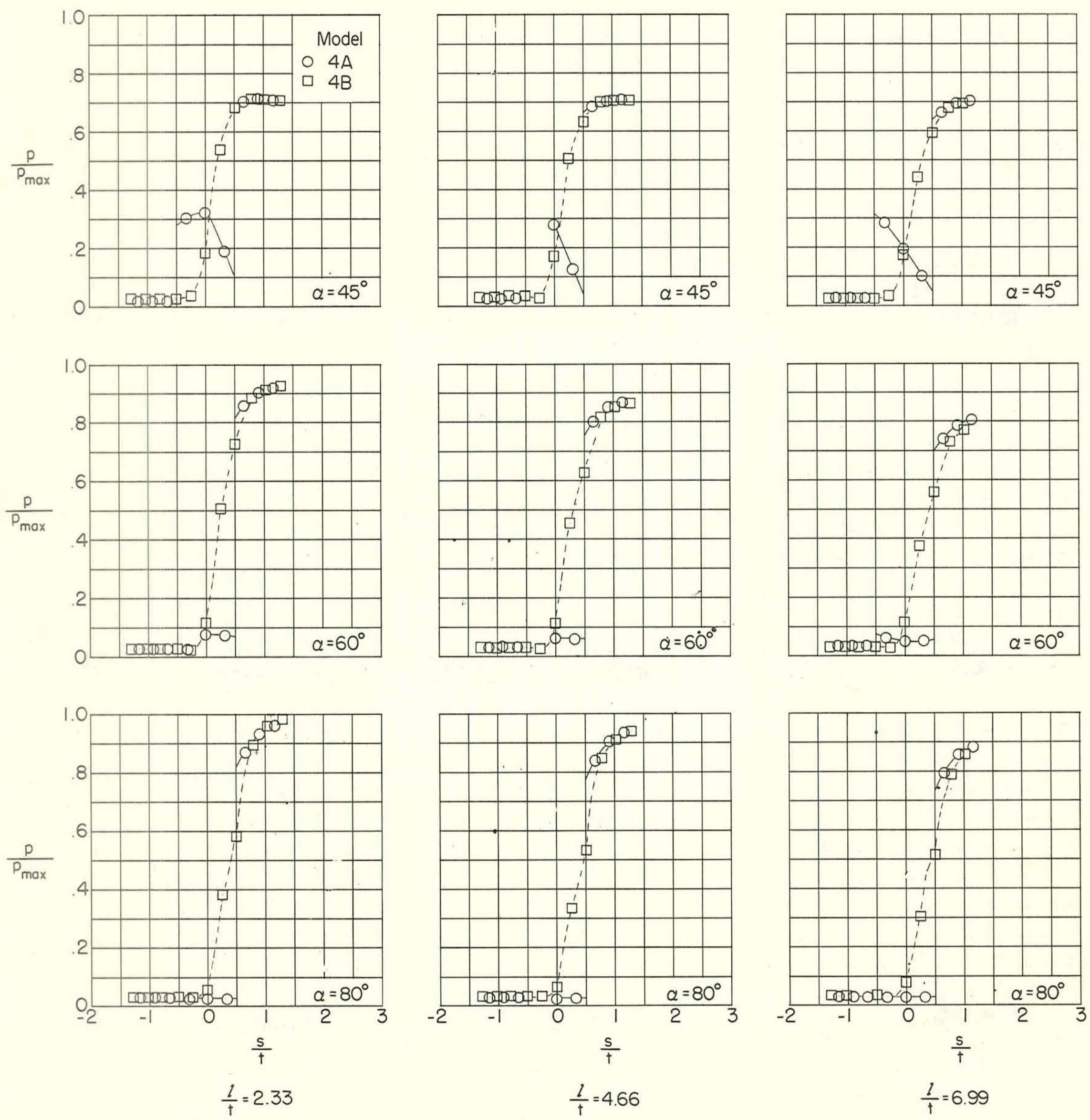

(d) Models 4A and 4B; $\Lambda = 60^\circ$.

Figure 12.- Continued.

L-1552

L-1552

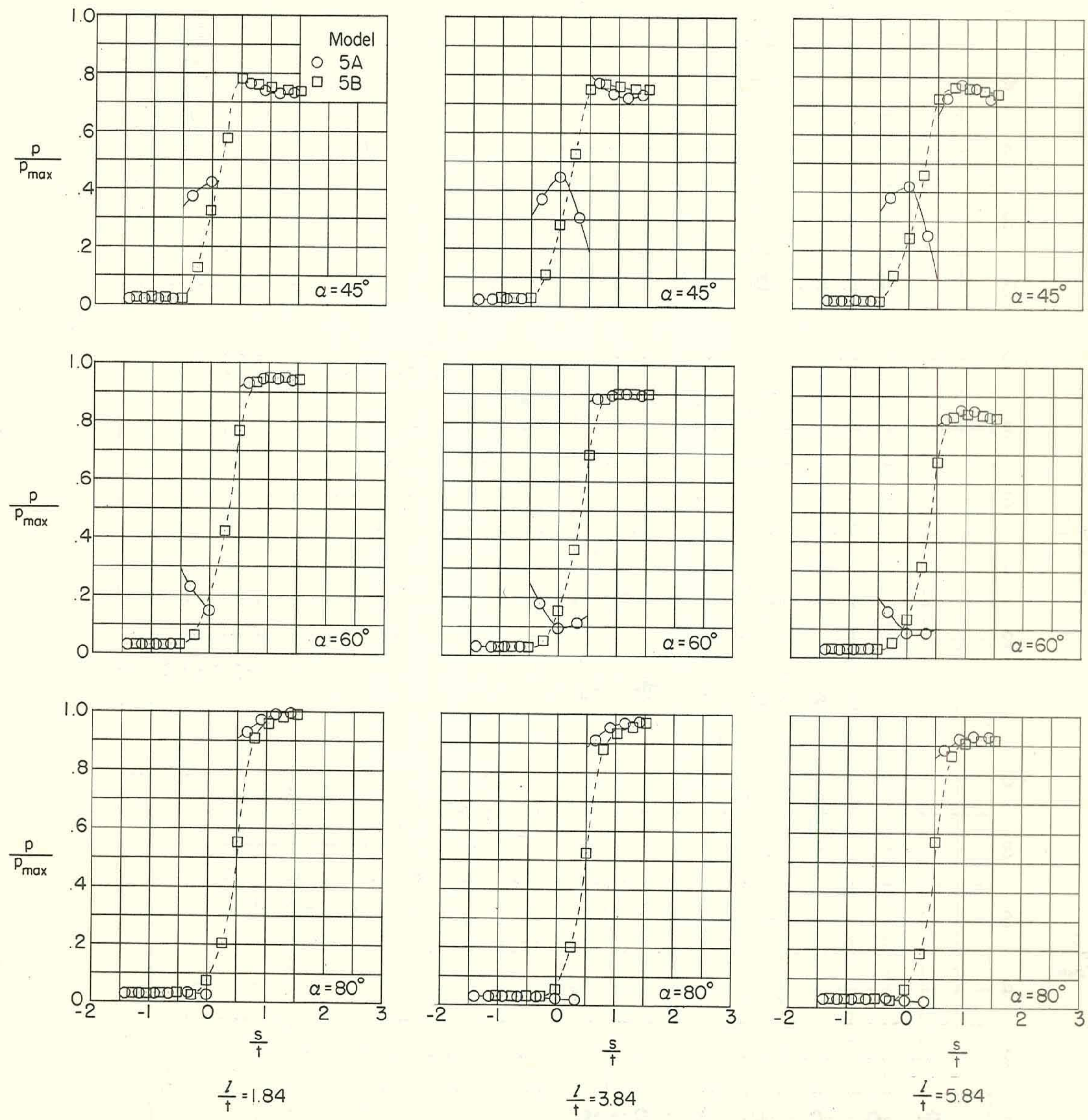

(e) Models 5A and 5B; Λ = 50°.

Figure 12.- Concluded.

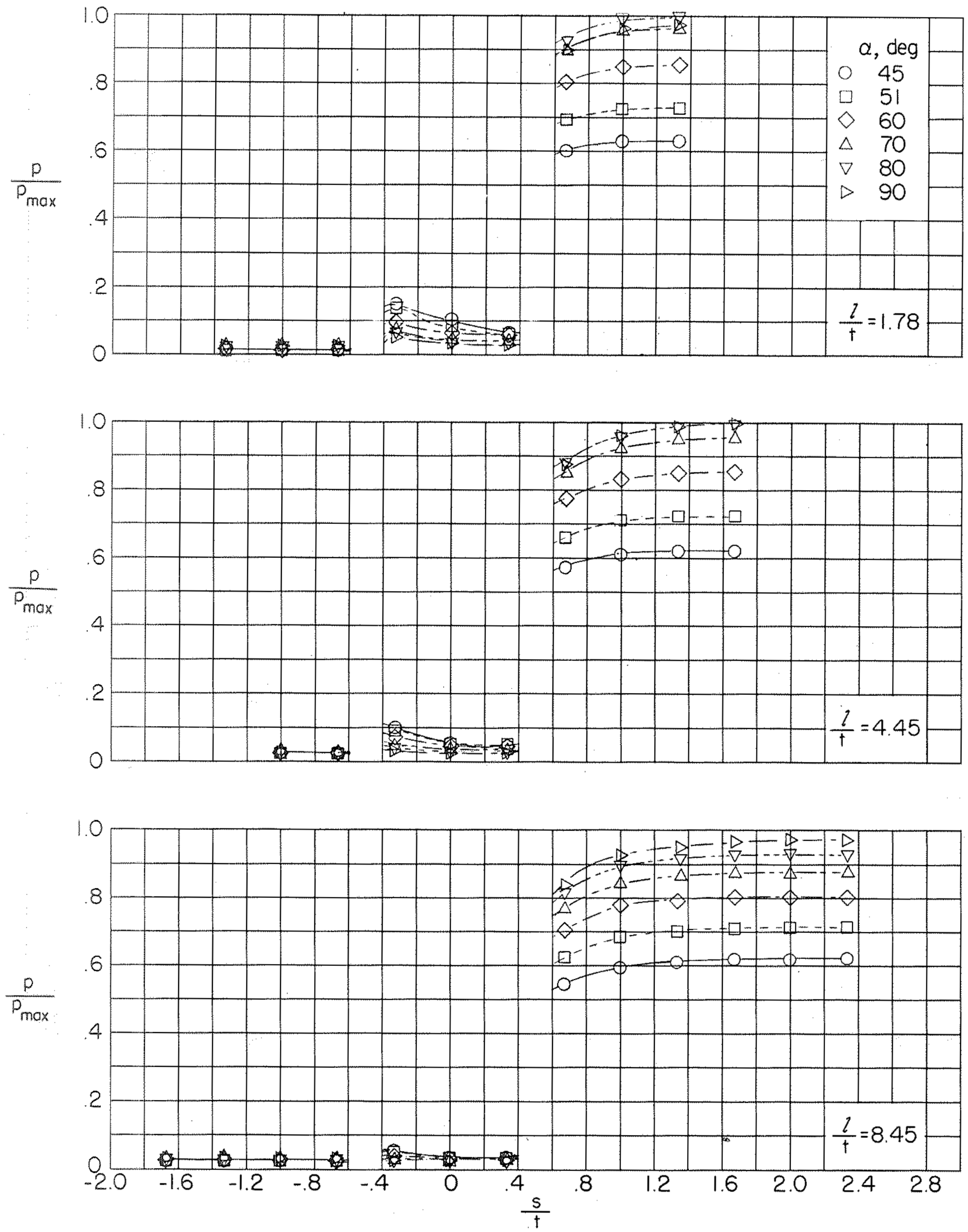

(a) Model 1A; Λ = 80°.

Figure 13.- Effect of angle of attack on the pressure distributions over the basic A-series models (square leading edge).

L-1552

L-1552

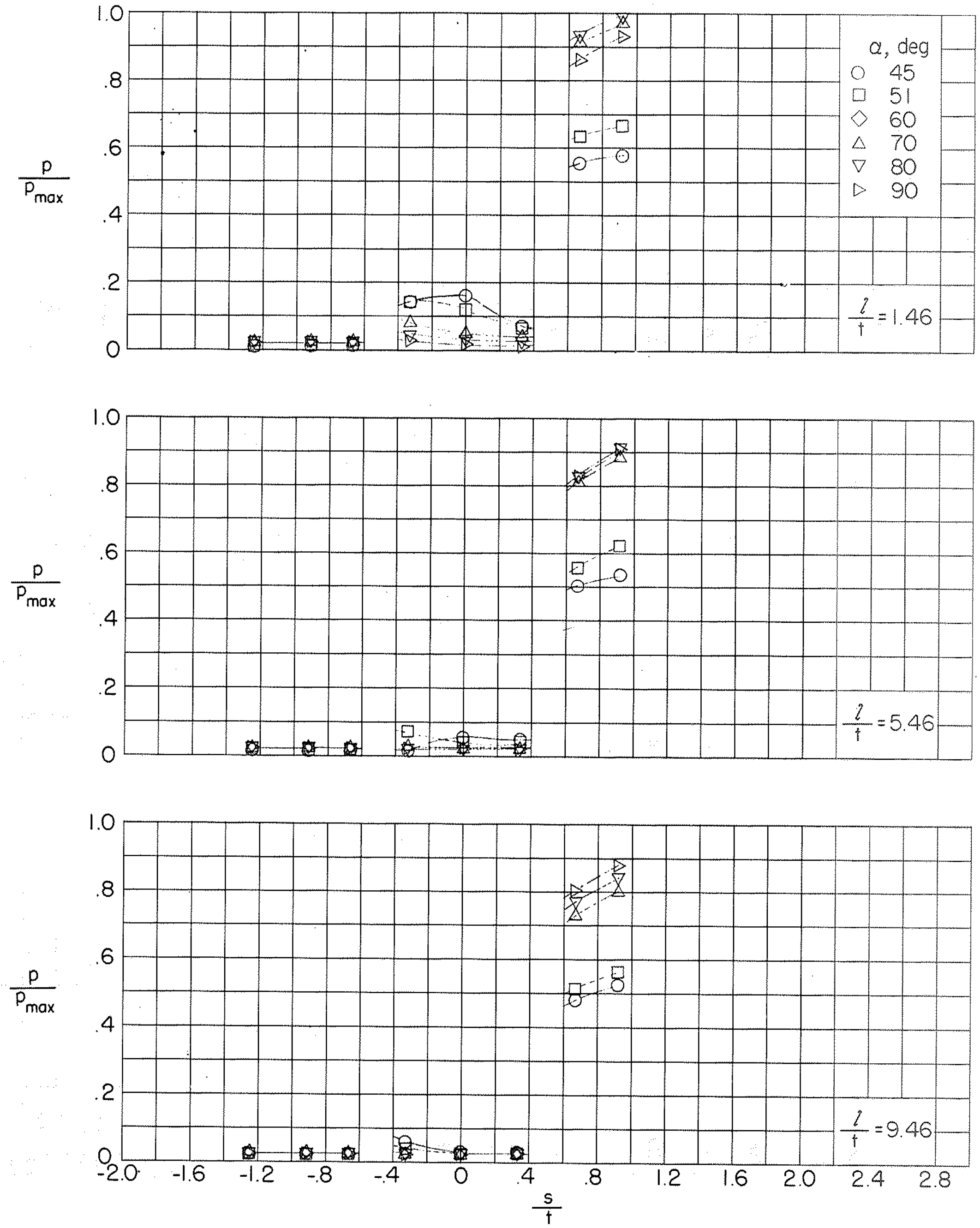

(b) Model 2A; Λ = 75°.

Figure 13.- Continued.

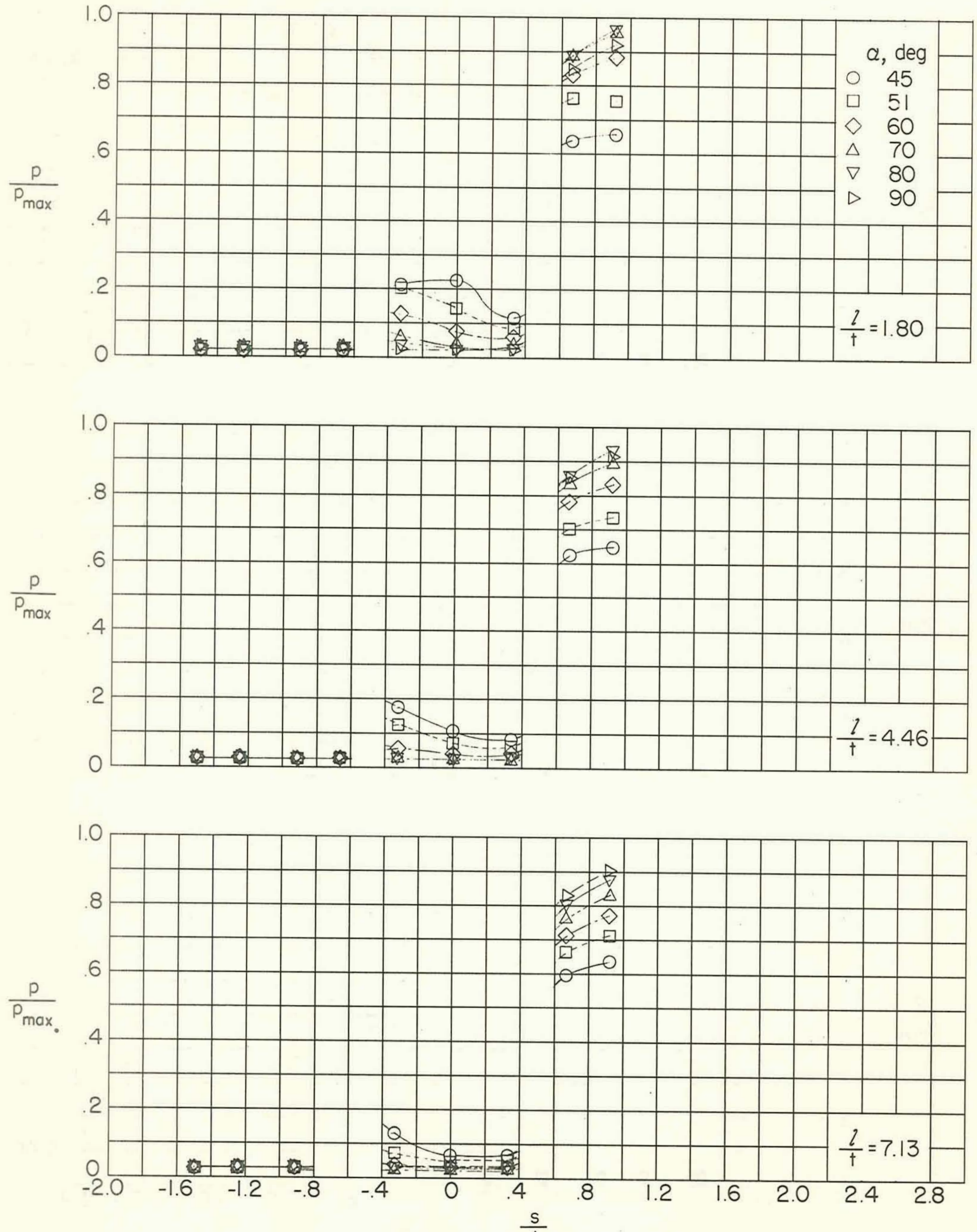

L-1552

(c) Model 3A; Λ = 70°.

Figure 13.- Continued.

L-1552

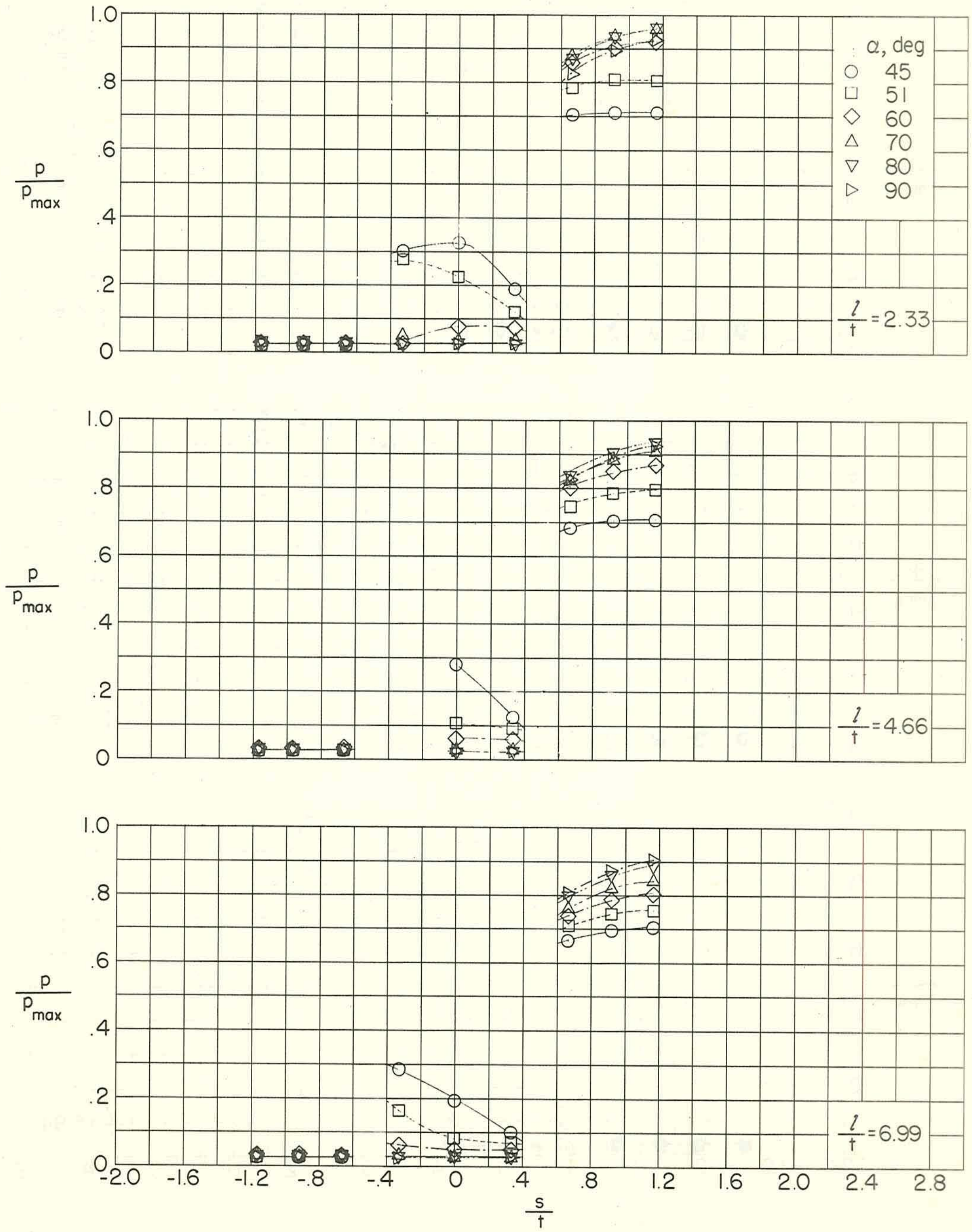

(d) Model 4A; Λ = 60°.

Figure 13.- Continued.

[redacted]

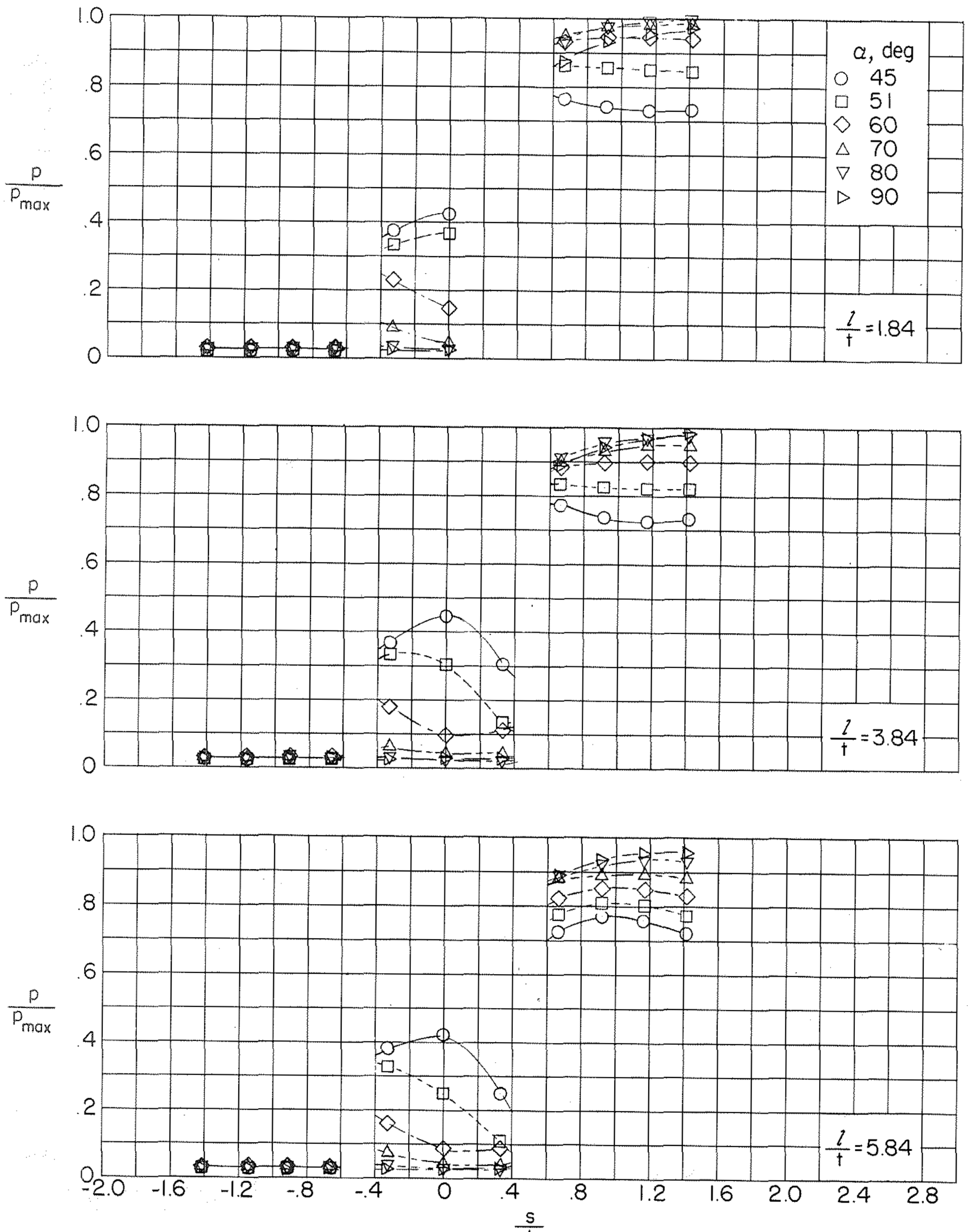

(e) Model 5A; Λ = 50°.

Figure 13.- Concluded.

L-1552

[redacted]

L-1552

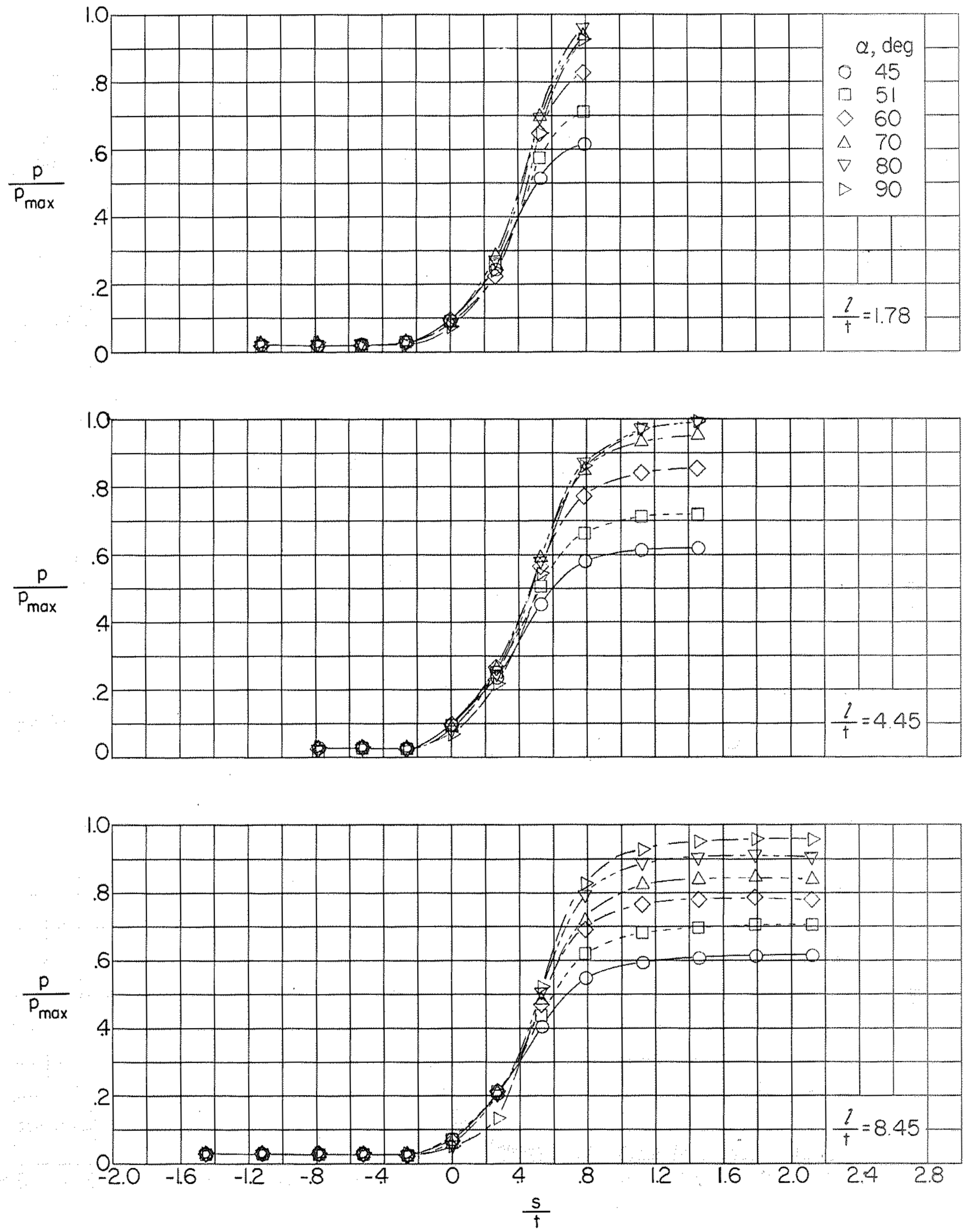

(a) Model 1B; $\Lambda = 80^{\circ}$.

Figure 14.- Effect of angle of attack on the pressure distributions over the basic B-series models (round leading edge).

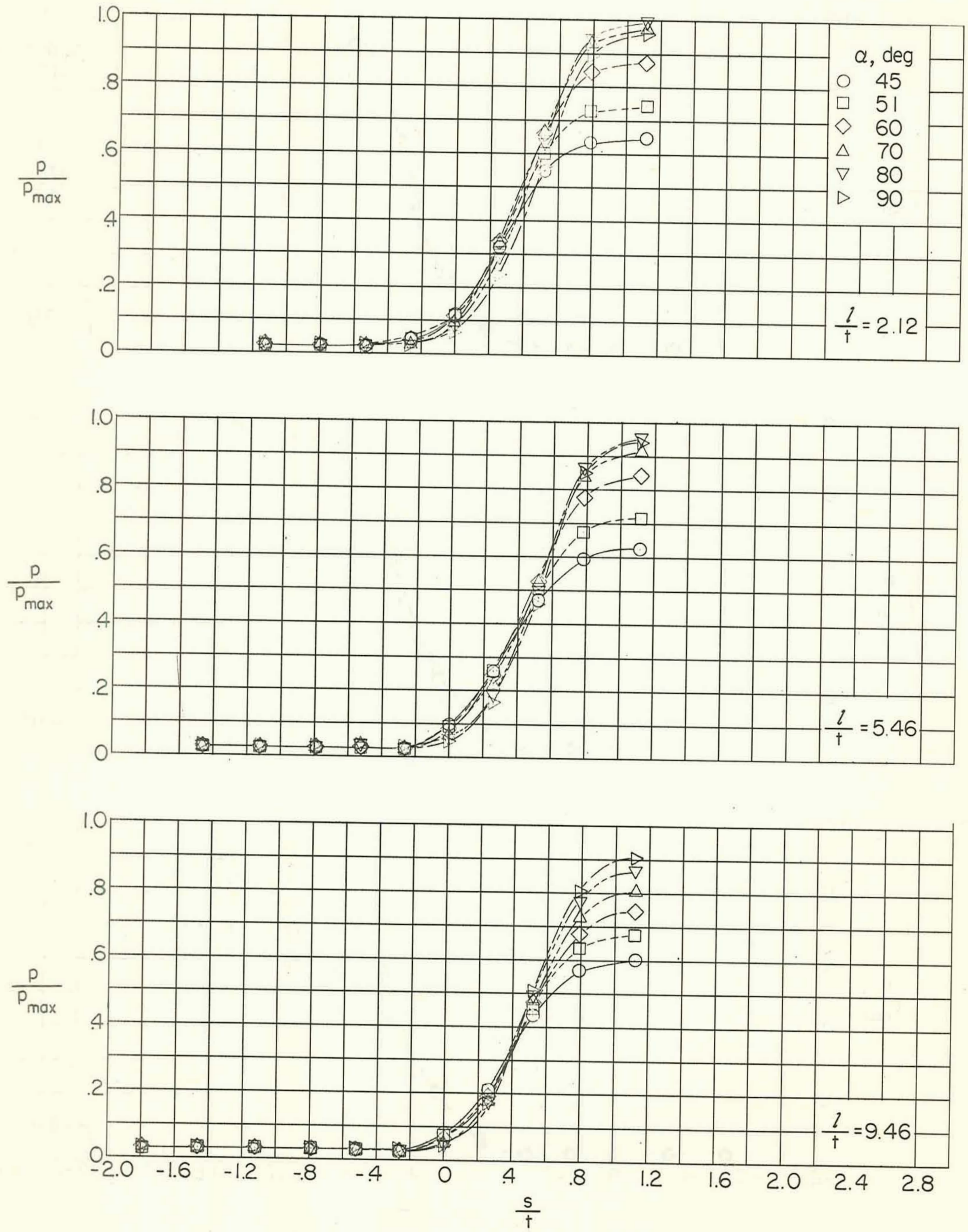

(b) Model 2B; Λ = 75°.

Figure 14.- Continued.

L-1552

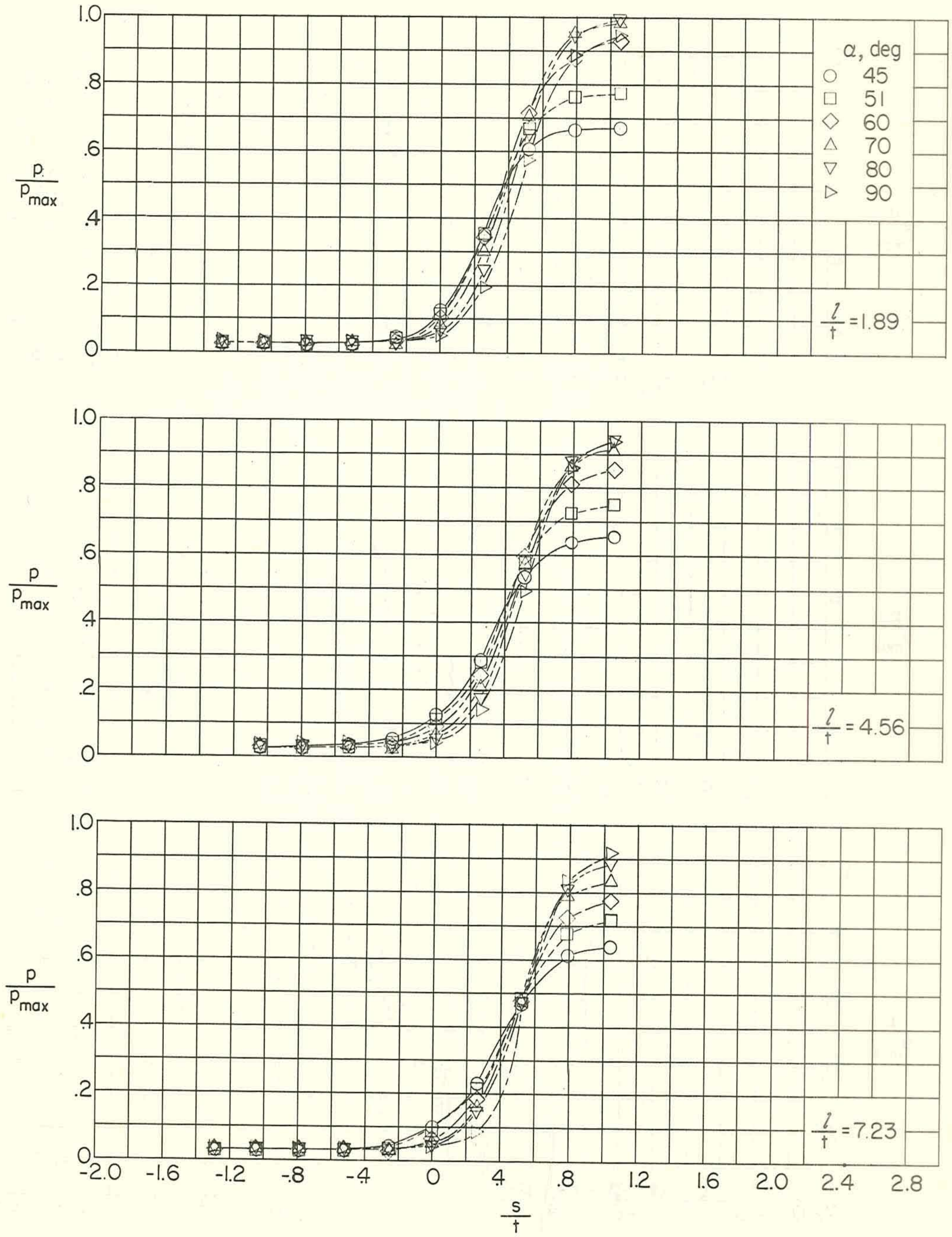

(c) Model 3B; $\Lambda = 70^{\circ}$.

Figure 14.- Continued.

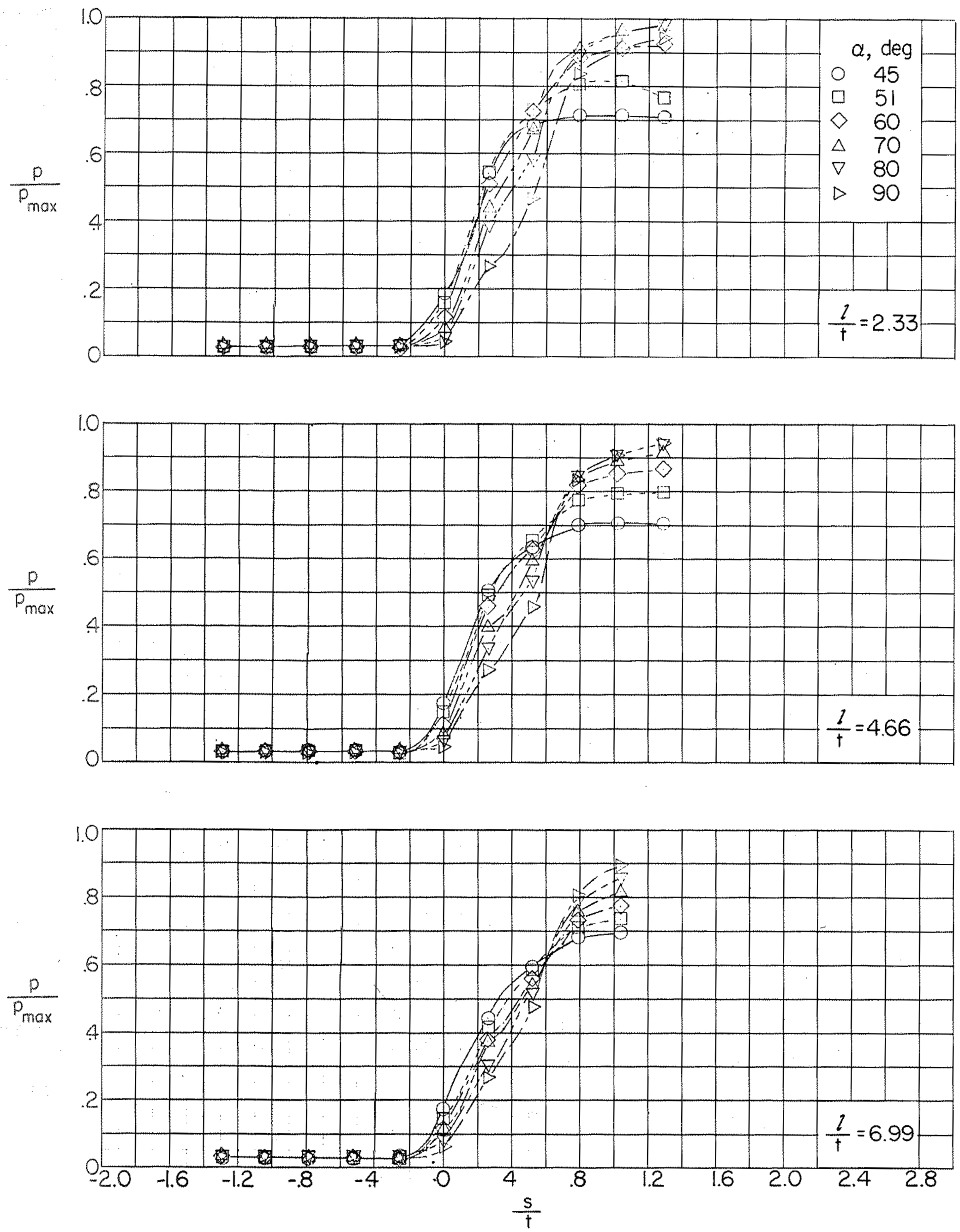

(d) Model 4B; Λ = 60°.

Figure 14.- Continued.

L-1552

L-1552

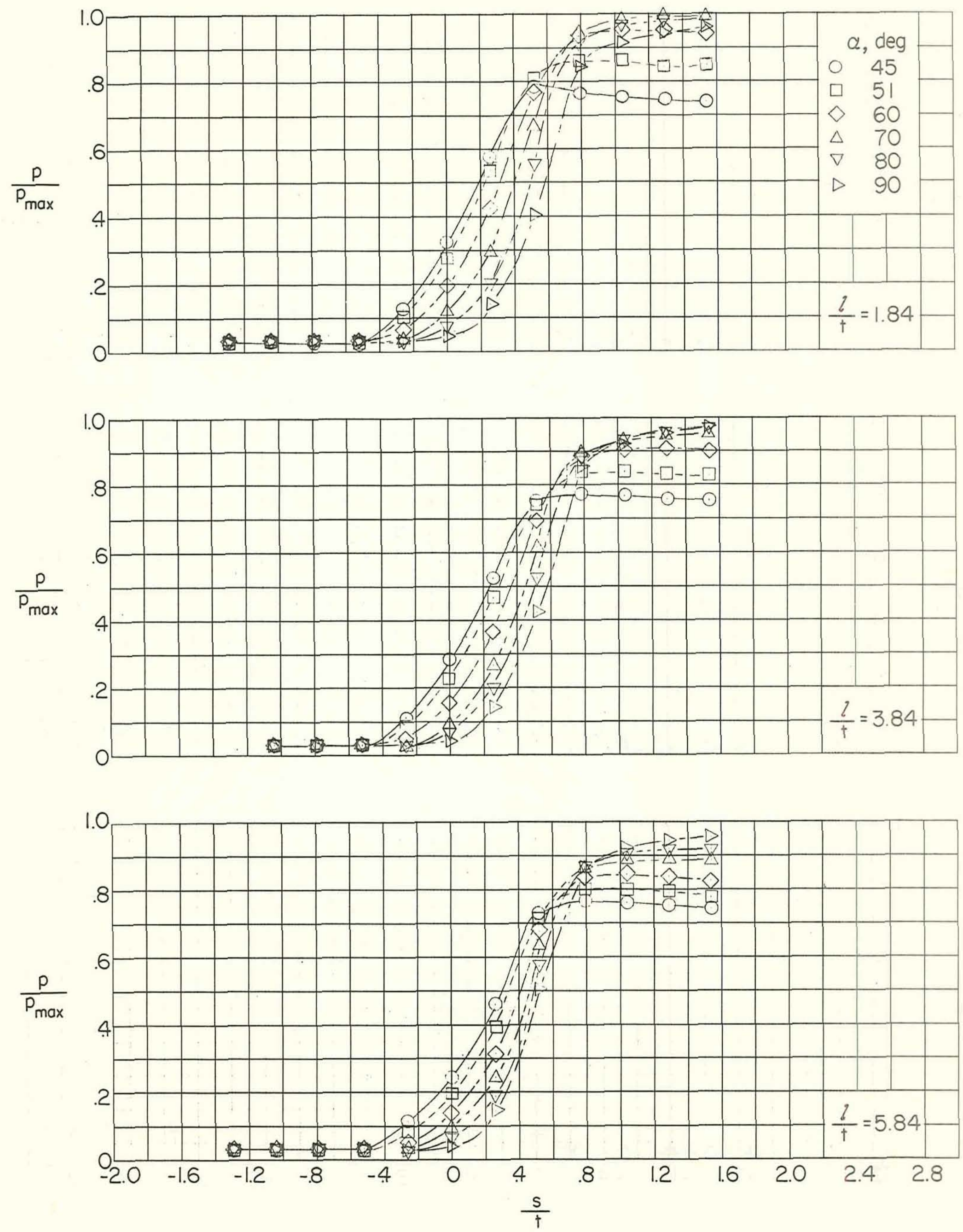

(e) Model 5B; $\Lambda = 50^{\circ}$.

Figure 14.- Concluded.

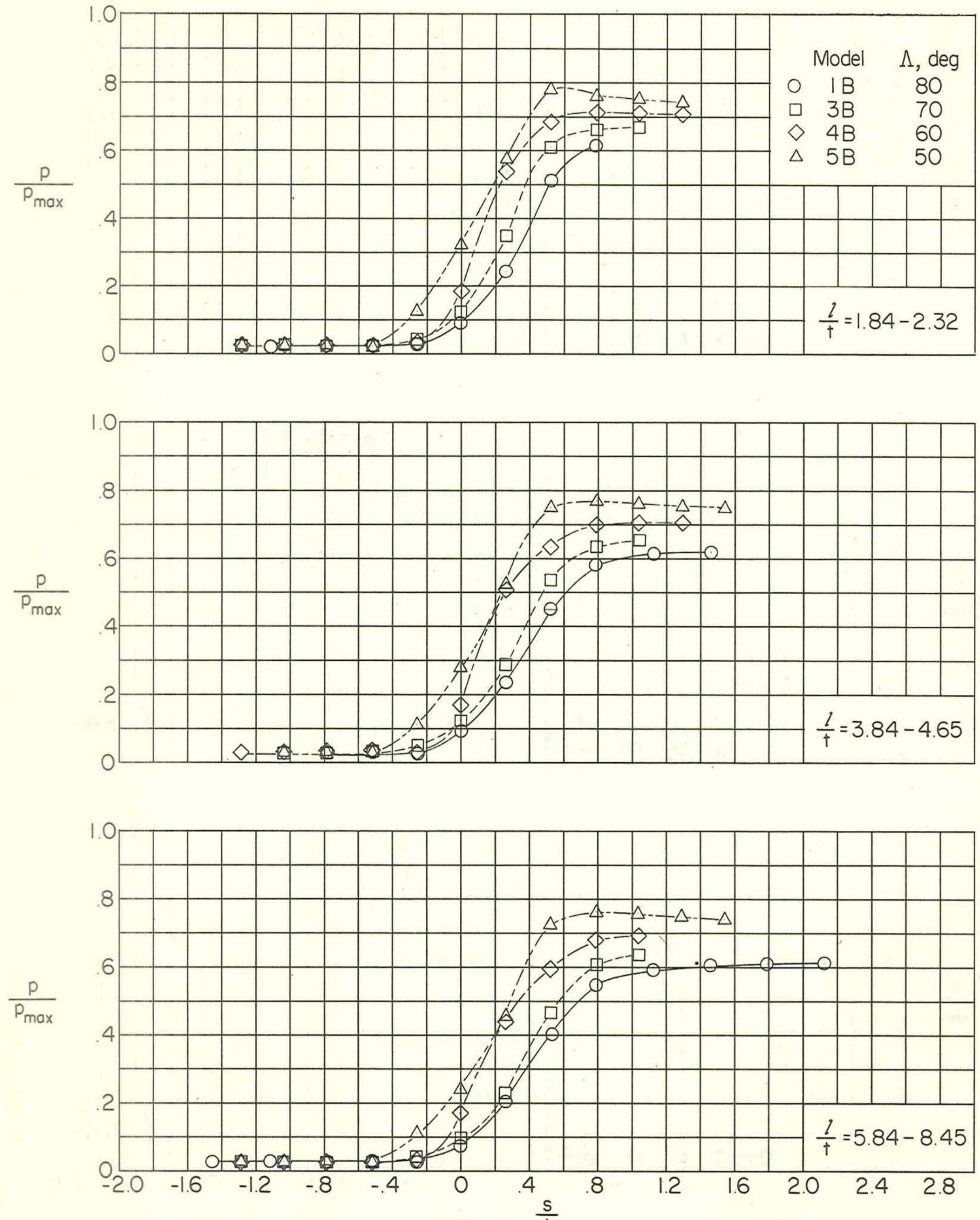

(a) $\alpha = 45^{\circ}$.

Figure 15.- Effect of wing sweep angle on the pressure distributions over the basic B-series models (round leading edge).

L-1552

L-1552

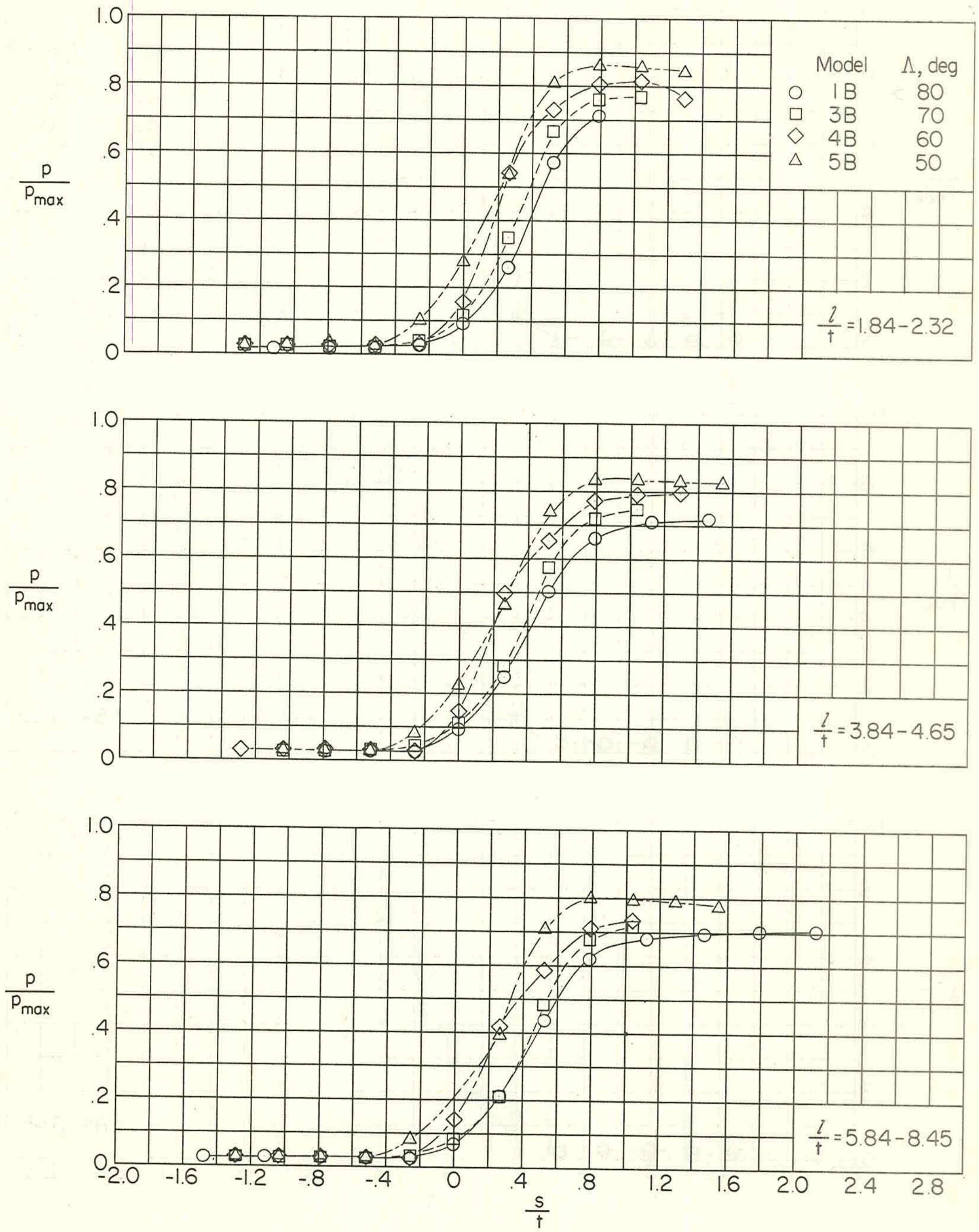

(b) $\alpha = 51^{\circ}$.

Figure 15.- Continued.

[redacted]

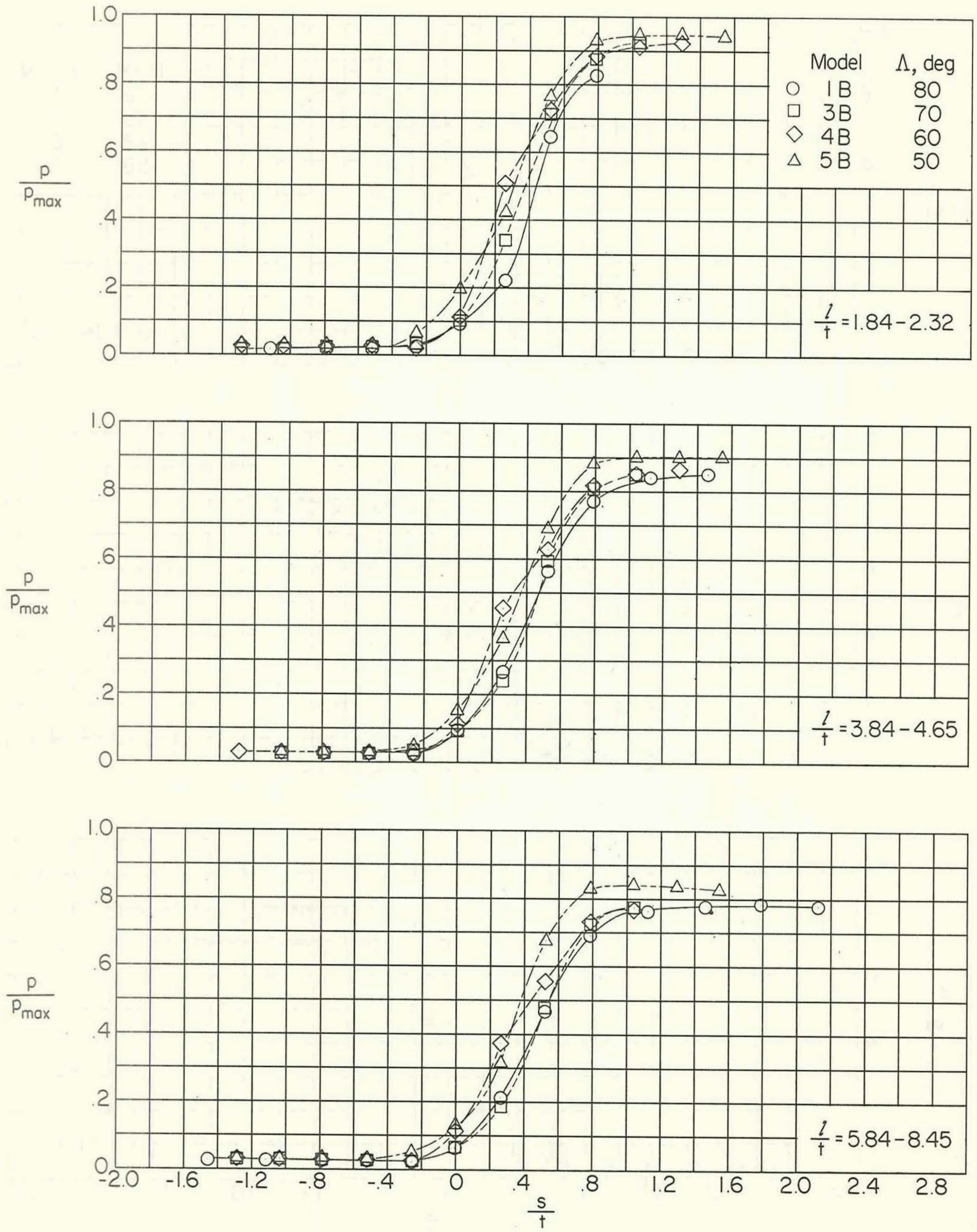

(c) $\alpha = 60^{\circ}$.

Figure 15.- Continued.

L-1552

L-1552

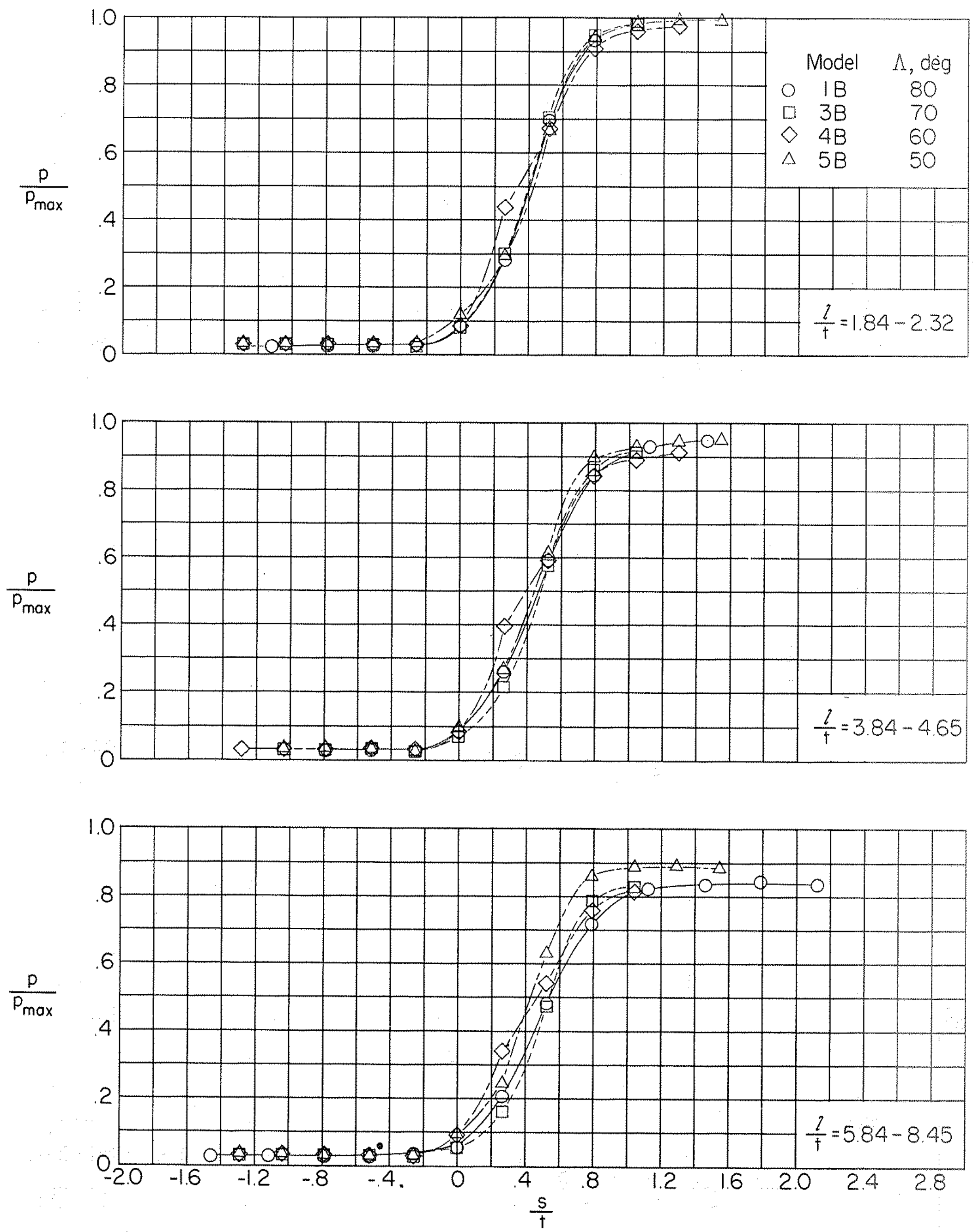

(d) $\alpha = 70^{\circ}$.

Figure 15.- Continued.

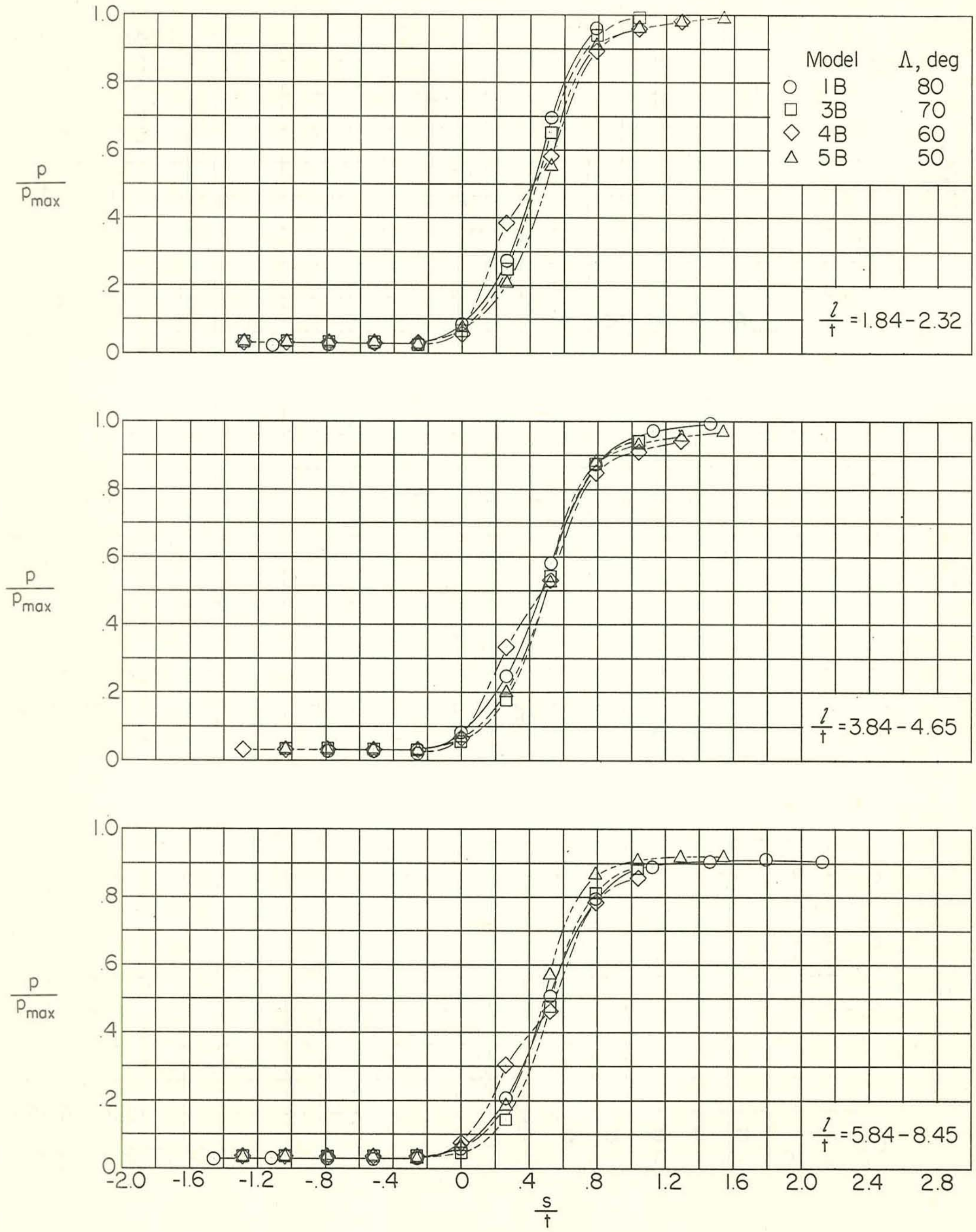

(e) α = 80°.

Figure 15.- Continued.

L-1552

L-1552

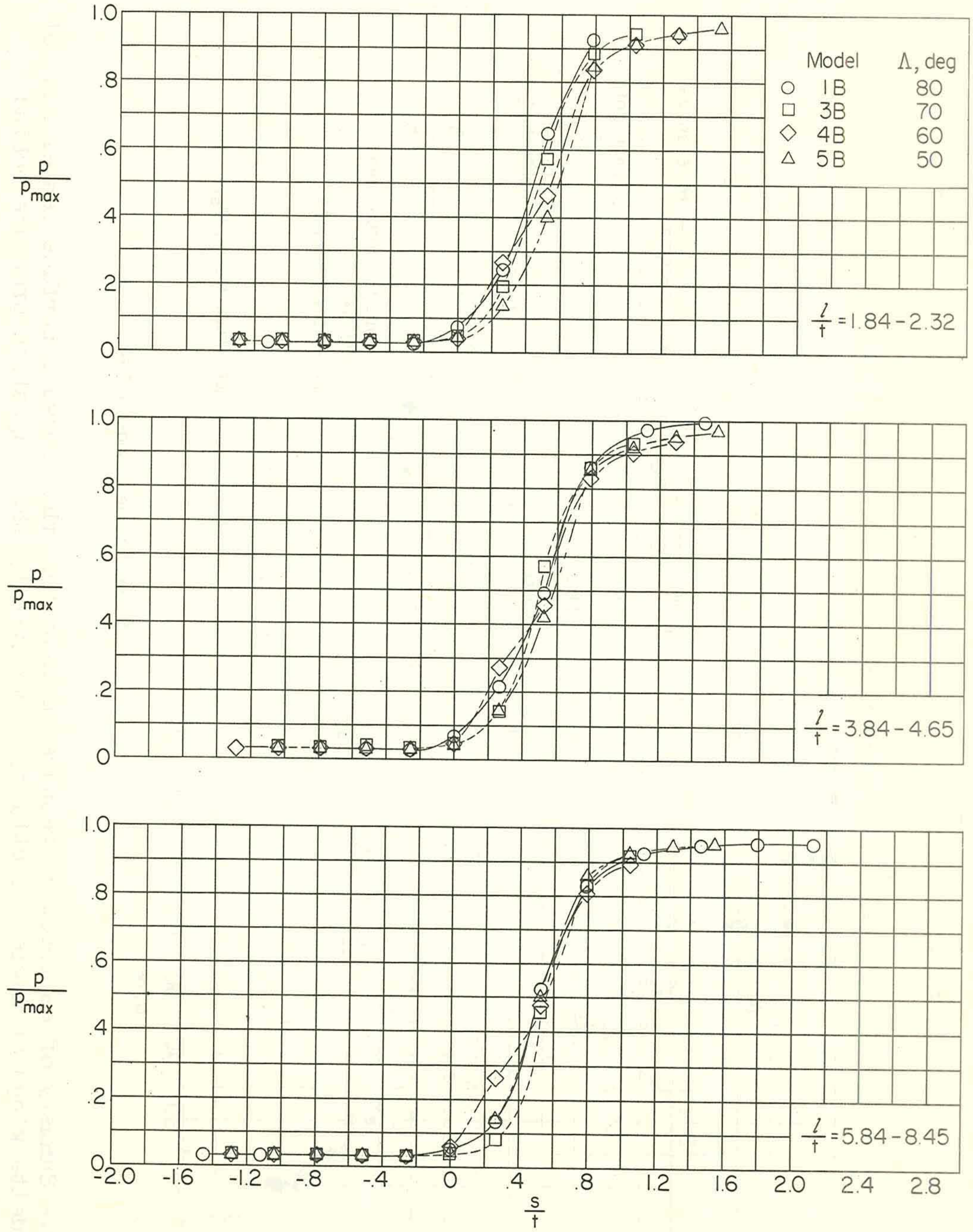

(f) $\alpha = 90^{\circ}$.

Figure 15.- Concluded.

[redacted]

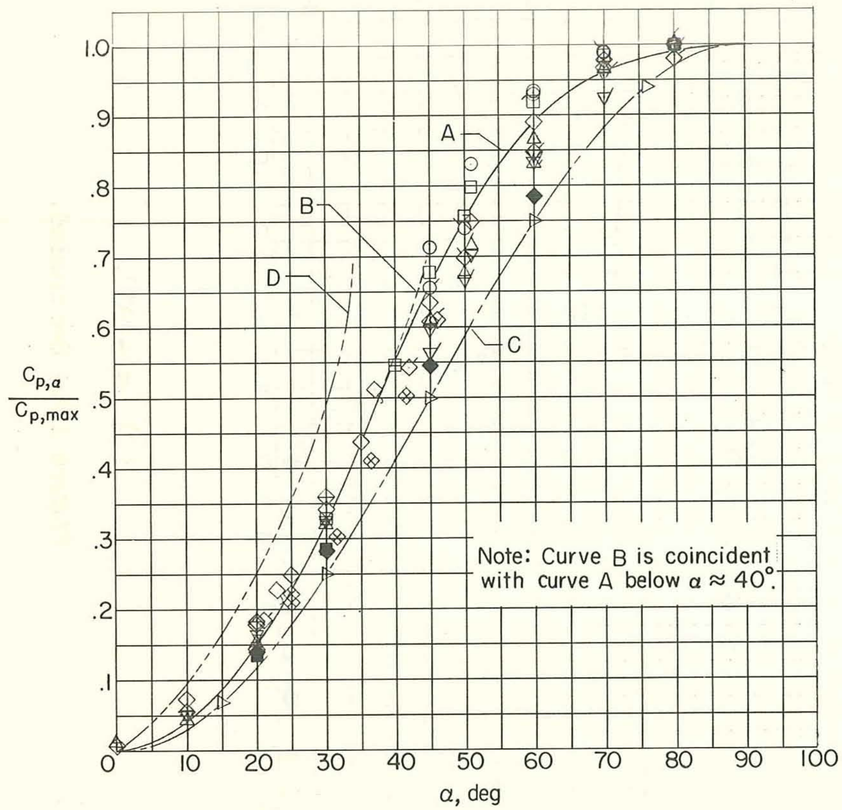

M	Λ, deg						References
	50	60	70	75	80	90*	
2.91	○	□	◇	△	▽		present data
4.65			◇				8
6.86	○		◇	△	▽	▷	8, 11, and unpublished data
8.00		⊞	◇	△	▽		9
9.6			◇				8
20-22		■	◆				15

A ———— 5-term hypersonic approximation (see appendix)

B -------- Oblique-shock theory, $M_\infty = \infty$ (ref. 16)

C ———— $\sin^2 \alpha$

D ———— Oblique-shock theory, $M_\infty = 2.91$

* Semi-infinite cylinder (ref. 6)

Figure 16.- Summary of asymptotic pressures measured on the windward surface center line of blunt delta wings at angles of attack, normalized by the stagnation pressure behind a normal shock.

[redacted]

L-1552

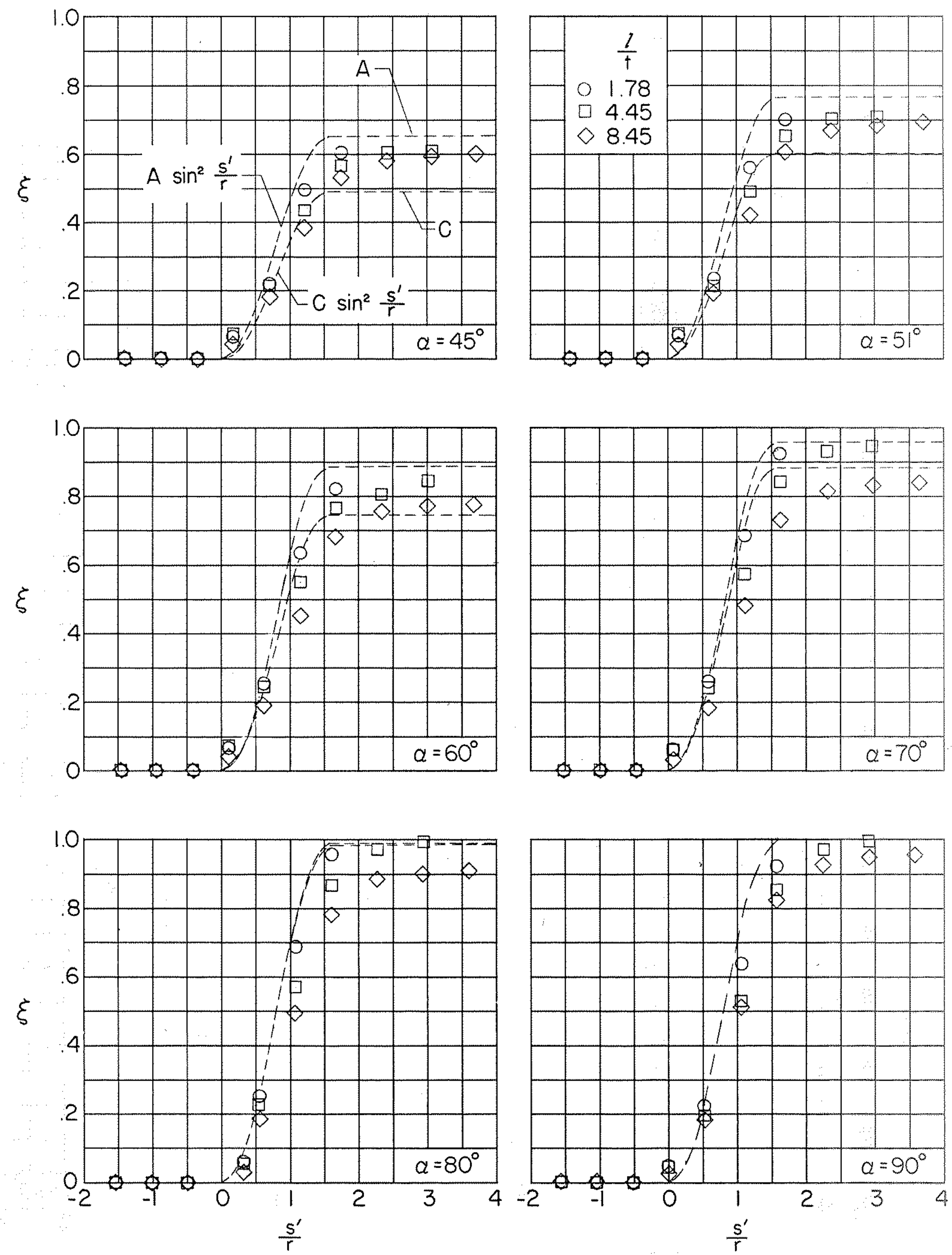

(a) Model 1B; Λ = 80°.

Figure 17.- Comparison of the pressure distributions obtained on the B-series models with an expression related to impact theory.

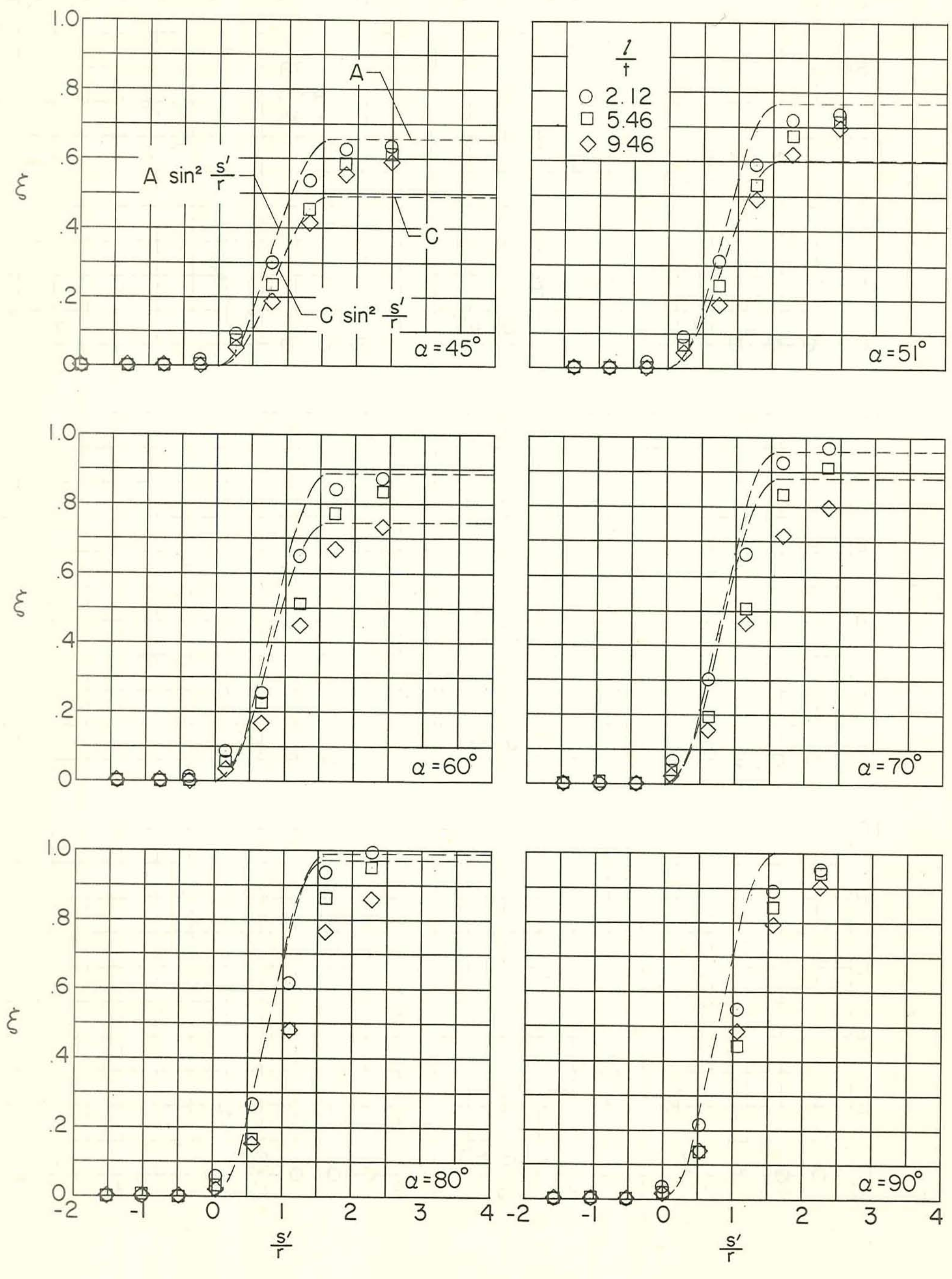

(b) Model 2(B); Λ = 75°.

Figure 17.- Continued.

L-1552

L-1552

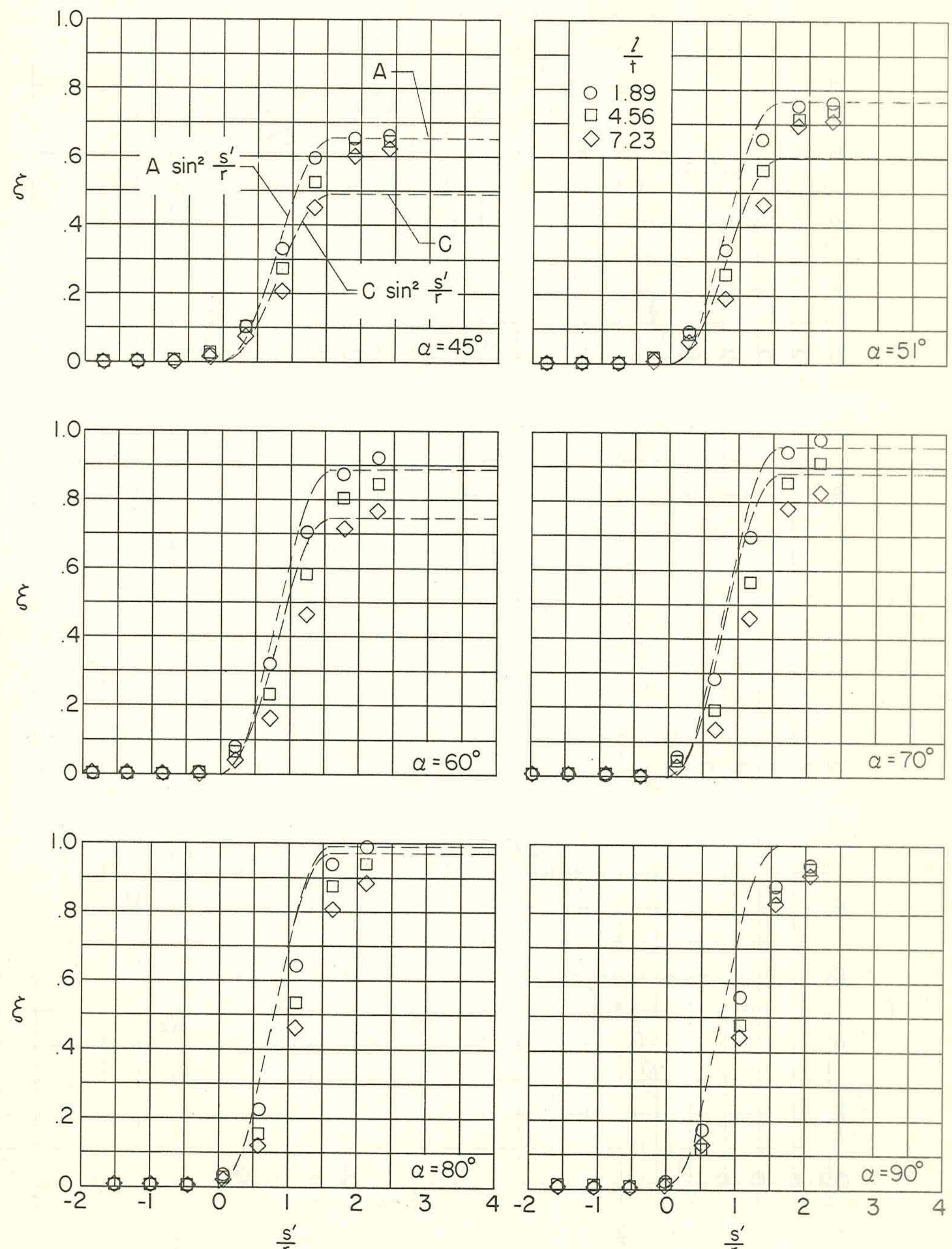

(c) Model 3 (B); $\Lambda = 70^{\circ}$.

Figure 17.- Continued.

[redacted]

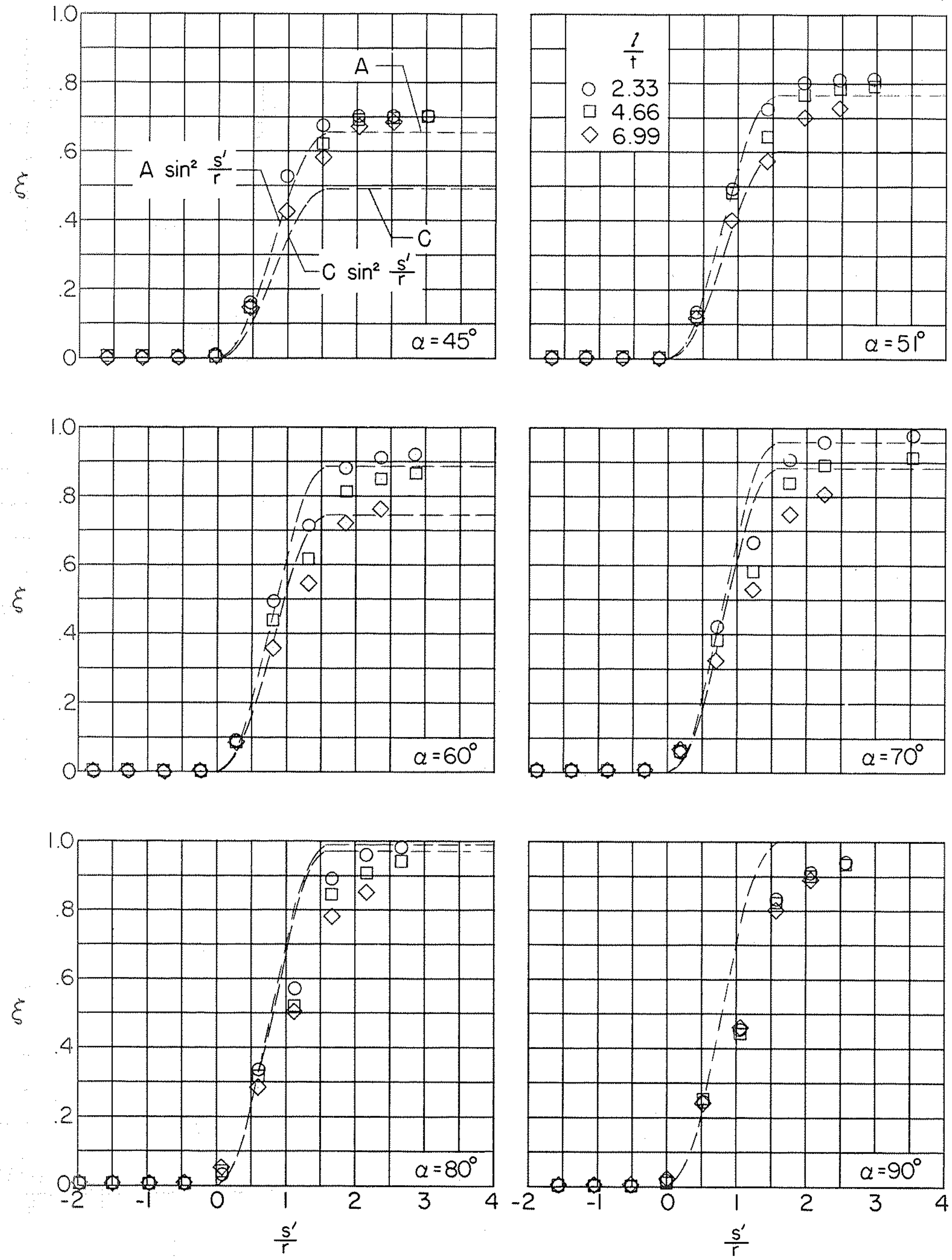

(d) Model 4B; Λ = 60°.

Figure 17.- Continued.

L-1552

[redacted]

L-1552

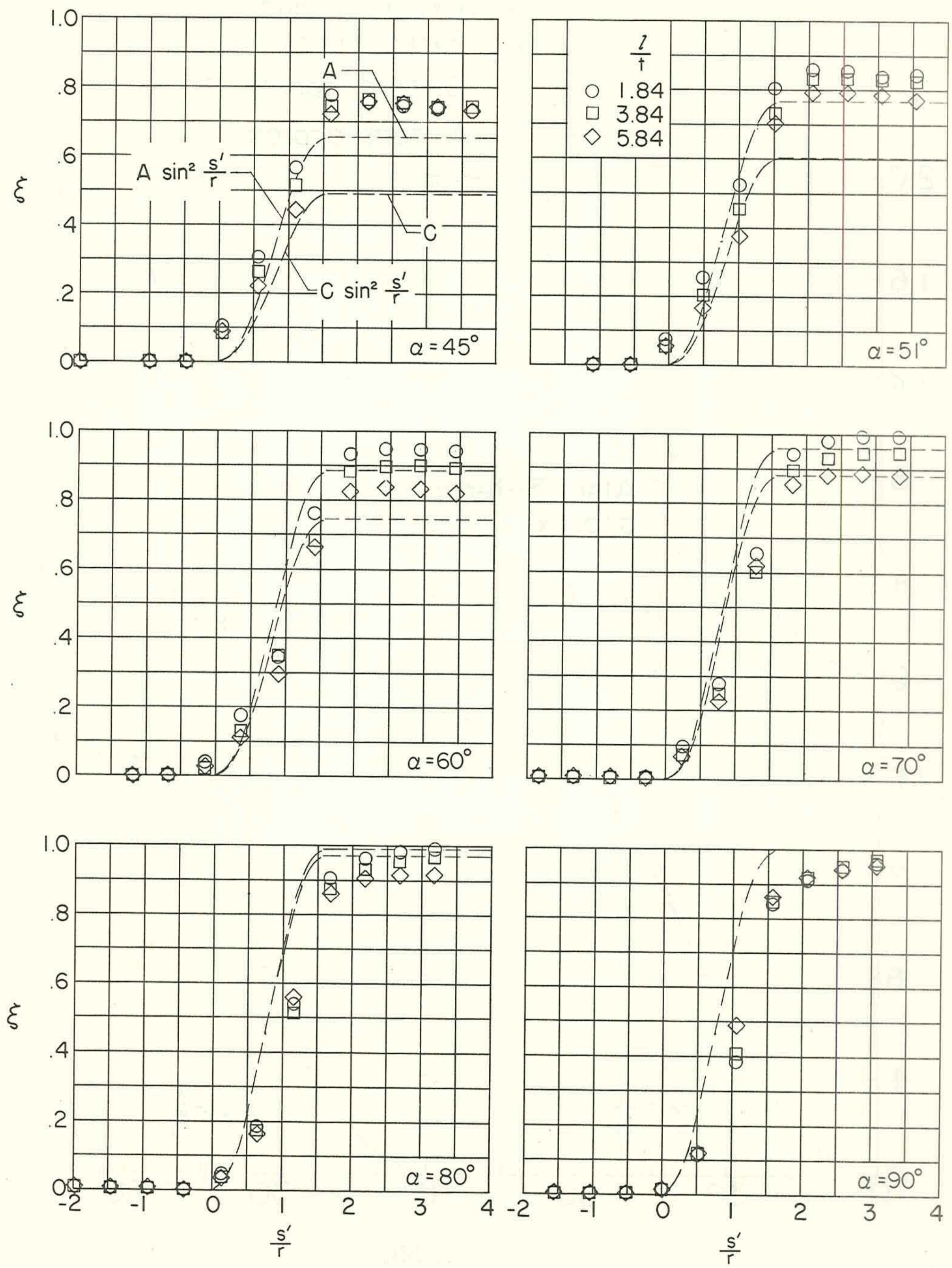

(e) Model 5B; Λ = 50°.

Figure 17.- Concluded.

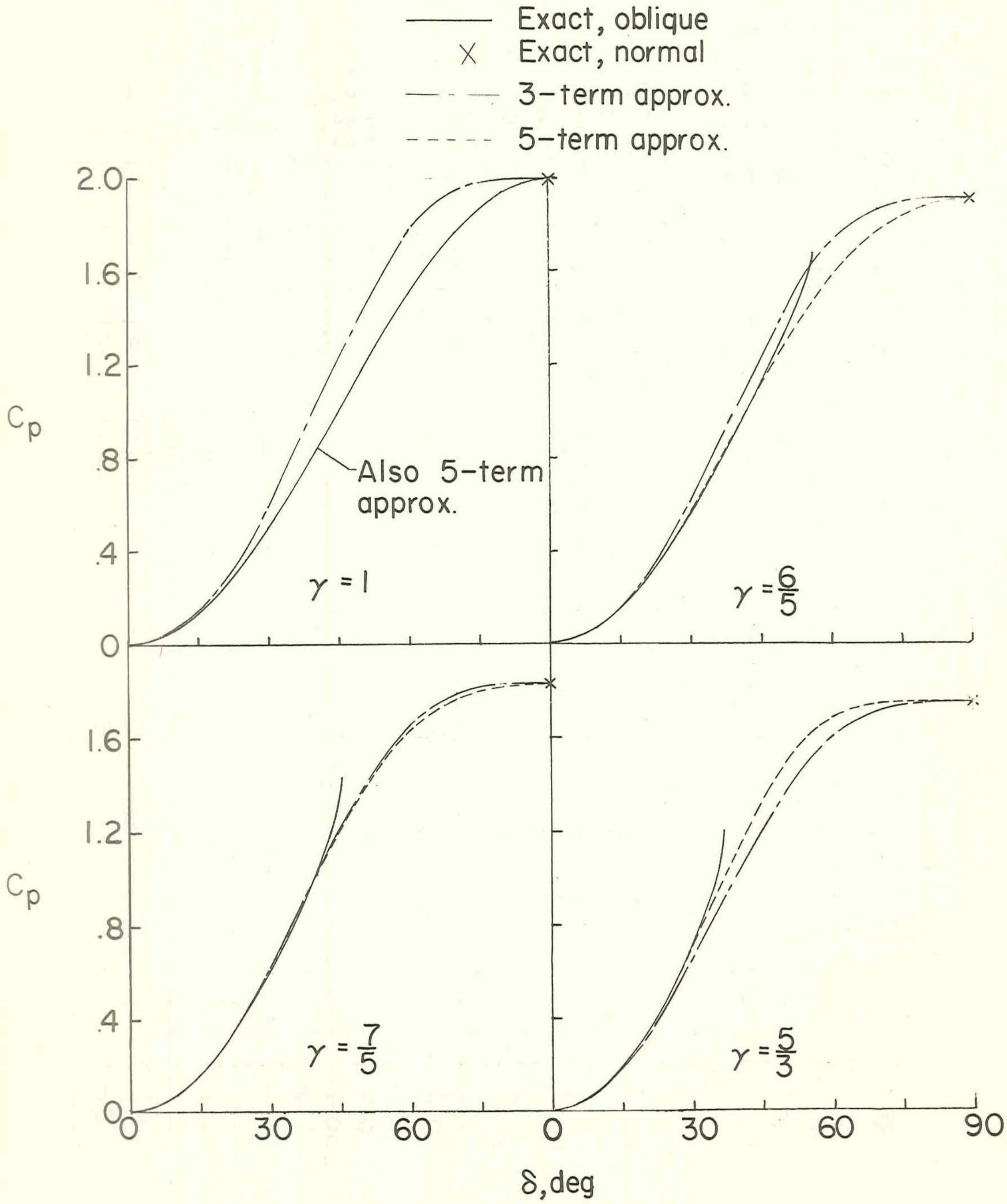

Figure 18.- Comparisons with exact shock theory for $M_\infty = \infty$ (from Love's work).

L-1552

CONFIDENTIAL

CONFIDENTIAL